UNIVERSITÉ DE BLIDA 1

Faculté de Technologie
Département d'Automatique et Électrotechnique

THÈSE DE DOCTORAT

en Automatique

Contribution to the modeling and control of continuum and deformable robots using artificial intelligence tools

Par
Abdelhamid GHOUL

Devant le jury composé de:

A. GUESSOUM	Professeur, U. of Blida 1	Président
K. BOUDJIT	MC A, U. de USTHB	Examinateur
A. MADDI	MC A, U. de Blida 1	Examinateur
K. KARA	Professeur, U. de Blida 1	Rapporteur

U. Blida 1, 13/07/2022

بسم الله الرحمن الرحيم

قَالُوا سُبْحَانَكَ لَا عِلْمَ لَنَا إِلَّا مَا عَلَّمْتَنَا إِنَّكَ
أَنتَ الْعَلِيمُ الْحَكِيمُ

سورة البقرة , الآية 31

DEDICATION

I dedicate this work to my grandfather **AZZI ABED** who supported me in the whole course of my life until the last day of his life.

And also I dedicate this modest work as a testimony of my great respect to my dearest father **GHOUL ABDELKADER**, and to my dearest mother **AZZI AICHA** for all their sacrifices, their love, their tenderness, their support and their prayers all along my studies. May Allah preserve your health and long life.

To my brothers, sister, grandparents, uncles, aunts, friends, classmates who shared their words of advice and encouragement to finish this work of doctorate.

ACKNOWLEDGEMENT

First and foremost, I thank Allah almighty, all powerful, to have given me the strength to survive, as well as the audacity and the patience to overcome all the difficulties.

The work presented in this thesis was carried out at the University Blida 1, Department of Automation and Power, Faculty of Technology, Blida, Algeria, under the supervision of Mr. **KARA KAMEL**, Professor at the University Blida 1, who supervised me throughout this thesis and who shared with me his brilliant intuitions. May he also be thanked for his availability and for the numerous encouragements that he lavished on me.

I express my gratitude to Mr. **GUESSOUM ABDELRAZAK**, Professor at the University Blida 1, agreed to chair the jury of this thesis.

My thanks also go to Mr. **BOUDJIT KAMEL**, professor at the University of Science and Technology Houari Boumediene, and Mr. **MADDI ABDELKADER**, professor at the University of Blida 1, who agreed to be examiners.

I express all my gratitude to Mr. **BENRABAH MOHAMED** Doctor at the University of sciences and technologies Houari Boumediene, for having agreed to answer my questions throughout this thesis.

It is impossible for me to forget Mr. **DJEFFAL SALMANE** Doctor in Mechanical Engineering for his precious help. He has always made all his possible to help me. In order not to forget anyone, my warm thanks are addressed to all those who helped me to realize this modest work.

ABSTRACT

Recently, continuum robots have emerged and are gaining great interest from a large number of researchers. Unlike standard rigid robots, continuum robots have an infinite degree of freedom and a flexible structure allowing them to operate in confined spaces and environments requiring a high level of dexterity and flexibility. However, continuum robots are characterized by a flexible structure and generate their movements by deforming, which make the operations of their kinematic modeling and control more difficult than those of rigid robots and still the subject of search that aims to develop accurate models and efficient control algorithms. The main objective of this thesis is to provide new methods for modeling and control of continuum robots using artificial intelligence tools, such as neural networks and meta-heuristic optimization algorithms.

Indeed, in this work the teaching learning based optimization algorithm is used to obtain the inverse kinematic model of continuum robots with constant curvature and variable length. The developed inverse kinematic model can accurately give the required coordinates to reach a given point in the work space, while avoiding possible static obstacles. Neural networks are also used to construct the inverse kinematic model of continuum robots with variable curvature.

The problem of dynamic modeling of continuum robots is considered in this work and a simplified dynamic model for variable curvature continuum robots is developed.

Also, two control algorithms are designed and their performance are evaluated using different reference trajectories. In the first algorithm, two proportional integral derivative controllers are used to control a variable curvature continuum robot. The parameters of these controllers are obtained using the adaptive particle swarm optimization algorithm. To ensure satisfactory control performance for a constant curvature continuum robot a second control algorithm based on the sliding mode control strategy is developed. This algorithm uses a nonlinear sliding surface and the adaptive particle swarm optimization algorithm to optimize the controller parameters. To conclude on the control performance of the proposed algorithm a comparative study is carried out.

RESUME

Récemment, les robots continus ont fait leur apparition et suscitent un intérêt croissant auprès d'un grand nombre de chercheurs. Contrairement aux robots rigides standards, les robots continus possèdent un degré de liberté infini et une structure flexible leur permettant d'opérer dans des espaces confinés et des environnements nécessitant un haut niveau de dextérité et de flexibilité. Cependant, les robots continus se caractérisent par une structure souple et génèrent leurs mouvements par déformation, ce qui rend les opérations de leurs modélisation cinématique et commande plus difficiles que celles des robots rigides et continuent à faire l'objet de travaux de recherches visant à développer des modèles précis et des algorithmes de commande efficaces. L'objectif principal de cette thèse de doctorat est de développer de nouvelles méthodes pour la modélisation cinématique et la commande de manipulateurs continus, en exploitant les outils de l'intelligence artificielle tels que les réseaux de neurones et les algorithmes d'optimisation méta-heuristique.

En effet, dans ce travail, l'algorithme d'optimisation basé sur l'enseignement et l'apprentissage est utilisé pour obtenir le modèle cinématique inverse de robots continus à courbure constante et longueur variable. Le modèle cinématique inverse développé peut donner avec précision les coordonnées requises pour atteindre un point donné dans l'espace de travail, tout en évitant d'éventuels obstacles statiques. Les réseaux de neurones sont également utilisés pour construire le modèle cinématique inverse de robots continus à courbure variable.

Le problème de la modélisation dynamique des robots continus est considéré dans ce travail, et un modèle dynamique simplifié pour les robots continus à courbure variable est développé.

De plus, deux algorithmes de commande sont développés et leurs performances sont évaluées en considérant différentes trajectoires de référence. Dans le premier algorithme, deux commandes de type proportionnel intégral dérivé sont utilisées pour commander un robot continu à courbure variable. Les paramètres de commande sont optimisés en utilisant l'algorithme d'optimisation par essaim de particules adaptatif.

Pour assurer des performances de commande satisfaisantes pour un robot continu à courbure constante, un deuxième algorithme de commande basé sur la stratégie de commande par mode glissant est développé. Cet algorithme utilise une surface de glissement non linéaire et l'algorithme d'optimisation par essaim de particules adaptatif pour optimiser les paramètres de commande. Afin de conclure sur les performances de commande de l'algorithme proposé, une étude comparative est effectuée.

الملخص

في الآونة الأخيرة ، ظهرت الروبوتات المستمرة و أصبحت تكتسب اهتمامًا كبيرًا بين عدد كبير من الباحثين. على عكس الروبوتات الصلبة التقليدية ، تتمتع الروبوتات المستمرة بدرجة لا نهائية من الحرية وهيكل مرن يسمح لها بالعمل في الأماكن والبيئات الضيقة التي تتطلب مستوى عالٍ من المهارة والمرونة. ومع ذلك ، تتميز الروبوتات المستمرة بهيكل مرن وتولد حركاتها عن طريق التشوه ، مما يجعل عمليات النمذجة الحركية والتحكم بها أكثر صعوبة من تلك الخاصة بالروبوتات الجامدة ولا تزال موضوع البحث الذي يهدف إلى تطوير نماذج دقيقة وخوارزميات تحكم فعالة . الهدف الرئيسي من هذه الأطروحة هو توفير طرق جديدة للنمذجة والتحكم في الروبوتات المستمرة باستخدام أدوات الذكاء الاصطناعي ، مثل الشبكات العصبية وخوارزميات التحسين الفوقية.

في الواقع ، في هذا العمل ، تم استخدام خوارزمية التحسين القائمة على التعلم التعليمي للحصول على النموذج الحركي العكسي للروبوتات المستمرة ذات الانحناء المستمر والطول المتغير. يمكن للنموذج الحركي العكسي المطور أن يعطي بدقة الإحداثيات المطلوبة للوصول إلى نقطة معينة في مساحة العمل ، مع تجنب العوائق الثابتة المحتملة. تُستخدم الشبكات العصبية أيضًا لبناء النموذج الحركي العكسي للروبوتات المستمرة ذات الانحناء المتغير.

تم النظر في مشكلة النمذجة الديناميكية للروبوتات المستمرة في هذا العمل وتم تطوير نموذج ديناميكي مبسط للروبوتات المتغيرة الانحناء.

كما تم تصميم خوارزميتين للتحكم وتقييم أدائهما باستخدام مسارات مرجعية مختلفة. في الخوارزمية الأولى ، تم استخدام اثنين من وحدات تحكم متناسبة متكاملة مشتقة للتحكم في روبوت مستمر بالانحناء المتغير. يتم الحصول على معلمات وحدات التحكم هذه باستخدام خوارزمية تحسين سرب الجسيمات التكيفية. لضمان أداء تحكم مرضٍ للروبوت المستمر ذو لانحناء المستمر ، تم تطوير خوارزمية تحكم ثانية بناءً على إستراتيجية التحكم في الوضع الانزلاقي. تستخدم هذه الخوارزمية سطحًا منزلقًا غير خطي وخوارزمية تحسين سرب الجسيمات التكيفية لتحسين معلمات وحدة التحكم. لاستنتاج فعالية التحكم للخوارزمية المقترحة تم إجراء دراسة مقارنة.

NOMENCLATURE

i	The cable index
j	The unit index
k	The section index
X_k	Cartesian coordinate X with respect to the local reference frame $\Re_{k-1}$
Y_k	Cartesian coordinate Y with respect to the local reference frame $\Re_{k-1}$
Z_k	Cartesian coordinate Z with respect to the local reference frame $\Re_{k-1}$
$A_{i,j,k}$	The point connecting the cables end and the unit mobile platform (j,k)
$B_{i,j,k}$	The point connecting end of cables and the cylindrical unit' fixed platform (j,k)
$\widehat{B}_{i,j,k}$	The point connecting end of the cables and the the conical unit' fixed platform (j,k)
T_{k-1}^{k}	Homogeneous transformation matrix (4×4) defining the reference frame R_k in R_{k-1}
$r_{j,k}$	The radii of the discs
X	The objective function
$\gamma_{i,k}$	Angle of arrangement of the segments in a rotating distance of 120 degrees
g	Gravity constant
t	Time
$\hat{\ell}_{i,j,k}$	Cable length i of the conical unit (j,k)
$\ell_{i,j,k}$	Cable length i of the cylindrical unit (j,k)
$l_{j,k}$	Length of the central axis of the flexible unit (j,k)
$d_{i,j,k}$	Bending radii for cables
R_{k-1}^{k}	Matrix (3×3) defining the orientation of the frame R_k in R_{k-1}
$v_{h,j}$	Linear velocity of the disc
$\theta_{j,k}$	Bending angle for each unit
κ_k	Curvature of the flexible section
w	Coefficient of inertia
F_i	The tension applied to the robot's cables
Q_k	Generalized forces
$U_{j,k}$	The position vector of each point located on the central axis of unit
h	Curvilinear abscissa
m_j	Mass of the discs

m_b	Mass of the stem
d_b	Diameter of the stem
E	Young module
I_b	Inertia moment of the stem
T	Total kinetic energy of the robot
d_b	Diameter of the stem
E	Young module
I_b	Inertia moment of the stem
T	Total kinetic energy of the robot
T_b	Kinetic energy of the stem
T_d	Kinetic energy of the discs
U	Total potential energy of the robot
U_p	Potential energy of the discs

LIST OF ABBREVIATIONS

BHA	Bionic Handling Arm
CBHA	Compact Bionic Handling Arm
DoF	Degree of Freedom
PSO	Particle Swarm Optimization
TLBO	Teaching Learning Based Optimization
FKM	Forward Kinematic Model
IKM	Inverse Kinematic Model
CC	Constant curvature
VC	variable curvature
CL	Constant Length
VL	Variable Length
OPID	Optimized Proportional Integral Derivative
OSMC	Optimized Sliding Mode Controller
ONSMC	Optimized Nonlinear Sliding Mode Controller

TABLE OF CONTENTS

LIST OF FIGURES

LIST OF TABLES

INTRODUCTION

Robotics increasingly attract researchers' interest over the past few decades, as it has become the solution to many problems in real world applications. Especially, when it comes to difficult and complex tasks that humans cannot handle or in industrial environments that may be hazardous to humans (for example near high temperatures and nuclear reactors or when dealing with chemical waste and sharp objects). As a consequence, the field of robotics has attracted more researchers to design more sophisticated robots to handle the required tasks. Initially, rigid robots were developed to perform specific tasks, for example in some military tasks, aerospace exploration and industrial operations because of their dexterity especially in repetitive tasks that require precision and rigidity.

Outside of industry, rigid robots have shown some drawbacks, in particular when it comes to surgery, rescue under buildings, inspection in hazardous environments and nuclear reactors which have labyrinth-like paths and small clustered environments. The deficiency of rigid robots is labeled to their rigid links and their inability to adapt with these kinds of paths. To this end, it would be tempting to find an alternative to these robots. Researchers have developed the so-called continuum bionic robots which can easily be adapted to any kind of paths thanks to their flexibility and high performance. Continuum robots are considered by a large number of researchers as an exciting and new technology because they have notable advantages such as flexibility, lightweight, inherent safety and so forth [1–12]. Continuum robots can also avoid obstacles, handle adjustable stiffness on irregular objects, and even adapt their body shape while maneuvering in an unknown and non-uniform environment. However, they still present an impediment to researchers, because of their complexity when it comes to modeling and control. Despite the fact that many researchers have come up with new methodologies to model them, yet they are not sufficiently reliable and further accuracy is required.

In this context, this thesis presents a modest contribution to the kinematics, dynamics modeling, and control of continuum robots.

In contrast to traditional robots with rigid and limited links, whose behavior was fully understood and studied, flexible continuum robots are more difficult to modeling and control which makes the full understanding of their behavior is more complex. The complexity of modeling and control of continuum robots is triggered by the variety of their properties, lack of rigidity, and their infinite degrees of freedom.

- **Motivation** : Rigid robots are employed in a vast range of applications, however the tasks that can manage are limited. The use of continuum robots in the other hand can be extended to a wider scope of areas due to their flexibility and dexterity. However, their modeling and control is still ongoing in a slow pace which prevents their dissemination and full benefit. This motivated us to dive in this promising alternatives in the aim of boosting their development.

- **Objectives of the thesis** : The main objective of this project is to provide new methods for the modeling and control of continuum and deformable robots using artificial intelligence tools such as neural networks and meta-heuristic optimization algorithms.

- **Contribution** : The obtained results in this work can be summarized as follows: an inverse kinematic model of a variable length continuum robot with constant curvature was proposed using a powerful meta-heuristic optimization method called teaching learning based optimization with the ability to make a robot dexterously avoid obstacles. Furthermore, an inverse kinematic model of a constant length continuum robot with variable curvature was developed using artificial neural networks. Then, a dynamic model of a continuum robot with variable curvature was developed using the Euler-Lagrange approach and the obtained differential equation was solved using the Runge-Kutta method. Finally, an efficient controller to control continuum robots that gives good accuracy and effectiveness event in presence of external disturbances was proposed.

- **Organization of the manuscript** : This thesis is organized into four chapters. The *Chapter 1* focuses on the state of art of continuum robots. In the 1st part, we present the different types of continuum robots and their usage in various fields. In the 2nd part of the state of the art we present some recent studies on kinematic, dynamic modeling and control approaches. In *Chapter 2* a geometrical description of a flexible continuum robot is given. Then, the

forward kinematic modeling of a single unity, a flexible section, and the whole robot are derived. In addition, a comparison is made between the workspace of a continuum robot with constant and variable curvature. Finally, a particular case study of a variable-length continuum robot is studied. *Chapter 3* is dedicated to inverse kinematic modeling. Firstly, the inverse kinematic model of a single section with constant curvature is analytically calculated. Then, the inverse kinematic model of a multi-section continuum robot with CC and VC was solved using meta-heuristic algorithms and artificial neural networks, respectively, as consequence of analytical methods inability to deal with equations complexity. Finally, the *last chapter* deals with a dynamic study of a continuum robot with variable curvature as well as developing efficient controllers to continuum robots.

- **List of publications** :
  Ghoul, A., Kara, K., Benrabah, M., and Hadjili, M, L. "Optimized Nonlinear Sliding Mode Control of a Continuum Robot Manipulator,". J Control Autom Electr Syst. pp.1-9, 2022. https://doi.org/10.1007/s40313-022-00914-1.

  Ghoul, A., Kara, K., Djeffal, S., Benrabah, M., and Hadjili, M, L. "Artificial Neural Network for Solving the Inverse Kinematic Model of a Spatial and Planar Variable Curvature Continuum Robot,". Archive of Mechanical Engineering. 2022.

  Ghoul, A., Kara, K. Djeffal, S., Benrabah, M., and Hadjili, M, L. "Inverse Kinematic Model of Continuum Robots Using Artificial Neural Network,". 19^{th} IEEE International Multi-Conference on Systems, Signals & Devices. April 2022. Setif, Algeria.

  Ghoul, A., Kara, K. Benrabah, M., and Nasri, B. "Control of Continuum Robots Using Two Optimized PID Controllers,". 2^{nd} Conference on Electrical Engineering (CEE'21). April 2021. Algiers, Algeria.

CHAPTER 1

STATE OF THE ART

1.1 Introduction

In this chapter an overview of the latest findings of researchers in the field of continuum robots' design, modeling and control are provided. In fact, this literature review is crucially important to clarify the encountered difficulties related to these robots compared to rigid robots. To this end, we first present the classification and definition of this type of continuum robots. Then, their modeling and controlling methods are thoroughly addressed.

1.2 Definition

Continuum robots are modern, flexible and biologically inspired [12–22] such as elephants' trunks, snakes, octopus' arms, tentacle and appendices. They have the ability to track, bend and maneuver in small and cluster pathways due to their flexible links and infinite degrees of freedom. These newly emerged robots attract great interest among research community due to its superiority over classical robots, which leads to their omnipresence in various fields, especially in the medical and the industrial ones.

Figure. 1.1: (a). BHA trunk robot; (b). Snake robot; (c). octopus arm robot

1.2.1 Types and design of continuum bionic robots

Recently, many researches focused on the graceful design and the flexibility of continuum robots, which make them compatible with a wide range of applications, in contrast to traditional robots that are unable to deal with dangerous and cluster environments due to their rigid and limited links. To this end, several models and designs have been proposed by the continuum robots' research community. The first continuum robot (Tensor arm manipulator) (Figure 1.2) was developed in 1967 by V. C. Anderson and R. C. Horn [23, 24], which contains a group of plates linked together by solid bonds as a backbone that is guided by an enormous number of tendons passing through small apertures in the disks (Figure 1.4) which make its control process very difficult.

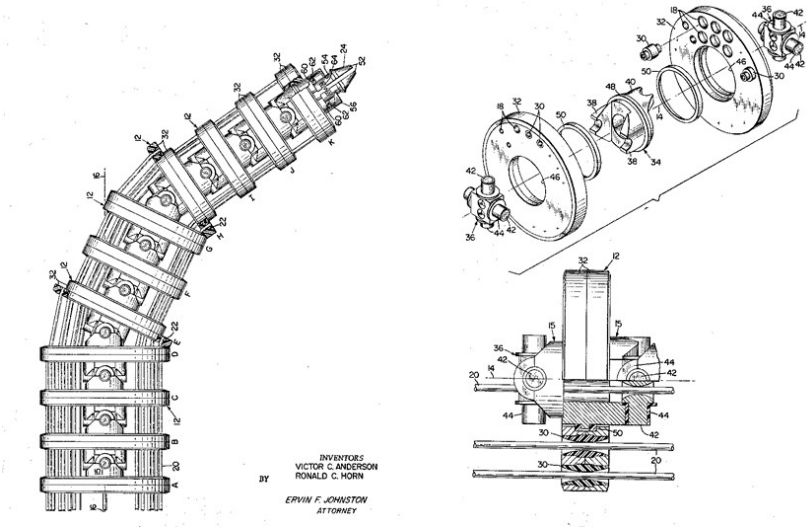

Figure. 1.2: (left) Tensor arm manipulator (right) partial cross-section of the plate [23]

Before the year 2000, some works were done for the development of continuum robots. In 1994, a continuum robot was proposed by Chirikjian [25] which simulates the movements of worms and snakes during exploration and inspection of twisted and tight pipes. Then, within the framework of an international project funded by the european union authority for the purpose of making up an under-sea tool dedicated to investigation, a prototype of a three-finger hydraulic continuum robot (Figure 1.3) was designed by Amadeus Company in 1996 [26, 27].The Amadeus robot, controlled by three independent motors, has the ability to grasp irregular shaped objects and able to avoid external disturbances due to its superior flexibility. In 1999, a continuum robot was developed by Walker with four sections (Figure 1.4), each section is separately actuated by a group of cables [28, 29].

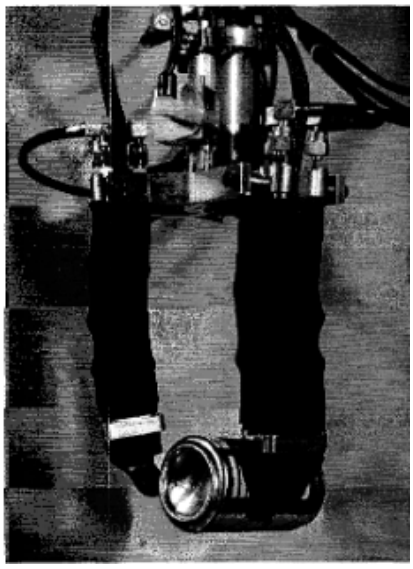

Figure. 1.3: Amadeus robot's fingers [26]

Figure. 1.4: Clemson Elephant Trunk Robot [28].

In the first beginning of 2000s, researchers paid great attention to the field of biologically inspired robots. Dozens of designs for continuum robots that simulate biological structures were developed and built, in particular, there were those who made their way to adopt elephant trunks to design and build these robots, most notably the Bionic Handling Assistant (BHA) robot. BHA was created by Festo company as shown in Figure 1.5, it won the German Future Prize in 2010, as it was designed from poly amide allowing it greatly bend over the needed position. This robot contains three sections with three tubes as backbones, each of its section has two degrees of

freedom and actuated by air pressure inside the tubes [30, 31]. Similarly to BHA, a robot, having two sections and named Robotino® XT (Figure 1.6) was designed by the same company. This robot is able to handle easy-to-deform objects [32].

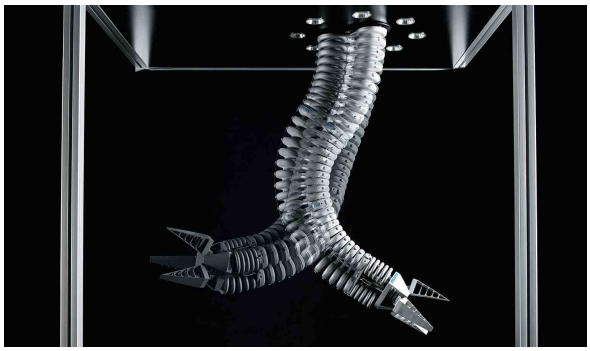

Figure. 1.5: BHA Robot.

Figure. 1.6: Robotino® XT Robot.

Since pneumatic actuator provide robots with much more energy to handle heavy objects, artificial pneumatic muscles were also adopted to design OctArm robots (Figure 1.7) by M. D. Grissom, I. D. Walker, where they built up an OctArm V robot consisting of three sections [33] and an OctArm IV robot with four sections [34], where each section contains three pneumatic muscles. OctArm robots are characterized by their force and flexible nature because it does not contain rigid links and elements in their structures. However, the thing that prevented working on them is their high response time than other designs.

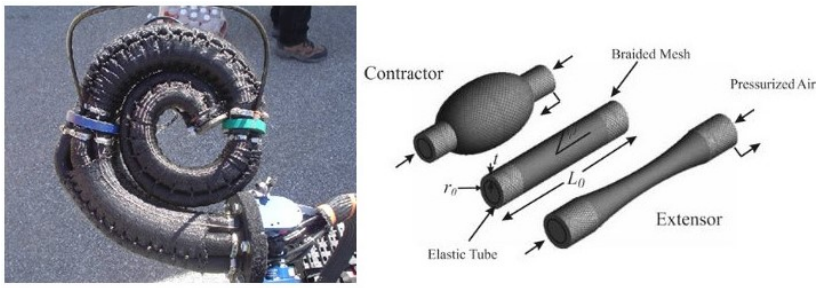

Figure. 1.7: (left) OctArm V robot ;(right) Muscle configuration [33]

In 2005, a robot that relies on air pressure and driven cables at the same time, named Air-Octor was created by I. D. Walker [35]. This robot contains two sections and each section has three degrees of freedom, where its curvature is controlled by cables that are extended and contracted by compressing the air inside the backbone. The backbone of air-octor robot contains a pneumatically pressurized chamber, which allows to extend its length up to 95 cm. It is very difficult to control it due to the combination of cables and pneumatic actuators. The simultaneous existing of cables and pneumatic actuation leads to air leakage, making it unusable in fields that require accuracy and efficiency in positioning. A new design for a hyper-redundant elephant trunk-like robot (Figure 1.8), was also developed by O. Salomon and A Wolf in 2012, consisting of 16 DoF and capable of bending 180°, with a length of about 80 cm and a diameter of about 7.7 cm [36]. Its great endurance, rigidity and high accuracy make it compatible with operations that require precision and dexterity.

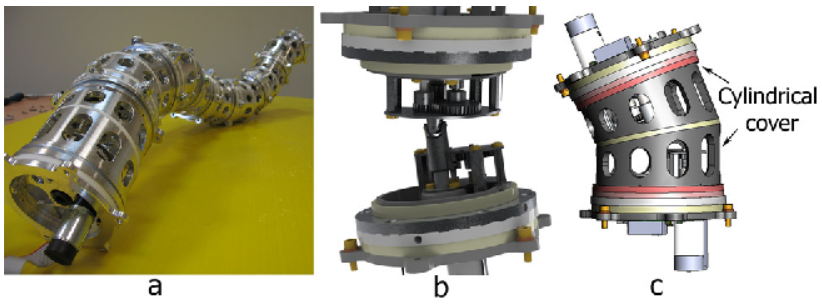

Figure. 1.8: (Left) Hyper- redundant elephant trunk; (Right) One section from the robot [36]

The octopus is an interesting model for the development of soft and continuum robots due to its high ability to deform and bend in all directions, it has distinctive muscular structure named muscular hydrostat. In 2009, an octopus arm-like robot was proposed by Laschi [37] that can expand, contract and bend in all directions due to a

group of longitudinal and transverse artificial muscles. To control the longitudinal and transverse muscles of a two-section continuum robot with eight DoF, artificial muscles powered by compressed air were adopted by Guglielmino and his group in 2010 [38]. This robot, also showed the ability to change its muscular diameter, which allows it to pass through small spaces yet the problem of this type of pneumatic arm robots is their weakness in terms of power capacity. In 2012, a robot that simulates the octopus arm was proposed by same researchers (Figure 1.9) [39], which has a remarkable ability to deal with rigid objects due to its rigidity compared to others, where its bending is controlled by a set of cables.

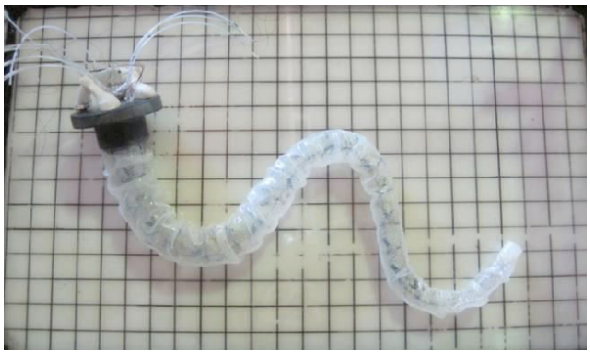

Figure. 1.9: Octopus-like robotic arm [39].

Always in the same context of robots that mimic the octopus arms, M.Sfakiotakis and his group were able, in 2013, to develop a robot that completely look like an octopus as shown in Figure 1.10. It has the ability to paddle under water at a speed of about 0.2 from its body length per second [40]. Then, in 2015, an octopus model, having high deformation named OCTOPUS robot, was developed by M.Cianchetti [41]. This robot contains eight arms, the front ones are used to hold things and elongate, while the rear ones are used to push the robot to move forward.

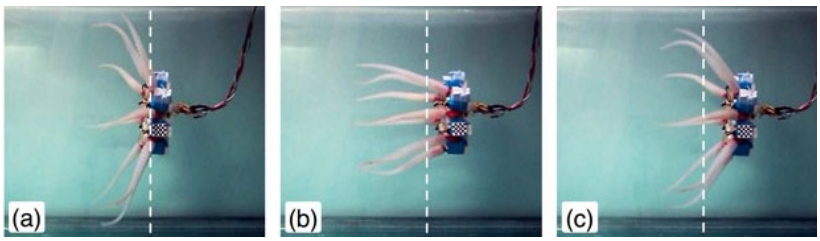

Figure. 1.10: Octopus-inspired swimming robot [40].

Snakes are perhaps the most prominent models that can be adopted in the design of continuum robots for their ability to move and navigate in narrow and curved spaces.

That is why this type of robot has been widely used, especially in the surgical fields. Their benefits reside in reducing pain and treatment time during medical surgeries. Especially, in the case of the surgeries where the robot has to go through tiny and tight spaces using endoscopic cameras as shown in Figure 1.11, it can also roll and rotate in all directions [42].

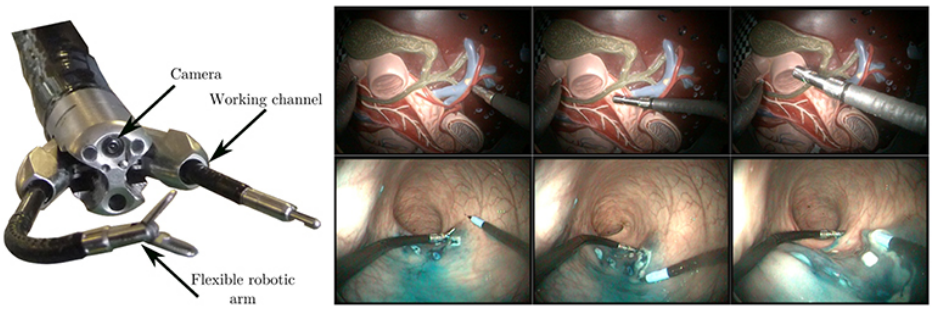

Figure. 1.11: Continuum robot using in minimally invasive surgery [43].

In the past decade, several manipulators such as snakes have been designed to be used in medical applications, which is an important advance in this field. The colonoscopy is a very important medical tool for diagnosing various diseases, but despite its importance, it causes a lot of pain and inconvenience to the patient due to the friction caused by manual guidance inside the human body. Therefore, a snake-like colonoscopy (Figure 1.12) was developed in 2009 by Haiyan Hu and his group to reduce patient inconvenience. This robot, has a flexible structure bending over a length of 600 mm and a diameter of about 12 mm, it has 5 sections with 10 DoF and guided by two DC motors through cables [44].

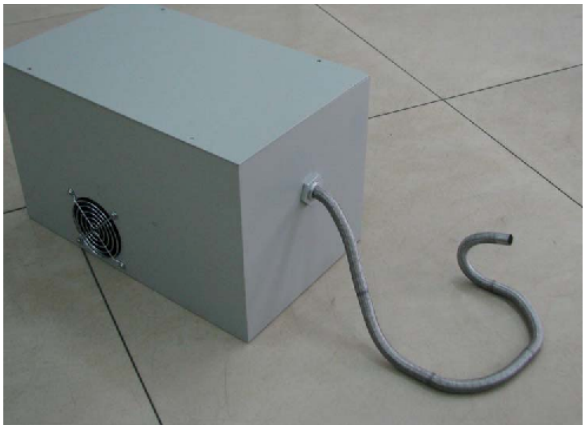

Figure. 1.12: The colonoscopy continuum robot [44].

Minimally invasive surgery is one of the most successful applications of surgical robotics. That is why many models have been proposed and designed to do this type of application, where a continuum robot was designed to perform minimally invasive surgeries by Bo Ouyang in 2016 (Figure 1.13). This robot, consists of three parts and a set of disks along the spine made of super-flexible nitinol and guided by four tendons [45]. In order to reduce the size of these robots and increase their rigidity that is necessary for minimally invasive surgery, some improvements have been added to the structure of these robots by adding a shoulder joint and an elbow joint with gear articulated configuration and a wrist joint with continuum configuration. These improvements (Figure 1.14) were done by Teng Wang in the year 2020 [46].

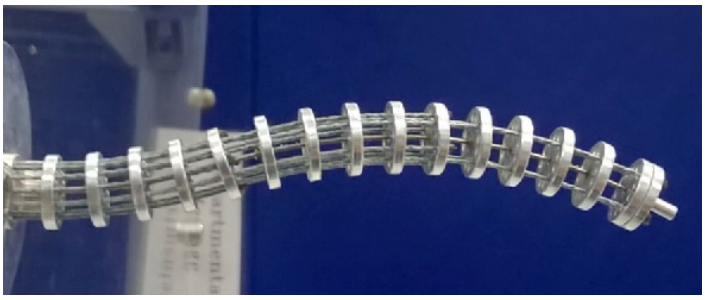

Figure. 1.13: Three-segment continuum robot prototype developed by Bo Ouyang [45].

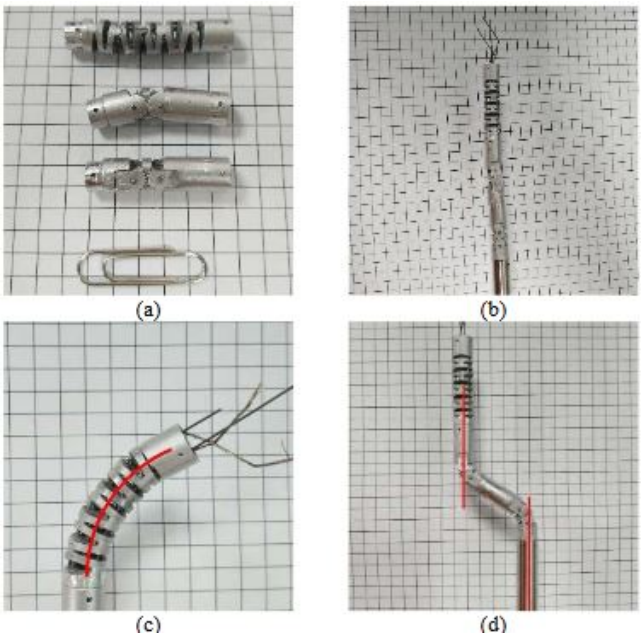

Figure. 1.14: Prototype of the designed snake-like surgical robot by Teng Weng. (a) shoulder, elbow and wrist joint (b) prototype of the assembled robot arm (c) bending of the continuum wrist (d) parallel lateral movement of the shoulder-elbow joint [46].

Recently, by adopting several highly flexible backbones as driven cables for actuation, Nabil Simaan and his team were able to create continuum robots capable of providing satisfactory accuracy and skill in several other surgical operations [47–51] such as cystectomy, throat surgery, surgical suturing, and knot tying (Figures 1.15,1.16).

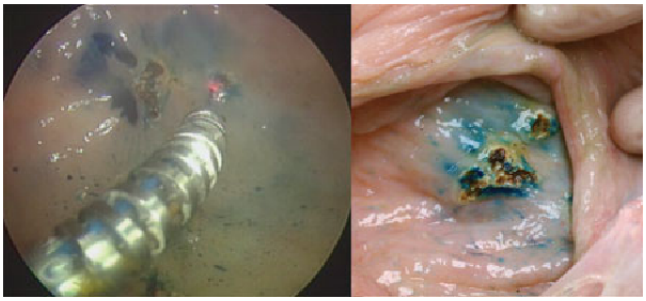

Figure. 1.15: Cystectomy using multi-backbone continuum robot [48].

Figure. 1.16: Suturing and knot tying using a multi-backbone continuum robot.

Although the majority of snake-like robots that have been adopted in the medical fields are cable-driven robots, a group of other structures has been relied on active channels as a backbone formed from a group of pre-curved tubes as shown in Figure 1.17. which depends on the energy that is produced by the stored flexibility in tubes. This type of robot, is characterized by its very small diameter, which is approximately 0.8 mm, allowing the robot to freely navigate and reduce the unwanted collisions against tissues yet its disadvantage appear in its limited curvature and rigidity [52].

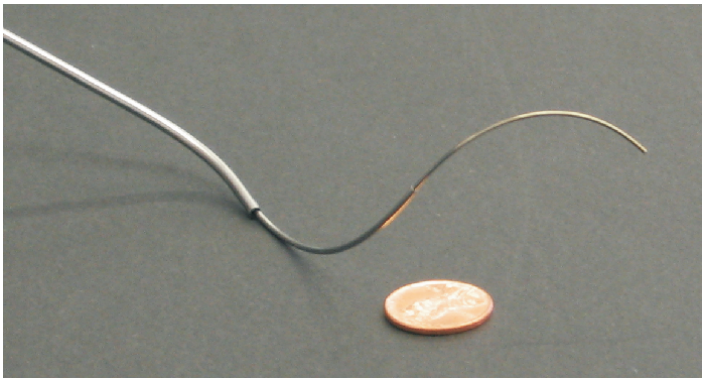

Figure. 1.17: Surgical robot made of active cannulas tube [52].

Despite the ingenuity of these types of robots, they may remain incapable to work on blood vessels due to many limitations related to the inability to penetrate inside these tiny vessels. To address these limitations, the so-called ferromagnetic soft continuum robots have emerged. They rely on flexible fibers in their structure and permanent magnets or magnetic particles that can be remotely controlled [53]. Figure 1.18 shows the ingenuity and ability to guide these magnetic robots inside blood vessels.

Figure. 1.18: Ferromagnetic soft continuum robots inside blood vessels [53].

Snake-like robots are not exclusively limited to medical fields. In fact, some companies that depend on these robots have appeared in other fields, especially in applications that require mobility and exploration in their spaces. The robots developed by OC Robotics company to explore and inspect the engineering parts and components (Figure 1.19), such as engines and aircraft, are an example of these robots . The actuation of their curvature is based on the cables and a mobile platform.

Figure. 1.19: Snake Arm Robots Developed by OC Robotics.

1.2.2 Classification principle

Continuum robots can be generally classified according to the type of their skeleton (backbone). Indeed, they are classified as single or multiple backbone (flexible backbone) robots. Single backbone robots (Figure 1.16) have a central structure that supports the passage of the actuation system along the manipulator body [10]. Many single skeleton robots have cables along their structure, which are equidistant by the disks attached to the skeleton as a means of transmission. The ends of the cables define the length of the section. Another classification of continuum robots is based on the actuation that can be intrinsic, extrinsic or hybrid. According to classification given by Figure 1.20, when the actuation system is integrated into the structure of the continuum robots and the force is applied directly to the spine, it is called intrinsic actuation system. The BHA manipulator (Figure 1.5) is a pneumatically operated intrinsic robot. Extrinsic actuation is defined as actuation that applies torque and force to the robot spine from outside the robot structure. Hybrid actuation has both intrinsic and extrinsic actuation. Typically, the central cavity of extrinsically actuated robots is operated by an actively controlled actuator. Many models of hybrid-actuated robots have pneumatic actuation [54, 55].

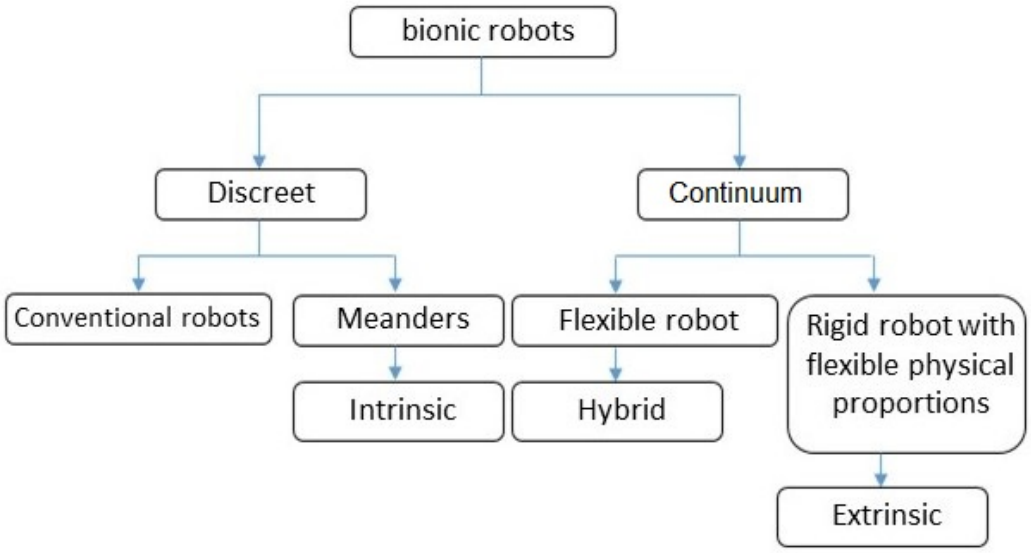

Figure. 1.20: Continuum robots types [56]

1.3 Modeling and control approaches

Unlike traditional robots with rigid and finite links, whose behavior has been fully understood and studied, continuum robots still suffer from many impediments in particular when it comes to modeling [57, 58] and control [59]. This is due to the diversity of their characteristics and methods of operation, as reported in section 1.2.1. These variations led to the lack of generalized models and approaches, hindering the development of modeling and control techniques, and provokes scientific competition between researchers. Moreover, there are increasing difficulties due to these robots' lack of rigidity and complex mechanical behavior. Despite these obstacles that faced the research community in the kinematic, dynamic modeling of continuum robots and their control, several concepts and contributions have been proposed, especially in kinematic modeling, which can be classified into: qualitative approaches aiming at learning the problem by using learning algorithms, quantitative approaches which are based on analytical methods and seek to find a direct mathematical relationship between inputs and outputs of the system, and hybrid approaches that depend on qualitative and quantitative approaches.

1.3.1 Forward kinematic model

Kinematic modeling is an essential step for a successful control of robots, because it describes the robots' poses, their cartesian coordinates, their positions, and the velocities of their links, as well as their geometric models. It also defines the relationship between the configuration and task spaces. Continuum robots usually include non-rigid links, which makes their sections completely deformable when controlling their rotating or prismatic joints, making their modeling very complex. Several kinematic models of different continuum robots have been developed in the literature. As far as the forward kinematic models, researchers relied on quantitative approaches that require good knowledge of the robot's kinematic behavior. The cosserat rod theory which is based on the model calculation without specific assumptions has been pursued, through which more accuracy to describe the movement of the robot can be achieved. It depends on solving a set of balance equations between the internal force, position, orientation and internal torque of the robot [58]. Despite the advantages of this approach, it suffers from significant disadvantages, as it contains a system of partial differential equations [60], which leads to the complexity of the model and makes it require great computational power. Whereas, the so-called rigid-links model, adopted by [61, 62], is based on dividing the curvature of the robot into several sections that act as solid links. This division allows simplifying the model and ease the adoption of methods based on rigid robots and enables the calculation of dynamic models [63]. Although, this approach considers an important assumption that leads to behaviors which are far from reality and leads to a lack of accuracy when dealing with obstacle avoidance. Perhaps, the modeling assuming constant curvature which depends on the arc geometry, is the most widely used method for extracting forward kinematic models for most continuum robots, because of its interesting advantages [57, 64–76]. Static curvature models have made it possible for researchers to remove many computational complexities compared to cosserat rod models, which makes them amenable to finding analytical solutions related to dynamic models and real-time control applications [64, 69, 70]. In order to simulate the accuracy of the behavior of real robots and cover its workspace , the idea of variable curvature is proposed, which is based on dividing each section of the robot into several other parts that have constant curvature [31]. Variable curvature idea theoretically gives the robot greater flexibility. This methodology has been simplified by suggesting a relationship between each section' parts separately [77], it facilitates the mission of adopting the variable curvature when integrating it in dynamic models and reducing the time of complex calculations that are necessary to obtain the control signals.

1.3.2 Inverse kinematic model

Inverse kinematic models are no less important than other models. By using these models, the robot is manipulated according to the desired paths, in its workspace, through the cartesian coordinates of the robot's end effector. Inverse kinematic modeling is one of the most difficult problems to be dealt with in continuum robotics research. Basically speaking, the inverse kinematic model can be figured out using analytical methods by calculating the inverse Jacobian matrix of the robot, but in most cases when it comes to infinite degrees of freedom of the robot that leads to infinite solutions (redundancy) and the analytical methods become impossible to be used. In quantitative approaches, some researchers have suggested analytical methods to overcome the inverse models. In the work developed by [78] the generation of the robot's workspace has been replaced by the egg curve to simplify the problem in terms of computational complexity and convergence speed. Egg curve approach theoretically showed no problems towards singularities . An analytical IKM for a continuum robot was developed using interval analysis by [79]. This technique has the advantage of dealing with the uncertainties that encounter the system and can also be adopted in the control operations. By adopting D-H techniques and the Closed-Loop Inverse Kinematic motion (CLIK) algorithm some researchers have solved the inverse models of these robots [80]. Based on the FKM and by adopting two quantitative approaches based on Newton Raphson iterative method and damped least square method, the IKM of CBHA robot has been solved [81]. Despite the multiplicity of quantitative approaches, they remain far from what is required because of the multiple assumptions about them, which negatively affects their accuracy and efficiency. In contrast to quantitative approaches, qualitative approaches are considered the most reliable method in deriving inverse kinematic models, as many researchers relied on optimization algorithms (PSO, GA) through which the FKM is mainly adopted. Then formulating the distance between the robot's end-effector and the position on the prescribed trajectory as an objective function. [82–85]. By the same approach and based on a Sequential Quadratic Program (SQP) the robot is considered as a series of vertebrae along the backbone, the inverse kinematic model of the CBHA robot was derived [86]. Despite the accuracy of the developed optimization-based models, they suffer from the problem of time consumption, especially when it comes to real-time control operations. Therefore, some researchers have resorted to adopting neural networks which rely on obtaining a neural function that links between inputs outputs of the system. Approximate inverse kinematic model based on multi-layer neural networks and Radial Basis Function (RBF) neural networks was developed [87]. By adopting an

approach that solely relies on the sampling method and without prior knowledge of the system, a supervised learning inverse kinematic solutions are learned in order to develop the inverse kinematic model of the robot [88, 89]. Some researchers have also resorted to adopting hybrid approaches that combine the advantages of quantitative and qualitative approaches to develop more accurate inverse kinematics models for continuum robots [90]. In fact, these works have been developed depending on the constant curvature hypothesis of the kinematic model due to its simplicity compared to variable curvature. Very few works have been developed dealing with IKMs with variable curvature. In [88], finding out the global solution through supervised learning and the Forward And Backward Reaching Inverse Kinematic (FABRIK) algorithm [91] were applied to solve the IKM. In [92], kepler oval was implemented to solve the IKM of inextensible continuum robot. It starts by identifying the workspace of the robot, then it formulates the IKM through a binary equation, which consists of the oval equations. The particle swarm optimization algorithm and neural networks were adopted to solve the inverse kinematic models of continuum robots with variable curvature in [77, 93] respectively.

1.3.3 Dynamic modeling

In contrast to the kinematic modeling of robots, dynamic modeling remains an active field for research. Several methods and theories have been adopted in order to derive the dynamic models of continuum robots, such as the Kane theory or the so-called virtual-power principle was adopted to develop a dynamic model for a continuum robot, taking into account the curvature along the robot, by adopting a set of kinematic variables [94]. With the same principle, a model of a continuum underwater robot was calculated, taking into account the hydrodynamics and physical constraints, which make the model adaptable to various environments [95]. This theory has also been adopted in several other works [96]. Based on the Euler–Lagrange method, which depends on the kinematic and potential energies of the system, several dynamic models were derived [67, 97–103], where all external forces were taken into account, including the friction forces of cables with disks as in [104]. Considering the robot as a composite material by applying a modified non-linear material model from Kelvin-Voigt to embody the hyper viscosity dynamics of the robot, the same Lagrange approach was used in [105] to extract the dynamic model of a continuum robot. Several other researchers have also taken different other methods to derive the dynamic models of continuum robots, among which we mention the Newton-Euler method [106, 107] and the classical cosserat series and the rod method [21, 58, 108, 109].

1.3.4 Control approaches

Broadly speaking, very few researchers were interested in the control of continuum robots. Control of continuum robots can be made through qualitative as well as quantitative approaches. For the development of control algorithms that depend on the robots model, it is necessary to have a good knowledge of the kinematic models, especially the inverse ones. Several methods based on the sliding mode control, that it is capable of dealing with non-linear systems under uncertainties, were developed [110–114]. A modified sliding function and fuzzy inference engine were used to solve the problem of chattering phenomenon and nonlinear equivalent dynamic formulation problem in the uncertain system, which is applied to the control unit, making it more robust than conventional sliding mode controller and simple fuzzy sliding mode controller [112]. The same control approach was also adopted on a model free of assumptions that is derived from the Cosserat-Rod theory and avoiding costly calculations by adopting a numerical method known as the general α-method. On the other hand, methods based on learning and adaptation have been considered, these methods depend on collecting data from the system without taking into account the complexity resulting from the models. The adaptive approach based on the Kalman filter given in [115], which depends only on two steps, gives accurate control in real-time. A control algorithm with two sub-controllers was proposed, The first sub-controller, based on the distal supervised learning scheme, deals with the stationary CBHA's behaviors; whereas the second based on adaptive control handles non-stationary behaviors [116]. Several models based on learning were also proposed that had a role in the development of other controllers [117–120].

1.4 Conclusion

In this chapter, a detailed literature overview on design, modeling and control of continuum bionic robots has been given. In the first part, the most prominent types of flexible robots developed by researchers were introduced. In the second part, methods of kinematic and dynamic modeling of this type of robots were thoroughly presented. Finally, some control approaches that have been applied on continuum robots were discussed.

This literature study allowed us to know the various methods and methodologies for dealing with continuous robots, and identify the obstacles and problems facing the development of these robots in terms of their design, modeling, and control.

CHAPTER 2

FORWARD KINEMATIC MODELING

2.1 Introduction

The forward kinematic model is the set of relationships that allow finding the position of the robot end-effector according to the operating coordinates; unlike rigid robots, the variables that express the configuration of a flexible robot change with respect to the robot's morphology and its type of actuation. For this reason, research on the modeling of flexible continuum robots investigates other means to develop exhaustive kinematic models taking into account maximum of specificities and mechanical properties of the studied robot. To this end, the main objective of this chapter is to establish the forward kinematic model of a flexible continuum robot with variable and constant curvature. First, a general description of the continuum robots is presented by defining the parameters and variables. After that, the forward kinematic modeling problem is formulated and explained. Finally, the workspace is graphically presented based on the established forward kinematic model of continuum robots with both (VC) and (CC) as well as a case study of a variable-length continuum robot with CC.

2.2 Geometric description of cable-driven continuum robot

A cable-driven continuum robot is one of the most commonly used types. Cable-driven continuum robots consist of a flexible backbone with disks that are separated from each other by the same distance, and attached to the backbone.

In most of these robots, the cable is considered as a straight or smooth helical curve. The cables pass through holes that are located on the disks to guide the robot and make it bend to the desired position.

2.2.1 Geometry of the whole profile of the considered robot

Developing a thorough description of the behavior and the morphology of continuum robots are the first major step that is needed to derive precise kinematic models, which themselves help to simulate the movements and the behavior of these robots. Therefore, several models have been proposed by researchers for the geometric description of continuum robots assuming constant curvature [57, 68, 79, 121] and variable curvature [31, 77].

The kinematics description of the variable curvature continuum robot depicted in Figure 2.1 is briefly presented, whose profile is similar to a backbone curve. This complex structure has two conically shaped sections. Each section k is mounted at the base of its first conical unit, while the remaining conical units are sequentially stacked on top. Each section has two degrees of freedom, a bending angle ($\theta_{j,k}$) and an orientation angle ($\varphi_{j,k}$) actuated by three independent cables.

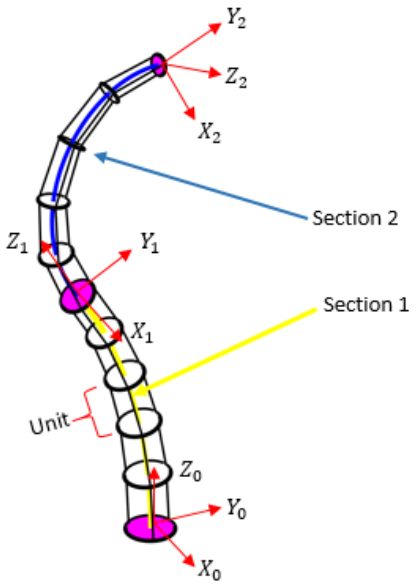

Figure. 2.1: Two-section continuum robot with its coordinate frames for each section k

To have a simplified description of the continuum robot under consideration, the profile of the whole section is assimilated into a curve formed by a serial concatenation of circular arcs, (Figure 2.2) which represents the robot central axis [85].

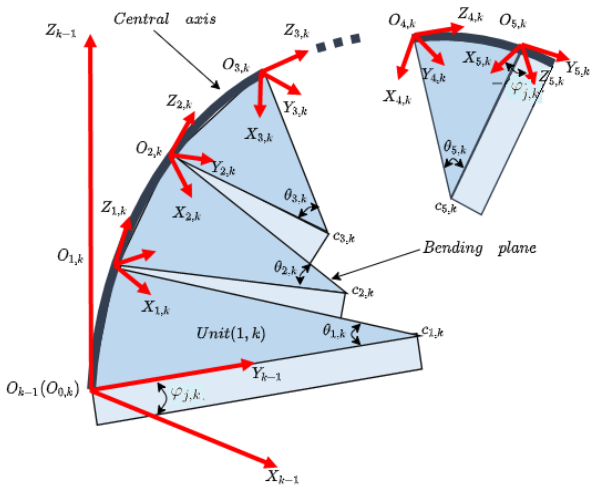

Figure. 2.2: Frames placements on the central axis for each unit

A detailed illustration of a conical shape unit showing arc parameters and geometric properties is discussed in the following.

2.2.2 the Geometry of a unit

Grasping the geometry of a single conical unit paves the way to understanding the remaining units that constitute the backbone of the robot. Each unit consists of two platforms (Figure 2.3), which can be virtual as in the case of CBHA or real as in our case.

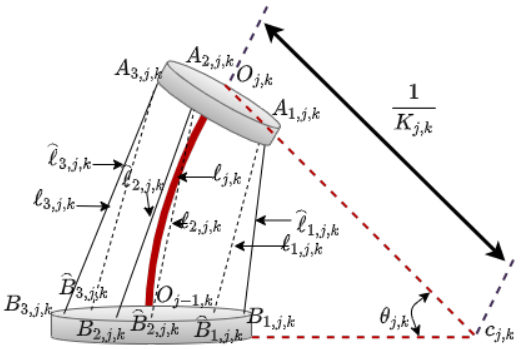

Figure. 2.3: Description of a conical and cylindrical unit and its cables

In the general case, the base of the unit is fixed and the upper part is mobile. They are connected by three segments.

For constant curvature continuum robot, each unit of the robot has a lower and an upper disk which have the same diameters (cylindrical shaped unit) and connected through the points $A_{i,j,k}$ and $\widehat{B}_{i,j,k}$. For variable curvature continuum robot, each unit has two disks with different diameters (conical shaped unit) and connected through $B_{i,j,k}$ and $A_{i,j,k}$ $(i = 1, 2, 3)$. Interestingly, the differentiation of the disks' diameters paves the way to establishing an equation which relates the units with each other as it is explained in detail in [77].

The length of cable that connects the disks of a cylindrical unit is denoted by $\ell_{i,j,k}$ and the length of cable that connects the disks of a conical unit is denoted by $\hat{\ell}_{i,j,k}$. Each cylindrical unit is parameterized by its orientation angle $\varphi_{j,k}$, its bending angle $\theta_{j,k}$, and its curvature $\kappa_{j,k}$.

2.2.3 The attached frames on the robot's backbone

In this section, we define the different frames that must be attached to the general geometry of a flexible robot. First, the center of the upper platform of each section k is referenced by a frame named R_k. Then, a frame R_O is fixed at the base of the first section as shown in Figure 2.4.

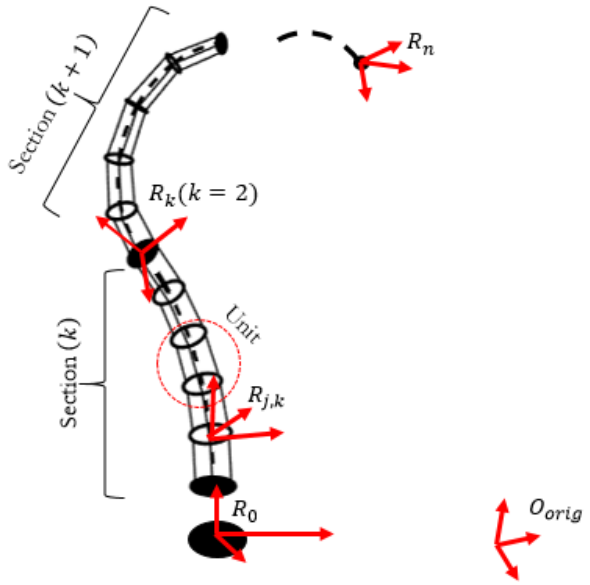

Figure. 2.4: Placement of frames on the structure of a flexible manipulator

In order to calculate the FKM of each unit constituting the robot, an intermediate reference frame $R_{j,k}$ is assigned to the center of the platform of each unit (j,k).

The description of a flexible section from its base to its end is as follows: the indices of the units j increase from 1 to m, and for each intermediate platform (j,k), the distance between the central axis and the anchor points is noted $r_{j,k}$ (Figure 2.3). The unit (j,k), is modeled as an inextensible arc of a circle. This unit has one end fixed at the origin of the reference frame $O_{j-1,k}$, the other end $O_{j,k}$ is located at a point in the reachable workspace as shown in Figure 2.3.

2.3 Modeling assumptions

Before starting the modeling of the considered robot, it is necessary to point out the different used assumptions, on which the mathematical development throughout this work is based. The previously developed work to model the central axis of flexible continuum robots is based on the constant curvature [73], which considers the deformation of the robot sections as a circular arc. The researchers purposefully used it because it facilitates the calculation of kinematic models. However, the constant curvature does not show a better imitation of the central axis of the continuum robot. For this reason, recent research has opened new doors to modeling the central axis of the continuum robot, which describe in detail the deformation of each unit of the robot as an arc of a circle, typically called variable curvature [31].

The assumptions considered for modeling variable curvature along this thesis can be summarized as follows [77]:

- The flexible continuum robot is described as an open kinematic chain of n sections.
- Each section is a set of conically equidistant units.
- Each conical shape unit is modeled as an inextensible circular arc having its individual parameters.
- The cable lengths are homogeneously fragmented along the robot.
- Robot deformations at sections and units are done without torsion (neglected torsion).

In the last section, a particular case is taken into account where the robot's backbone can be extensible

2.4 Forward kinematic model

The forward kinematic model consists of calculating the position and the orientation of the flexible continuum robot's end-effector as a function of the cable lengths. The FKM for the considered robot in this work can be derived in three steps:

- The FKM of a conical shape single unit.
- The FKM of a single section.
- The FKM of a multi-section flexible continuum robot.

2.4.1 FKM of a single conically shaped unit

As shown in Figure 2.3, an elaborate description of the conical and cylindrical shape of the flexible continuum robot is described.

Overall, the FKM of a conical shape unit consists of representing the operational coordinates $X_{j,k}$ as a function of the length of the cables $\widehat{Q}_{j,k}$ through the arc parameters $K_{j,k}$, and which is obtained by two transformations, the first is the specific transformation and the second is the independent one. Both transformations will be discussed in detail in the rest of this chapter.

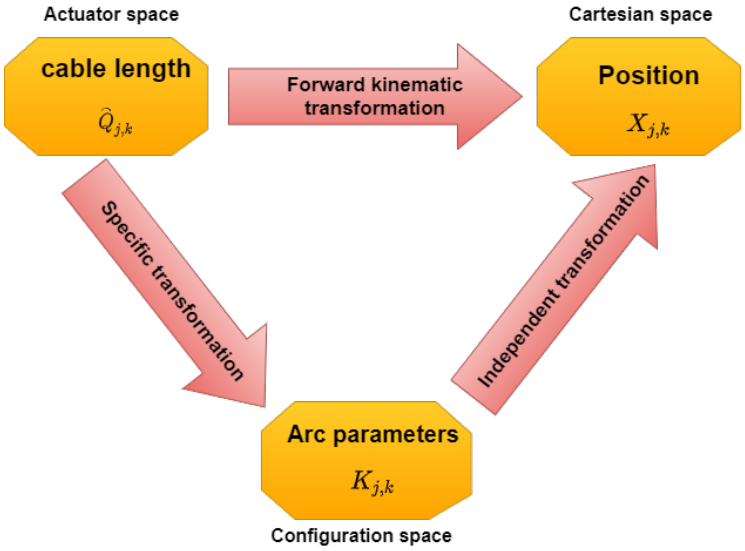

Figure. 2.5: Global view of the modeling

Assuming that each unit deforms in the form of an arc. The geometric parameters of each unit can be illustrated in a three-dimensional frame as follows:

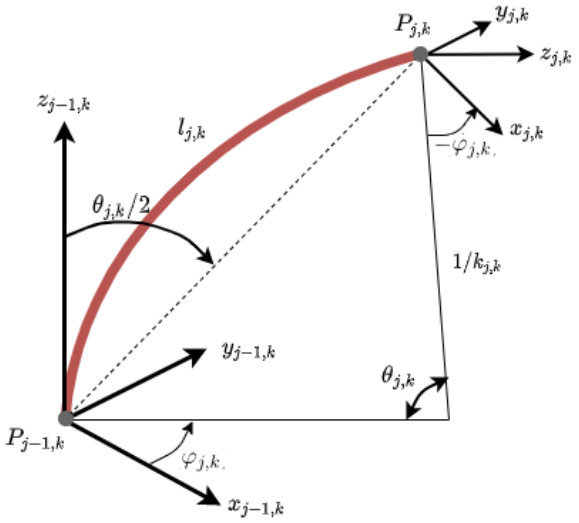

Figure. 2.6: The geometric parameters of a circle arc in 3D space

The homogeneous transformation can be written by the following equation [57] :

$$T_{j,k}^{j-1,k} = \begin{bmatrix} R_{j,k}^{j-1,k} & O_{j,k}^{j-1,k} \\ 0_{1\times 3} & 1 \end{bmatrix} \tag{2.1}$$

with $R_{j,k}^{j-1,k}$ and $O_{j,k}^{j-1,k}$ are respectively the (3×3) matrix and the (3×1) vector defining the orientation and the position of the reference frame origin $R_{j,k}$ in the reference frame $R_{j-1,k}$.

Based on the previously defined assumptions, the orientation matrix $R_{j,k}^{j-1,k}$ is given by the following equation [68]:

$R_{j,k}^{j-1,k} = rot\left(Z_{j-1,k}, \varphi_{j,k}\right) rot\left(Y_{j-1,k}, \theta_{j,k}\right) rot(Z_{j-1,k}, -\varphi_{j,k})$

$$= \begin{bmatrix} c^2\varphi_{j,k}c\theta_{j,k} + s^2\varphi_{j,k} & c\varphi_{j,k}c\theta_{j,k}s\varphi_{j,k} - c\varphi_{j,k}s\varphi_{j,k} & c\varphi_k s\theta_{j,k} \\ c\varphi_{j,k}c\theta_{j,k}s\varphi_{j,k} - c\varphi_{j,k}s\varphi_{j,k} & s^2\varphi_{j,k}c\theta_{j,k} + c^2\varphi_{j,k} & s\varphi_{j,k}s\theta_{j,k} \\ -c\varphi_{j,k}s\theta_{j,k} & -s\varphi_{j,k}s\theta_{j,k} & c\theta_{j,k} \end{bmatrix} \tag{2.2}$$

with : $c. = \cos(.)$ and $s. = \sin(.)$

The position vector is defined as follows:

$$O_{j,k}^{j-1,k} = \begin{cases} \frac{l_{j,k}}{\theta_{j,k}}\left(1 - \cos\left(\theta_{j,k}\right)\right)\cos\left(\varphi_{j,k}\right) \\ \frac{l_{j,k}}{\theta_{j,k}}\left(1 - \cos\left(\theta_{j,k}\right)\right)\sin\left(\varphi_{j,k}\right) \\ \frac{l_{j,k}}{\theta_{j,k}}\sin\left(\varphi_{j,k}\right) \end{cases} \tag{2.3}$$

2.4.1.1 Specific transformation

In order to show the length of the cables in the orientation matrix, a specific transformation is established. It expresses the length of the cables $\ell_{i,j,k}$, of each unit (j,k) as a function of the arc parameters which are the orientation angle $\varphi_{j,k}$, the bending angle $\theta_{j,k}$ $[rad]$ and its curvature $\kappa_{j,k}$ $[1/mm]$. First, the orientation angle $\varphi_{j,k}$ must be calculated.

As the diameter of each disk is calculated by a general equation that allows determining each of them as follows[77]:

$$r_{j,k} = r_{\max,k} - \frac{j}{k}\left(r_{\max,k} - r_{\min,k}\right) \tag{2.4}$$

with $r_{\max,k}$ and $r_{\min,k}$ are, respectively, the maximum and the minimum radius of the section k. When the orientation angle is equal to 0, the central axis of the unit takes the shape of a circular arc with the center $\left[d_{j,k},0,0\right]^T$.

Similarly, the points $A_{i,j,k}$ and $B_{i,j,k}$ where the cables are attached takes a place in an arc of circle of center $\left[d_{i,j,k},0,0\right]^T$. Based on these results, we can obtain the following equation:

$$l_{j,k}[mm] = \theta_{j,k} d_{j,k} = \frac{\theta_{j,k}}{\kappa_{j,k}} \tag{2.5}$$

The different curvature radii of the unit can be described by the equation (2.6) based on Figure 2.7, where $d_{j,k}$ is the radius of curvature of the unit (j,k) and $d_{i,j,k}$ is the radius of curvature for each cable.

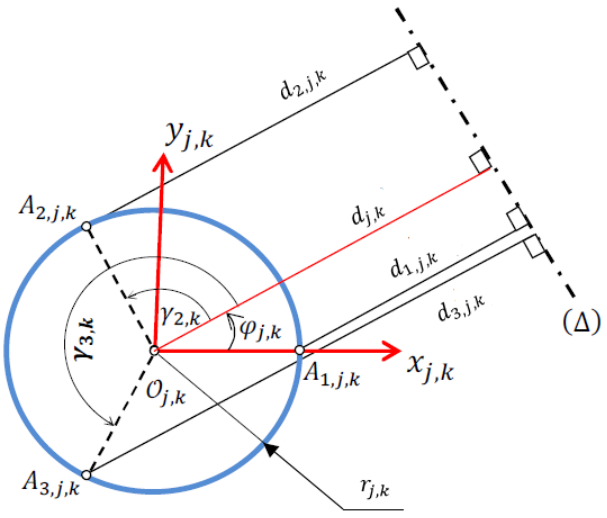

Figure. 2.7: Definition of the different curvature radii of the unit (j,k)

In addition, there is a relationship between the angle $\varphi_{j,k}$ and $\gamma_{i,k}$ $(i = 1, 2, 3)$. with $\gamma_{1,k} = -\varphi_{j,k}, \gamma_{2,k} = \frac{2\pi}{3} - \varphi_{j,k}, \gamma_{3,k} = -\frac{2\pi}{3} - \varphi_{j,k}$. Through the Figure 2.7, the radius of curvature can be expressed as follows:

$$\begin{cases} d_{1,j,k} = d_{j,k} - r_{j,k}\cos\left(\gamma_{1,k}\right) \\ d_{2,j,k} = d_{j,k} - r_{j,k}\cos\left(\gamma_{2,k}\right) \\ d_{3,j,k} = d_{j,k} - r_{j,k}\cos\left(\gamma_{3,k}\right) \end{cases} \tag{2.6}$$

Based the equation (2.5) and by multiply the three values of the equation (2.6) by $\theta_{j,k}$, we can obtain the following equation:

$$\begin{cases} \ell_{1,j,k} = l_{j,k} - r_{j,k}\theta_{j,k}\cos\left(\gamma_{1,k}\right) \\ \ell_{2,j,k} = l_{j,k} - r_{j,k}\theta_{j,k}\cos\left(\gamma_{2,k}\right) \\ \ell_{3,j,k} = l_{j,k} - r_{j,k}\theta_{j,k}\cos\left(\gamma_{3,k}\right) \end{cases} \tag{2.7}$$

According to equation (2.7), one way to get $\varphi_{j,k}$ out of this equation is to subtract member by member the second equation from the first equation and the third equation from the first equation as follows:

$$\begin{cases} \ell_{1,j,k} - \ell_{2,j,k} = r_{j,k}\theta_{j,k}\left(\cos\left(\gamma_{2,k}\right) - \cos\left(\gamma_{1,k}\right)\right) \\ \ell_{1,j,k} - \ell_{3,j,k} = r_{j,k}\theta_{j,k}\left(\cos\left(\gamma_{3,k}\right) - \cos\left(\gamma_{1,k}\right)\right) \end{cases} \tag{2.8}$$

By dividing the equations member by member (2.8), we obtain the following equation:

$$\frac{\ell_{1,j,k} - \ell_{2,j,k}}{\ell_{1,j,k} - \ell_{3,j,k}} = \frac{\left(\cos\left(\frac{2\pi}{3} - \varphi_{j,k}\right) - \cos\left(-\varphi_{j,k}\right)\right)}{\left(\cos\left(-\frac{2\pi}{3} - \varphi_{j,k}\right) - \cos\left(-\varphi_{j,k}\right)\right)} \tag{2.9}$$

After applying the trigonometric properties to equation (2.9) we find the following equality

$$\frac{\ell_{1,j,k} - \ell_{2,j,k}}{\ell_{1,j,k} - \ell_{3,j,k}} = \frac{\cos\left(\frac{2\pi}{3}\right)\cos\left(\varphi_{j,k}\right) + \sin\left(\frac{2\pi}{3}\right)\sin\left(\varphi_{j,k}\right) - \cos\left(-\varphi_{j,k}\right)}{\cos\left(-\frac{2\pi}{3}\right)\cos\left(\varphi_{j,k}\right) + \sin\left(-\frac{2\pi}{3}\right)\sin\left(\varphi_{j,k}\right) - \cos\left(-\varphi_{j,k}\right)} \tag{2.10}$$

After simplification the equation (2.10) becomes:

$$\frac{\ell_{1,j,k} - \ell_{2,j,k}}{\ell_{1,j,k} - \ell_{3,j,k}} = \frac{-\frac{1}{2}\cos\left(\varphi_{j,k}\right) + \frac{\sqrt{3}}{2}\sin\left(\varphi_{j,k}\right) - \cos\left(-\varphi_{j,k}\right)}{-\frac{1}{2}\cos\left(\varphi_{j,k}\right) - \frac{\sqrt{3}}{2}\sin\left(\varphi_{j,k}\right) - \cos\left(-\varphi_{j,k}\right)} \tag{2.11}$$

In the following, a detailed procedure for obtaining the arc parameters is established .

- 1^{st} simplification :
  $\frac{1}{2}\ell_{1,j,k}\cos\left(\varphi_{j,k}\right) - \frac{\sqrt{3}}{2}\ell_{1,j,k}\sin\left(\varphi_{j,k}\right) - \ell_{1,j,k}\cos\left(\varphi_{j,k}\right) + \frac{1}{2}\ell_{1,j,k}\cos\left(\varphi_{j,k}\right) + \frac{\sqrt{3}}{2}\ell_{2,j,k}\sin\left(\varphi_{j,k}\right) + \ell_{2,j,k}\cos\left(\varphi_{j,k}\right) = -\frac{1}{2}\ell_{1,j,k}\cos\left(\varphi_{j,k}\right) + \frac{\sqrt{3}}{2}\ell_{1,j,k}\sin\left(\varphi_{j,k}\right) - \ell_{1,j,k}\cos\left(\varphi_{j,k}\right) + \frac{1}{2}\ell_{3,j,k}\cos\left(\varphi_{j,k}\right) - \frac{\sqrt{3}}{2}\ell_{3,j,k}\sin\left(\varphi_{j,k}\right) + \ell_{3,j,k}\cos\left(\varphi_{j,k}\right)$
- 2^{nd} simplification :
  $-\sqrt{3}\ell_{1,j,k}\sin\left(\varphi_{j,k}\right) + \frac{1}{2}\ell_{2,j,k}\cos\left(\varphi_{j,k}\right) + \frac{\sqrt{3}}{2}\ell_{2,j,k}\sin\left(\varphi_{j,k}\right) + \ell_{2,j,k}\cos\left(\varphi_{j,k}\right) = \frac{1}{2}\ell_{3,j,k}\cos\left(\varphi_{j,k}\right) - \frac{\sqrt{3}}{2}\ell_{3,j,k}\sin\left(\varphi_{j,k}\right) + \ell_{3,j,k}\cos\left(\varphi_{j,k}\right)$
- 3^{rd} simplification :
  $-\sqrt{3}\ell_{1,j,k}\sin\left(\varphi_{j,k}\right) + \frac{3}{2}\ell_{2,j,k}\cos\left(\varphi_{j,k}\right) + \frac{\sqrt{3}}{2}\ell_{2,j,k}\sin\left(\varphi_{j,k}\right) = \frac{3}{2}\ell_{3,j,k}\cos\left(\varphi_{j,k}\right) - \frac{\sqrt{3}}{2}\ell_{3,j,k}\sin\left(\varphi_{j,k}\right)$
- 4^{th} simplification :
  $\frac{\sqrt{3}}{2}\left(-2\ell_{1,j,k} + \ell_{2,j,k} + \ell_{3,j,k}\right)\sin\left(\varphi_{j,k}\right) = \frac{3}{2}\left(\ell_{3,j,k} - \ell_{2,j,k}\right)\cos\left(\varphi_{j,k}\right)$
- 5^{th} simplification :
  $\frac{\sin(\varphi_{j,k})}{\cos(\varphi_{j,k})} = \frac{\sqrt{3}(\ell_{3,j,k} - \ell_{2,j,k})}{(-2\ell_{1,j,k} + \ell_{2,j,k} + \ell_{3,j,k})}$

Finally, we obtain following formula for the orientation angle:

$$\varphi_{j,k} = \tan^{-1}\left(\frac{\sqrt{3}\left(\ell_{3,j,k} - \ell_{2,j,k}\right)}{2\ell_{1,j,k} - \ell_{2,j,k} - \ell_{3,j,k}}\right) \tag{2.12}$$

After having determined the orientation angle, we calculate the radius of curvature using the previously mentioned equation (2.7) by summing the three members:

$$3l_{j,k} = \ell_{1,j,k} + \ell_{2,j,k} + \ell_{3,j,k} + r_{j,k}\theta_{j,k}\left(\cos\left(\gamma_{1,k}\right) + \cos\left(\gamma_{2,k}\right) + \cos\left(\gamma_{3,k}\right)\right) \tag{2.13}$$

Through Figure 2.7, we can write:

$$\sum_{i=1}^{3}\cos\left(\gamma_{i,k}\right) = 0 \tag{2.14}$$

This makes it possible to write:

$$l_{j,k} = \frac{\ell_{1,j,k} + \ell_{2,j,k} + \ell_{3,j,k}}{3} \tag{2.15}$$

Substituting the equation (2.5) and (2.15) into the equation (2.6), and after trigonometric simplifications, the formula of the curvature's radius can be expressed as follows:

$$d_{j,k} = \frac{1}{\kappa_{j,k}} = \frac{r_{j,k}\left(\ell_{1,j,k} + \ell_{2,j,k} + \ell_{3,j,k}\right)}{2\cdot\sqrt{\ell_{1,j,k}^2 + \ell_{2,j,k}^2 + \ell_{3,j,k}^2 - \ell_{1,j,k}\ell_{2,j,k} - \ell_{1,j,k}\ell_{3,j,k} - \ell_{2,j,k}\ell_{3,j,k}}} \tag{2.16}$$

The last parameter of the arc is the bending angle $\theta_{j,k}$, which can be calculated by substituting the equations (2.15) and (2.16) into (2.5), we then obtain:

$$\theta_{j,k} = \frac{2 \cdot \sqrt{\ell_{1,j,k}^2 + \ell_{2,j,k}^2 + \ell_{3,j,k}^2 - \ell_{1,j,k}\ell_{2,j,k} - \ell_{1,j,k}\ell_{3,j,k} - \ell_{2,j,k}\ell_{3,j,k}}}{3r_{j,k}} \tag{2.17}$$

Finally, the expressions for the arc of a circle can be summarized in the equation (2.18) :

$$\begin{cases} \varphi_{j,k} = \tan^{-1}\left(\frac{\sqrt{3}\left(\ell_{3,j,k} - \ell_{2,j,k}\right)}{2\ell_{1,j,k} - \ell_{2,j,k} - \ell_{3,j,k}}\right) \\ \theta_{j,k} = \frac{2 \cdot \sqrt{\ell_{1,j,k}^2 + \ell_{2,j,k}^2 + \ell_{3,j,k}^2 - \ell_{1,j,k}\ell_{2,j,k} - \ell_{1,j,k}\ell_{3,j,k} - \ell_{2,j,k}\ell_{3,j,k}}}{3r_{j,k}} \\ \kappa_{j,k} = \frac{2 \cdot \sqrt{\ell_{1,j,k}^2 + \ell_{2,j,k}^2 + \ell_{3,j,k}^2 - \ell_{1,j,k}\ell_{2,j,k} - \ell_{1,j,k}\ell_{3,j,k} - \ell_{2,j,k}\ell_{3,j,k}}}{r_{j,k}\left(\ell_{1,j,k} + \ell_{2,j,k} + \ell_{3,j,k}\right)} \end{cases} \tag{2.18}$$

Knowing that each unit has a conical shape, the equations (2.18) must be expressed in terms of the cable lengths $\widehat{\ell}_{i,j,k}$ instead of $\ell_{i,j,k}$. Therefore, according to the assumption mentioned before; each conical shape unit is modeled as an inextensible arc with its individual arc parameters and deforms at small angles, the relationship between these two cable lengths is given by the law of cosines [31]:

$$\widehat{\ell}^{\,2}_{i,j,k} = \ell_{i,j,k}^2 + \left(r_{j-1,k} - r_{j,k}\right)^2 - 2\ell_{i,j,k}\left(r_{j-1,k} - r_{j,k}\right)\cos\left(\beta_{i,j,k}\right) \tag{2.19}$$

with :

$$\cos\left(\beta_{i,j,k}\right) = \sin\left(\frac{\kappa_{j,k} l_{j,k}}{2}\right)\cos\left(\frac{2}{3}\pi\left(k-1\right) - \varphi_{j,k}\right)$$

After solving the equation (2.19), the cables length $\ell_{i,j,k}$ can be expressed as follows:

$$\begin{aligned} \ell_{i,j,k} = & \sqrt{\widehat{\ell}^{\,2}_{i,j,k} - \left(r_{j-1,k} - r_{j,k}\right)^2 + \left(r_{j-1,k} - r_{j,k}\right)^2 \cos^2\left(\beta_{i,j,k}\right)} \\ & + \left(r_{j-1,k} - r_{j,k}\right)\cos\left(\beta_{i,j,k}\right) \end{aligned} \tag{2.20}$$

According to equation (2.20), the length of the cable $\ell_{i,j,k}$ is in function of the cable lenghts $\widehat{\ell}_{i,j,k}$, the disks's radius $(r_{j-1,k} - r_{j,k})$ and the angle $\beta_{i,j,k}$. To find an approximate analytical solution between the lengths of the conical unit cable $\widehat{\ell}_{i,j,k}$ and the configuration state $\kappa_{j,k}$, the influence of $\beta_{i,j,k}$ on the lengths of the cylindrical unit cable according to equation (2.20) must be negligible. Since the unit's conical shape cannot be changed, angles $\beta_{i,j,k}$ close to $\frac{\pi}{2}$ are required. This can be achieved by choosing a high number of units, because the bending angle $\theta_{j,k}$ of the unit decreases

with an increasing number of units per section. In this case, the equation (2.20) simplifies to :

$$\ell_{i,j,k} = \sqrt{\widehat{\ell}^{\,2}_{i,j,k} - \left(r_{j-1,k} - r_{j,k}\right)^2} \tag{2.21}$$

2.4.1.2 Independent transformation

To express the cartesian coordinates $\left(x_{j,k}, y_{j,k}, z_{j,k}\right)$ in terms of the arc parameters, we substitute equation (2.18) into (2.3), the cartesian coordinates $\left(x_{j,k}, y_{j,k}, z_{j,k}\right)$ as a function of the cable lengths can be expressed as follows:

$$\begin{cases} x_{j,k} = \frac{r_{j,k}\left(\ell_{1,j,k}+\ell_{2,j,k}+\ell_{3,j,k}\right)}{M_{j,k}} \sin^2\left(\frac{M_{j,k}}{3r_{j,k}}\right) \cos\left(\tan^{-1}\left(\frac{\sqrt{3}\left(\ell_{3,j,k}-\ell_{2,j,k}\right)}{2\ell_{1,j,k}-\ell_{2,j,k}-\ell_{3,j,k}}\right)\right) \\ y_{j,k} = \frac{r_{j,k}\left(\ell_{1,j,k}+\ell_{2,j,k}+\ell_{3,j,k}\right)}{M_{j,k}} \sin^2\left(\frac{M_{j,k}}{3r_{j,k}}\right) \sin\left(\tan^{-1}\left(\frac{\sqrt{3}\left(\ell_{3,j,k}-\ell_{2,j,k}\right)}{2\ell_{1,j,k}-\ell_{2,j,k}-\ell_{3,j,k}}\right)\right) \\ z_{j,k} = \frac{r_{j,k}\left(\ell_{1,j,k}+\ell_{2,j,k}+\ell_{3,j,k}\right)}{2M_{j,k}} \sin\left(\frac{2M_{j,k}}{3r_{j,k}}\right) \end{cases} \tag{2.22}$$

with : $M_{j,k} = 2 \cdot \sqrt{\ell^2_{1,j,k} + \ell^2_{2,j,k} + \ell^2_{3,j,k} - \ell_{1,j,k}\ell_{2,j,k} - \ell_{1,j,k}\ell_{3,j,k} - \ell_{2,j,k}\ell_{3,j,k}}$

2.4.2 FKM of a conical section

As mentioned before, a section k is a concatenation of m units. Moreover, each section deforms without torsional effect, so we can have the forward kinematic model of a section by the multiplication of transformation matrices, which can be expressed by the following relation:

$$T^{k-1}_{k} = T^{0,k}_{m,k} = \prod_{j=1}^{m} T^{j-1,k}_{j,k} \tag{2.23}$$

where $T^{j-1,k}_{j,k}$ is the (4×4) matrix defining the orientation and position of the origin of the reference frame $R_{j,k}$ in the frame $R_{j-1,k}$.

The parameters used for the considered section of the continuum robot are indicated in the Table 2.1.

Table 2.1: Parameters of the two-section flexible continuum robot

	Section (k=1)	Section (k=2)	Description
m_k	5 units	5 units	Number of units per section
L_k	300 mm	300 mm	Total length of the section
$r_{\min,k}$	17.5 mm	10 mm	Radial cable distance
$r_{\max,k}$	25 mm	17.5 mm	Radial cable distance

Table 2.2: Discs radii for each section of the robot

The discs radii (mm)	Section 1	Section 2
r_1 (base disc)	25	17.5
r_2	23.5	16
r_3	22	14.5
r_4	20	13
r_5	19	11.5
r_6	17.5	10

For a VC continuum robot, an approximate formula is developed in [77], which allows to express the bending angle of the robot's units in function of the first bending angle of the first unit in the same section.The developed formula is expressed as follows [77]:

$$\theta_{j,k} = \frac{r_{1,k}}{r_{j,k}}\theta_{1,k} \tag{2.24}$$

As the number of units increases, the accuracy of the solutions of the equation (2.24) also increases, that is, when the angle β_i is closer to $\frac{\pi}{2}$ (Figure 2.3). Therefore, using equation (2.24), the forward kinematic model of a single section can only be expressed by two variables $\theta_{1,k}$ and φ_k. This approximation leads to a remarkable simplification and reduction of the number of variables involved in the FKM.

2.4.3 FKM of the multi-section conical robot

Based on the equation (2.24), the identification of the robot's end-effector posture becomes relatively simple because the different unit angles will be expressed in terms of the bending angle of the first unit. Thus the forward kinematic model for a multi-section continuum robot (see Figure 2.1) can be easily found by successive multiplication of the independent transformation matrices for each section k and the transformation matrix of the static frame of reference. The resulting matrix is given by the following equation:

$$T_n^{orig} = \begin{bmatrix} A_n^{orig} & O_n^{orig} \\ 0_{1\times 3} & 1 \end{bmatrix} = T_0^{orig} \prod_{k=1}^{n} T_k^{k-1} \tag{2.25}$$

where the matrices T_0^{orig} and T_k^{k-1} represent the static transformation matrix and the independent transformation matrix of each flexible section respectively.

2.5 Workspace generation for a continuum robot

By definition, the workspace is the set of all positions accessible by the robot's end effector.

Figure 2.8 shows the possible positions that can be reached by the first section of the continuum robot, as well as by the continuum robot with two sections in two-dimensional representations. These points were obtained using the FKM, by varying the first bending angle for each section in the interval $\theta_{1,k} \in \left[-\frac{\pi}{8}, \frac{\pi}{8}\right]$.

On figure 2.8, we present some possible positions that the continuum robot's end effector can reach, which are designated by the letter A (dotted curved lines in red) as well as the positions of the first section of the robot designated by the letter B (dotted curved lines in yellow).

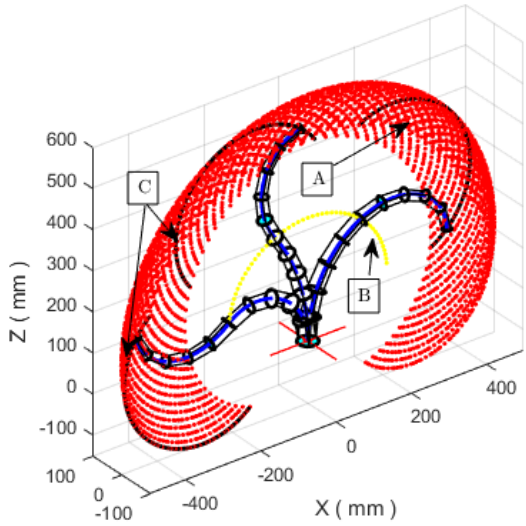

Figure. 2.8: 2D view of the continuum robot workspace at VC

2.5.1 Comparison between the workspace of a continuum robot with VC and CC

In this section, we compare the workspace of a flexible continuum robot with constant and variable curvature. Lets start with the comparison of a single section of the continuum robot, the characteristics of each section are shown on Table 2.1. The first bending angle and orientation of the section are varied in the interval $\left[0, \frac{\pi}{5}\right]$ and $[-\pi, \pi]$ respectively.

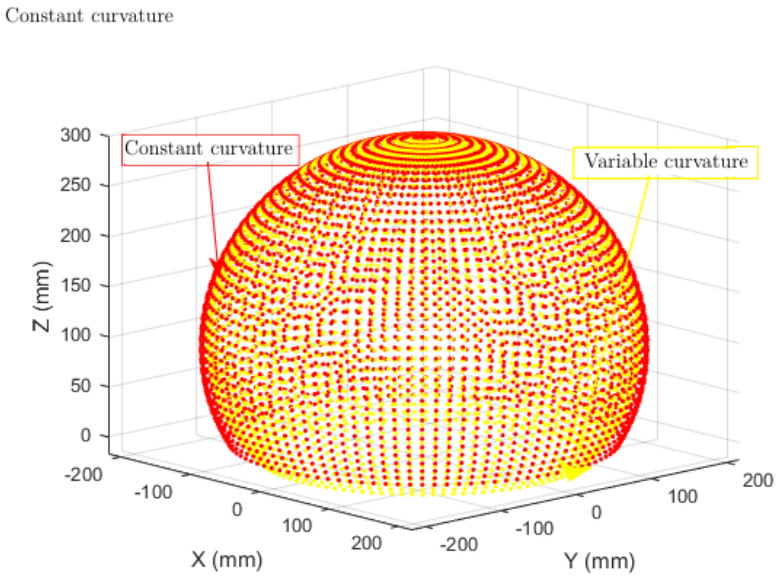

Figure. 2.9: 3D view of the workspace of a CC and VC section

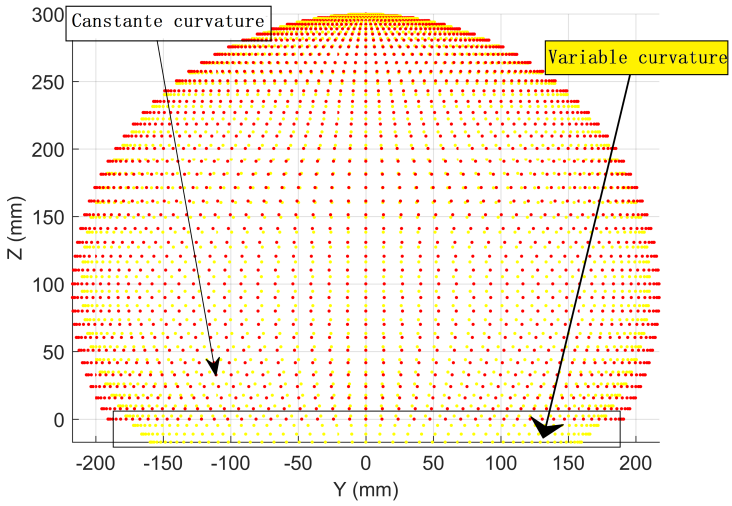

Figure. 2.10: View in the YZ plane of the workspace of a CC and VC section

As it can be seen in Figures 2.9 and 2.10, the idea of variable curvature is able to produce bending angles with increasing curvature, namely, the end point of the section can reach much more curved positions with respect to the constant curvature.

In the second example, we vary the first bending angle for each section in the same range $\theta_{j,k} \in \left[-\frac{\pi}{8}, \frac{\pi}{8}\right]$.

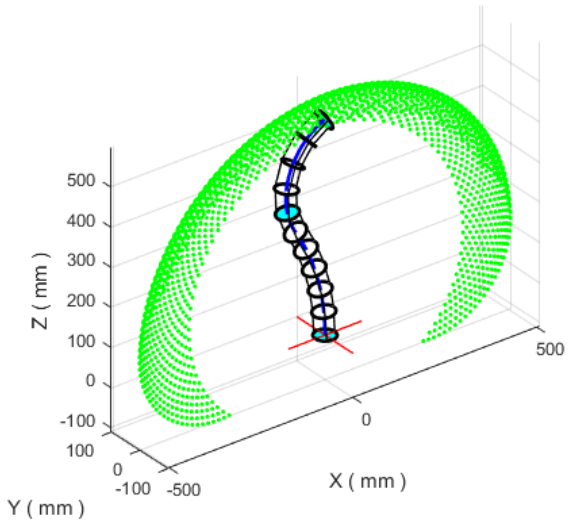

Figure. 2.11: 2D workspace view for a flexible continuum robot with constant curvature : $r_{\max} = r_{\min} = 25mm$

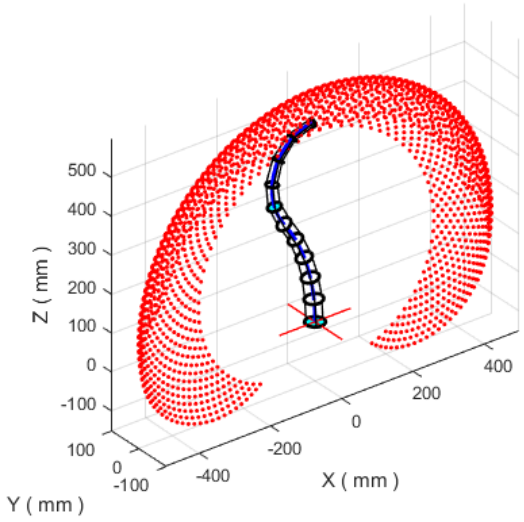

Figure. 2.12: 2D workspace view for a flexible continuum robot with variable curvature: $r_{\max} = 25mm, r_{\min} = 10mm$

Figures 2.11 and 2.12 show the workspace of a flexible continuum robot with CC and VC respectively. Comparatively, the end effector of a VC flexible continuum robot can reach much more curved positions than a CC continuum robot as shown in Figure 2.13.

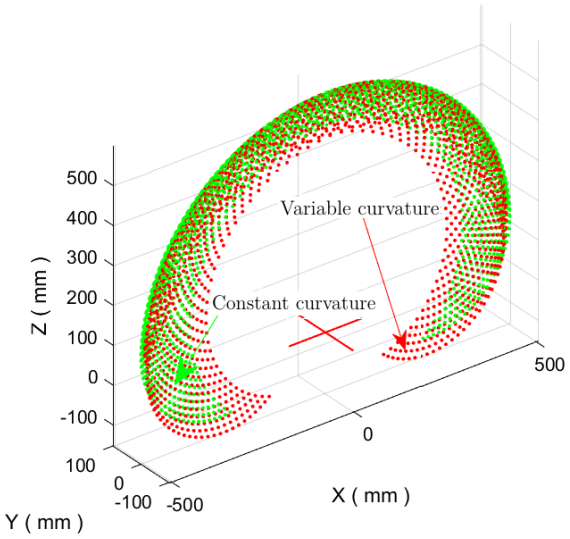

Figure. 2.13: Comparison of workspace for a flexible continuum robot with CC and VC

2.6 Case study of a variable-length continuum robot with CC

Continuum robots with variable length have the ability to extend their links allowing the robot to have a larger workspace compared to a non-variable length continuum robot. Broadly speaking, continuum robot with variable length can extend its backbone according to the needed task as it shown in Figure 2.14.

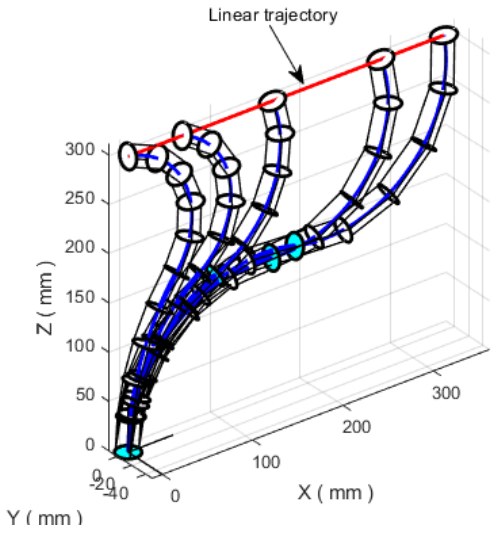

Figure. 2.14: VL continuum robot following a linear trajectory

The considered robot in this section consists of two sections ($n = 2$), the sections' backbone range from 100 mm (contraction) to 300 mm (extension), that is, the maximum length extension of the robot's backbone can reach out to 600 mm and can be shortened to 200 mm. Furthermore, each section has five disks with the same diameters.

Table 2.3: Parameters of the considered flexible continuum robot

	Section 1	Section 2	Description
m_k	5 units	5 units	Number of units
$l_{\min,k}$	100 mm	100 mm	Minimum contraction length in each section
$l_{\max,k}$	300 mm	300 mm	Maximum extension length in each section
r_k	12 mm	12 mm	Diameter of disks

The workspace of the considered continuum robot is shown in Figure 2.15 (red ball-like shape). The workspace is obtained from the robot's FKM using the bending angle $\theta_{1,2}$ that ranges between $[-\pi \quad \pi]$ and the rotation angles $\varphi_{1,2}$ that ranges between $[0 \quad \pi]$.

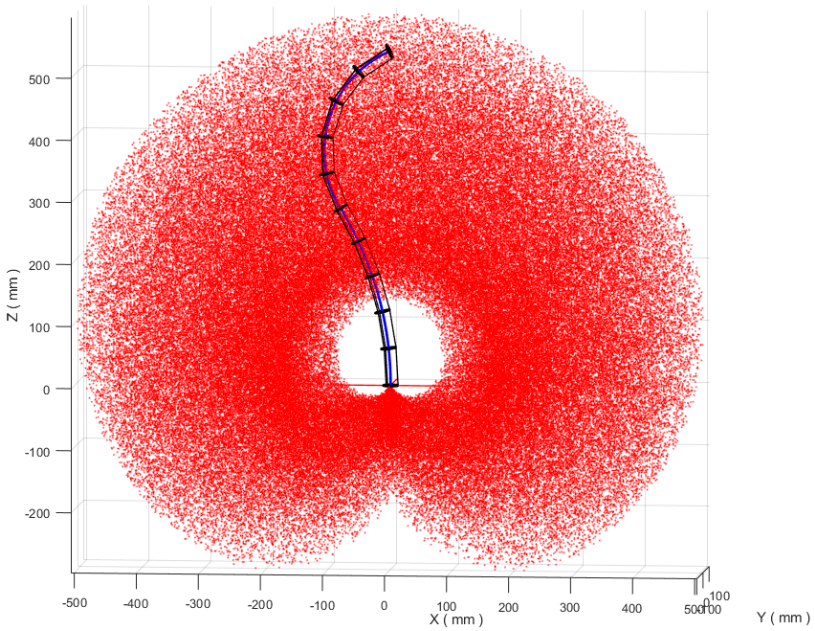

Figure. 2.15: 2D workspace for a VL two section continuum robot

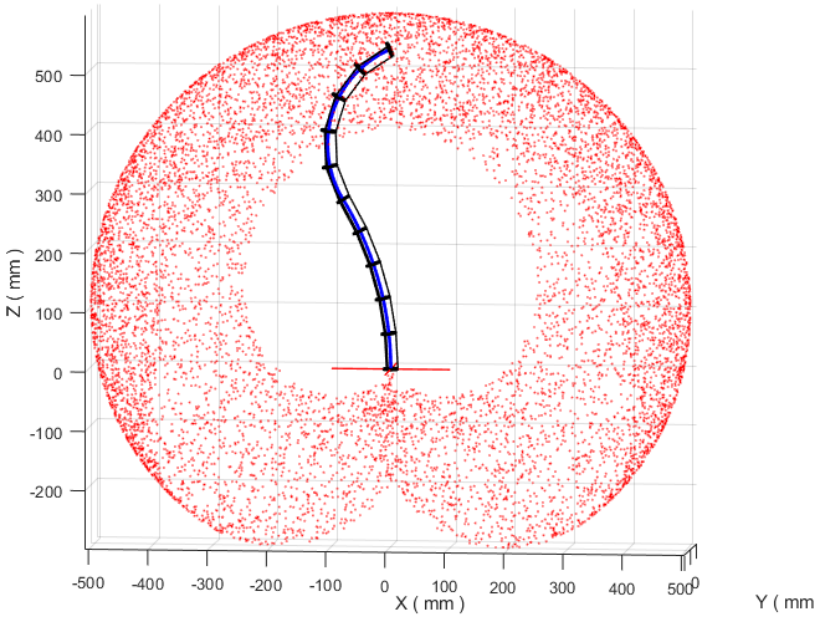

Figure. 2.16: 2D workspace for a constant length two section continuum robot

As it is shown in Figure 2.15, the 2D workspace of a two section continuum robot with variable length is illustrated by the curved red-dashed points. It is obviously clear that the robot's end effector can cover a large area within its workspace compared to a continuum robot with Constant Length (CL) as it is shown in Figure 2.16. Thanks to the extensibility of the robot's backbone, the workspace can be broadened according to the extreme limit of the backbone extension and contraction which help the robot to reach out to almost any possible position in its workspace. In Figure 2.16, it is noticeable that the constant length continuum robot's end effector misses a set of positions (blank ball-like shape) inside its workspace, which can be easily dealt with using VL continuum robot .

2.7 Conclusion

In this chapter, a comprehensive description of the structure and the behavior of a continuum robot with variable curvature was presented. Then, the forward kinematic model for this robot is calculated, namely the forward kinematic model of a unit which is obtained using the homogeneous transformation matrix through two steps: the specific transformation which expresses the relationship between the parameters of the arc and the cables' length, then the independent transformation which expresses the desired situation (position) as a function of the arc's parameters. The forward

kinematic model of the flexible section and the whole robot are obtained by a successive multiplication of the global geometric transformation matrices of units. We concluded this chapter with a comparison between the workspace of a flexible continuum robot with constant and variable curvature as well as a case study of a variable-length continuum robot with constant curvature.

CHAPTER 3

INVERSE KINEMATIC MODELING

3.1 Introduction

For any robotic system, the inverse kinematic model can be summarized as follows: for a given posture (position and orientation), we determine the necessary actuation variables that satisfy certain movement constraints. In the continuum robots' world, the inverse kinematic models are a very nonlinear problem, which is inferred by calculating the inverse function of forward kinematic models. IKMs can easily orient robots by cartesian position equations rather than curvature and rotational equations. But obtaining IKMs remains a difficult task, especially when it comes to multi-section continuum robots. In almost cases IKMs cannot be analytically calculated and have several problems that lie in the following:

- Unavailability of solutions when the target points are outside the robot's workspace.
- Several solutions or endless solutions when the target point can be reached by different configurations.

For the robots studied in this thesis, the inverse kinematic model consists in calculating the cable lengths and geometric parameters corresponding to the desired position of the robot's end-effector. In this chapter, meta-heuristic approach and artificial neural networks will be used to solve the inverse kinematic model of a VL continuum robot with constant curvature and a CL continuum robot with variable curvature respectively. The development of the used approaches to solve the IKMs is done through the forward kinematic models.

3.2 IKM of variable length continuum robot with constant curvature

In this section, the inverse kinematic model of a VL continuum robot with constant curvature is solved by specifying the arc's parameters corresponding to a desired posture of the robot's end-effector. First, we start with the analytical calculation of the inverse kinematic model of a single section continuum robot analytically. Then, the inverse kinematic model of a multi-section continuum robot is figured out using meta-heuristic methods.

3.2.1 IKM of VL single section continuum robot with constant curvature

The variable-length continuum robot with constant curvature at each point can be considered as a circular arc as it shown in Figure 3.1. Therefore, the inverse kinematic model of this robot can be solved by calculating the circular arc geometric parameters in the configuration space according to cartesian coordinates. The circular arc at each point has the following parameters:

- The curvature κ
- The orientation angle φ
- The bending angle θ
- The arc length(the robot's length) l

For the calculation of the arc parameters, according to the Figure 3.1, it is obviously clear that the angle of orientation φ can be expressed as follows [122] :

$$\varphi = arctan\left(\frac{y}{x}\right) \tag{3.1}$$

The center of the arc lies in the plane xy ; after rotation, this center must lie along the axis x. Therefore, the radius r of the center of this arc c lies in $(r,0)$ with respect to the plane xz.

The curvature κ can be determined by finding the distance between the origin and the center of the arc formed by the continuous section. By rotating P around the axis z by $-\varphi$, this creates $P^{'}$ such that $x^{'} = \sqrt{x^2+y^2}$, $y^{'} = 0$ and $z^{'} = z$.

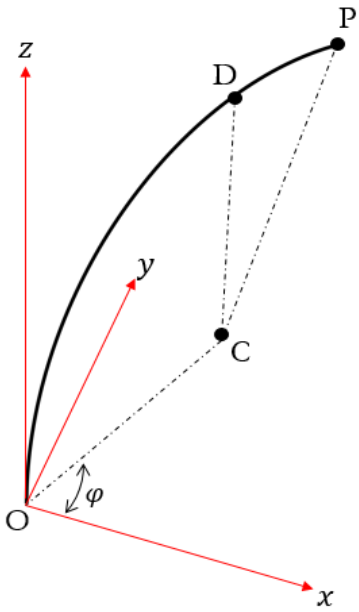

Figure. 3.1: 3D representation of the robot central axis

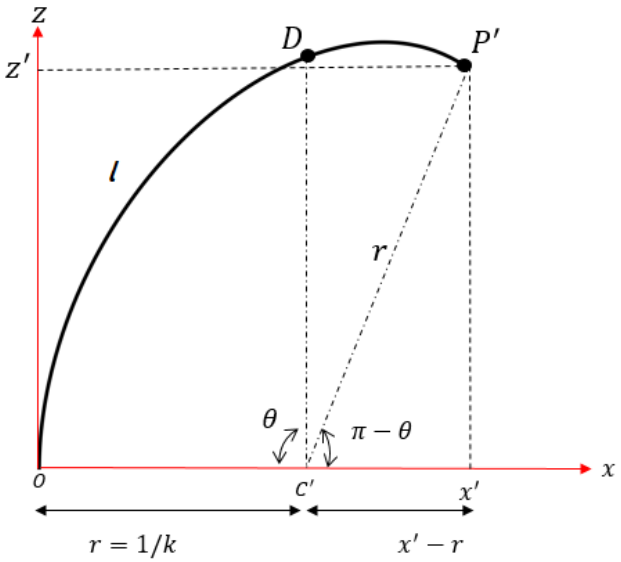

Figure. 3.2: 2D representation of the robot central axis

From the triangle $P^{'}c^{'}x^{'}$ (Figure 3.2), we have:

$$\left(x^{'}-r\right)^{2}+z^{'2}=r^{2} \tag{3.2}$$

After replacing $x^{'}$ an $z^{'}$ by their expressions we obtain:

$$\kappa = r^{-1} = \frac{2\sqrt{x^2+y^2}}{x^2+y^2+z^2} \tag{3.3}$$

The angle θ, as shown in the Figure 3.2, can be calculated from the curvature and the cartesian coordinates of P. Examining the triangle $P^{'}c^{'}x^{'}$ we can write:

$$\cos(\pi-\theta) = \frac{\left(x^{'}-r\right)}{r} \tag{3.4}$$

After that we obtain:

$$\theta = \pi - arccos\left(\frac{x^{'}-\kappa^{-1}}{\kappa^{-1}}\right) \tag{3.5}$$

After simplification, the expressions for the bending angle θ can be summarized in the equation (3.6) :

$$\theta = \pi - arccos\left(\frac{x^2+y^2-z^2}{x^2+y^2+z^2}\right) \tag{3.6}$$

Finaly, the length l is calculated from equations (3.3) and (3.6) as follows:

$$l = \left(\pi - arccos\left(\frac{x^2+y^2-z^2}{x^2+y^2+z^2}\right)\right)\left(\frac{x^2+y^2+z^2}{2\sqrt{x^2+y^2}}\right) \tag{3.7}$$

3.3 Solving the IKM of VL multi-section continuum robot with CC using metaheuristic optimization

Variable length continuum robots are usually adopted in applications that require in avoiding obstacles in enclosed spaces and labyrinth-like paths. To this end, in this section, the optimization algorithm called teaching learning based optimization (TLBO) is used to solve the inverse kinematic model of a variable length continuum robot with the ability to make the robot dexterously avoid static obstacles.

The main objective of adopting optimization algorithms unlike artificial neural network to solve the inverse kinematic model of this type of continuum robot is their ability to deal with obstacles simply by making the robot take the appropriate configuration to accomplish the required task.

3.3.1 Comparison of TLBO with other optimization algorithms

Generally, almost all optimization methods require specific parameters that have a crucial role on the algorithm' s functionality as well as its performance. Table 3.1 shows the required parameters for some metaheuristic algorithms. Unlike other optimization techniques, TLBO does not require any specific parameters, which makes it a handy algorithm to deal with the complicated problems of engineering. TLBO uses the best solution at each iteration to shift to the best existing solution in the population, which paves the way to a fast convergence.

Table 3.1: The required parameters for each algorithm

Algorithms	Required parameters
GA	Crossover probability, mutation rate, selection method
PSO	Acceleration constants, weight variation, maximum veclocity
ABC	Onlooker bees number, employed bees number, food sources number
HS	Range of each variable, pich rate, number of improvisation

3.3.2 Teaching learning based optimization algorithm

TLBO Algorithm is originally inspired from the process' effect of teaching a set of students. It was proposed by Rao et al [123] and Rao and Savsani [124]. The algorithm consists of two phases, teacher and learners phases. In the process of this algorithm, a set of learners is considered as population, the whole population is provided with various topics, which are supposed to be the variables of the optimization problem. The learners' results illustrate the fitness value of the optimization problem. The outstanding solution among the whole population is considered to be the teacher, while the variables are the objective function's parameters and its best value is the best solution to the considered problem.

3.3.2.1 Teacher phase

In the first phase, the teacher thoroughly tries to improve the mean result of the whole class according to the taught subject. At each attempt (iteration) i, there are m topics and n_p learners in a specific topic j. The best learner in the classroom is chosen as the teacher. The difference $d^{i}_{j,k}$ between the existing mean results of each topic and the

teacher result for each subject is given by :

$$d^{\mathrm{i}}_{\mathrm{j,k}} = r\left(X^{\mathrm{i}}_{\mathrm{j,k_{best}}} - T_F M^{\mathrm{i}}_{\mathrm{j}}\right) \tag{3.8}$$

where

$$M^{\mathrm{i}}_{\mathrm{j}} = \frac{\sum_{\mathrm{k=1}}^{n} X^{\mathrm{i}}_{\mathrm{j,k}}}{n} \tag{3.9}$$

and $X^{\mathrm{i}}_{\mathrm{j,k_{best}}}$ is the best selected learner's result in a topic j, T_F is a factor which can be either 1 or 2, r is a random number in the range [0,1], $M^{\mathrm{i}}_{\mathrm{j}}$ is the mean result. Based on equation (3.8), the existing solution is updated in the teacher phase as follows:

$$Xnew^{\mathrm{i}}_{\mathrm{j,k}} = X^{\mathrm{i}}_{\mathrm{j,k}} + d^{\mathrm{i}}_{\mathrm{j,k}} \tag{3.10}$$

where $Xnew^{\mathrm{i}}_{\mathrm{j,k}}$ is the updated value of $X^{\mathrm{i}}_{\mathrm{j,k}}$ which is sent to the learner phase.

3.3.2.2 Learner phase

In this particular phase, the learners enhance their level of knowledge by a random interaction among themselves. The learner can improve his/her knowledge by interacting with a learner who has more knowledge than him/her. The whole process can be mathematically formulated as follows:

$$\begin{cases} Xnew^{\mathrm{i}}_{\mathrm{j},A} = X^{\mathrm{i}}_{\mathrm{j},A} + r\left(X^{\mathrm{i}}_{\mathrm{j},A} - X^{\mathrm{i}}_{\mathrm{j},B}\right) & if \quad F^{\mathrm{i}}_{A} < F^{\mathrm{i}}_{B} \\ Xnew^{\mathrm{i}}_{\mathrm{j},A} = X^{\mathrm{i}}_{\mathrm{j},A} + r\left(X^{\mathrm{i}}_{\mathrm{j},B} - X^{\mathrm{i}}_{\mathrm{j},A}\right) & if \quad F^{\mathrm{i}}_{B} < F^{\mathrm{i}}_{A} \end{cases} \tag{3.11}$$

where A and B are two randomly selected learners, F^{i}_{A} and F^{i}_{B} are the fitness values of X_A and X_B for A and B , respectively. It is noteworthy to say that the aforementioned equations ((3.8), (3.10), (3.11)) are valid exclusively when it comes to minimization problems.

3.3.3 Objective function and problem formulation

The resolution of the IKM can be addressed using an objective function, which describes the distance between the prescribed position and the robot's end tip (Figure 3.3), where the lowest possible distance can be considered as a solution for a specifically prescribed position. The cost function contains the desired position coordinate and the robot's end tip coordinates it can be mathematically expressed as follows:

$$F = \sqrt{(P_{X_i} - X_{c_i})^2 + (P_{Y_i} - Y_{c_i})^2 + (P_{Z_i} - Z_{c_i})^2} \tag{3.12}$$

Furthermore, X_{c_i},Y_{c_i}, and Z_{c_i} represent the spatial coordinates of a located position on the prescribed trajectory. P_{X_i},P_{Y_i}, and P_{Z_i} represent the position of the robot's end tip obtained from the FKM. These positions represent the three first components of the fourth column of the matrix (2.25).

$$D^2_{\mathrm{j,k}} \leq \left(r_{obstacle} + r_{\mathrm{j,k}}\right)^2 \tag{3.13}$$

For the obstacle avoidance (Figure 3.3), the constraint given by (3.13) is considered and a specific penalty is added to the objective function.This function becomes as follows:

$$F = \sqrt{(P_{X_i} - X_{c_i})^2 + (P_{Y_i} - Y_{c_i})^2 + (P_{Z_i} - Z_{c_i})^2} + 1000 \cdot (D^2_{\mathrm{j,k}} \leq \left(r_{obstacle} + r_{\mathrm{j,k}}\right)^2) \tag{3.14}$$

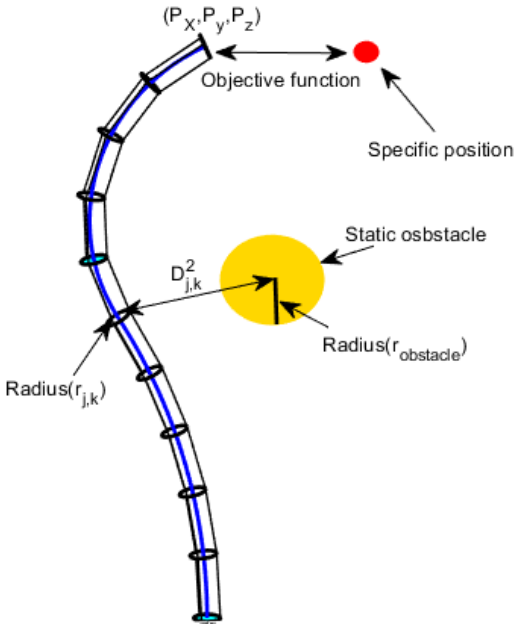

Figure. 3.3: Global view of the governing objective function and the adopted strategy for the obstacle avoidance.

where $r_{obstacle}$ is the radius of the spherical-like obstacle, and $r_{j,k}$ is the radius of the selected robot's disks.

3.3.4 TLBO implementation to solve the IKM of VL continuum robot

Three Simulation examples through Matlab are carried out. For the former, a 3D simulation of a two-section continuum robot with variable length following two types of trajectories, namely a linear and spherical trajectory, is considered. The needed variables to be found by the TLBO are (θ_1, ϕ_1, l_1) for the robot's first section and (θ_2, ϕ_2, l_2) for the robot's second section. The second simulation addresses a free-collision example during the follow up of a circular trajectory. In the third simulation, a 3D simulation of a three-section continuum robot during the follow up of a linear trajectory is carried out.

3.3.4.1 Step of the optimization algorithm

- Step 0: initialization
  - Choose the population size (n_p), the number of variables (m), the termination criterion (ϵ), the maximum number of iteration (k_{max}), the admissible maximum and minimum values for each variable ($X_{\mathrm{j}_{max}}, X_{\mathrm{j}_{min}}$).
  - For each point of the reference trajectory do the following steps:
- Step 1: initial solution
  - For $\mathrm{k} = 1 : n_p$
    - For $\mathrm{j} = 1 : m$
      - Choose randomly the initial solution as follows: $x^1_{\mathrm{j,k}} = rand(0,1) * (X_{\mathrm{j}_{max}} - X_{\mathrm{j}_{min}}) + X_{\mathrm{j}_{min}}$ where:r is a random number between 0 and 1
    - End
  - End
  - Select the desired reference trajectory point.
  - Set $\mathrm{i} = 1$
- Step 2: teacher phase
  - For $\mathrm{k} = 1 : n_p$
    - Evaluate the corresponding objective function (F_{k}) using equation (3.12).

- End
- Select the student who gives the minimum value of the objective function ($F_{\mathrm{k}_{best}}$) as a teacher.
- For $\mathrm{j} = 1 : m$
  - Calculate the mean result($M_{\mathrm{j}}^{\mathrm{i}}$) using equation (3.9).
- End
- For $\mathrm{j} = 1 : m$
  - Calculate the difference mean($d_{\mathrm{j}}^{\mathrm{i}}$) using equation(3.8).
- End
- For $\mathrm{k} = 1 : n_p$
  - For $\mathrm{j} = 1 : m$
    - Calculate the new solutions ($Xnew_{\mathrm{j,k}}^{\mathrm{i}}$) using equation (3.10).
  - End
- End
- For $\mathrm{k} = 1 : n_p$
  - Evaluate the new corresponding objective function ($Fnew_{\mathrm{k}}$) using the new solutions ($Xnew_{\mathrm{j,k}}^{\mathrm{i}}$) according to equation (3.12).
- End
- Apply a greedy selection between the new and the old solutions.

- Step 3: learners phase
  - Choose randomly a q pairs of solutions.
  - For $\mathrm{k} = 1 : n_p$
    - For $\mathrm{j} = 1 : m$
      - Calculate the new solutions ($Xnew_{\mathrm{j,k}}^{\mathrm{i}}$) using equation (3.11)
    - End
  - End
  - For $\mathrm{k} = 1 : n_p$
    - Evaluate the new corresponding objective function ($Fnew_{\mathrm{k}}$) using the new solutions ($Xnew_{\mathrm{j,k}}^{\mathrm{i}}$) according to equation (3.12)

  - End
  - Apply a greedy selection between the new and the old solutions.

- Step 4: iterative process
  - If $F_{\mathrm{k}_{best}} < \epsilon$ or $\mathrm{i} > \mathrm{k}_{max}$
    - Go to step 5
  - Else
    - $\mathrm{i} = \mathrm{i} + 1$
    - Go to step 2
  - End if

- Step 5: obtaining the final solution
  - Apply the computed best solution.
  - Go to step 1.

3.3.4.2 Variable length continuum robot following linear trajectory

In Figure 3.4, a two-sections continuum robot with variable length is accurately following the linear trajectory given by equation (3.15). It is noteworthy to say that without the added constraints $\theta_2 < 0$, $\phi_1 > 0$ and $\phi_2 < 10^{-5}$, there is an infinite number of solutions.

$$X = 10t; \quad Y = 0; \quad Z = 300 \tag{3.15}$$

with t = 0:0.1:35

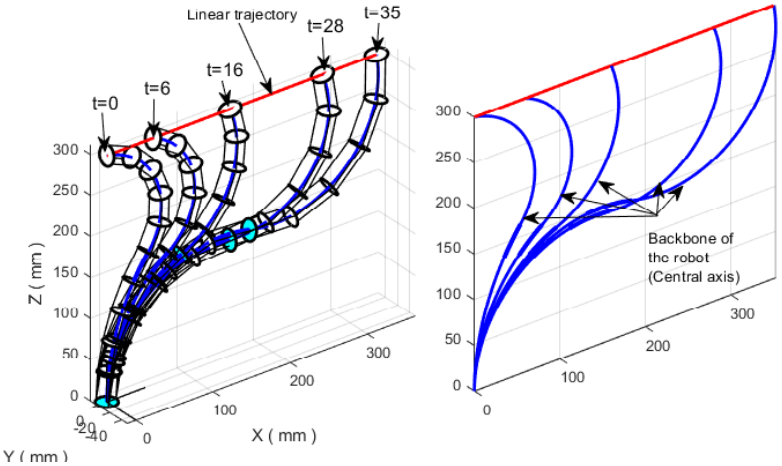

Figure. 3.4: (Left) VL continuum robot following the linear trajectory with constraints: $\theta_2 < 0$ and $\phi_1 > 0$, $\phi_2 < 10^{-5}$; (Right) Central axis of the robot.

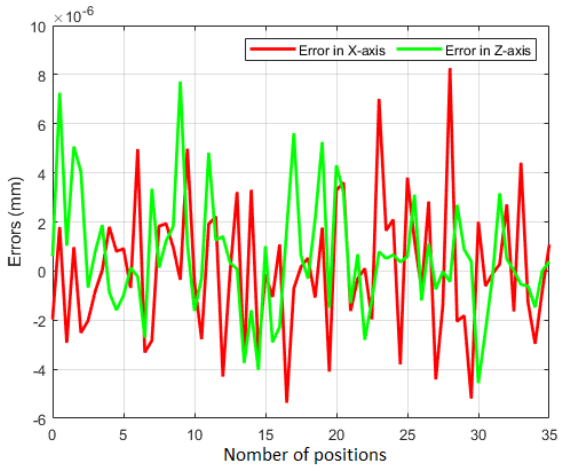

Figure. 3.5: Errors between the desired linear trajectory and that generated by TLBO

As it can be seen from Fig. 3.5 that the generated and desired trajectory overlap. As it can be seen in Figure 3.6, each position on the linear trajectory can be reached by the robot's end effector through at least three configurations (redundancy), for instance the robot can attain the position (t=16) on the linear trajectory through three different configurations with different backbone's length. To emphasize, the second configuration (Figure 3.6) has less longer backbone compared to the first and third configurations. Seemingly, the first and third configurations make the robot take lengthy backbone.

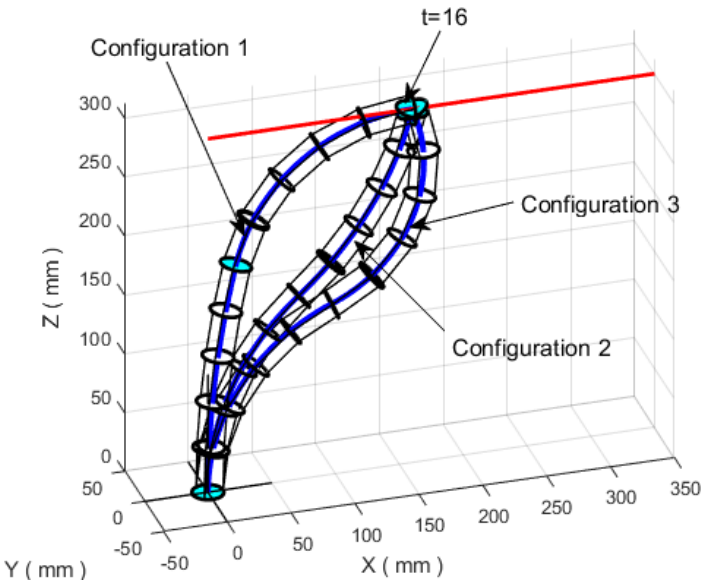

Figure. 3.6: Different configurations for the VL continuum robot following the linear trajectory (redundancy).

Since the purpose of the developed algorithm does not rely on finding the lowest extensibility of the robot's backbone, we have just taken a rondom solution (configuration) among the existing ones. Basically, the considered continuum robot varies its length according to each position thanks to its backbone's extensibility and which refers to the so called variable length continuum robot.

As it is shown in Figure 3.4, only one of the existing configurations (solutions) is taken which allows the robot to track the linear trajectory and that can be achieved by adding these constraints : $\theta_2 < 0$, $\phi_1 > 0$ and $\phi_2 < 10^{-5}$ to the objective function. For the first position (t=0) on the linear trajectory, the robot's backbone length is approximately 350 mm, while in the last position (t=35) the robot's backbone length takes a value of 540 mm (see Table 3.2).

Table 3.2: Cable lengths and backbone extensibility for some positions on the linear trajectory

Positions	$(t=0)$	$(t=6)$	$(t=16)$	$(t=28)$	$(t=35)$
Backbone length (mm)	350	360	370	480	540
Cable ℓ_1 (mm)	167.2657	168.3662	170.5898	218.7388	246.8439
Cable ℓ_2 (mm)	178.6907	185.4123	191.5741	248.9291	279.3553
Cable ℓ_3 (mm)	178.6907	185.4123	191.5741	248.9291	279.3553
Cable ℓ_4 (mm)	197.8896	204.3020	202.8323	262.8905	292.0712
Cable ℓ_5 (mm)	161.7734	165.7582	174.9679	226.0046	256.2625
Cable ℓ_6 (mm)	161.7734	165.7582	174.9679	226.0046	256.2625

3.3.4.3 Variable length continuum robot following a spiral trajectory

In the second simulation example, the spiral-like trajectory expressed by equation (3.16) is followed up by a variable length two-section continuum robot as shown in Figure 3.7.

$$\begin{cases} X = 50 - 5cos(2t) \\ Y = 50sin(2t) \\ Z = 350 - 5t \end{cases} \tag{3.16}$$

with t = 0:0.25:10

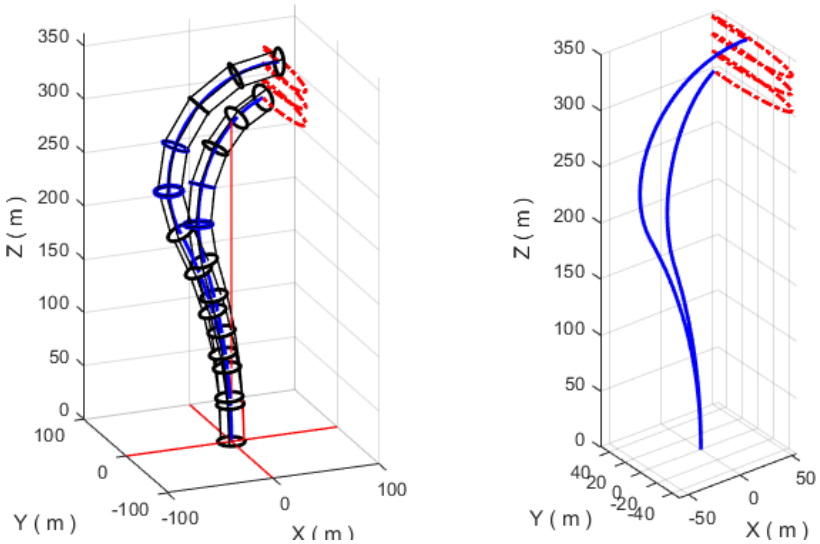

Figure. 3.7: (Left) Two configurations for the VL continuum robot following the spiral trajectory; (Right) Central axis of the robot following the spiral trajectory

This trajectory contains relatively small bending and orientation angles. Therefore it has been used to evaluate the performance of the TLBO. The generated bending and orientation angles from the TLBO algorithm to make the robot follow the spiral trajectory are shown in Figure 3.8.

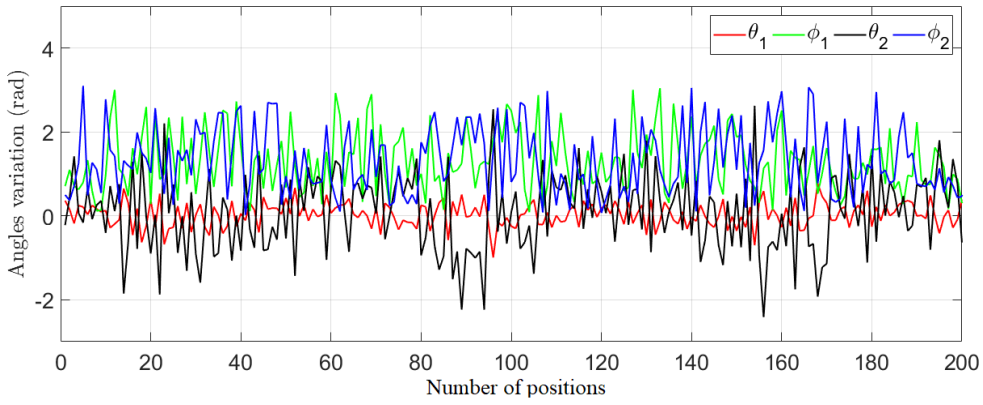

Figure. 3.8: Needed bending and orientation angles for the two-section continuum robot to follow the spiral trajectory

Although the tackled trajectory which is shown in Figure 3.7 is relatively difficult compared to the previously proposed trajectories, the TLBO managed to come up the proposed trajectory with minor errors (Figure 3.9).

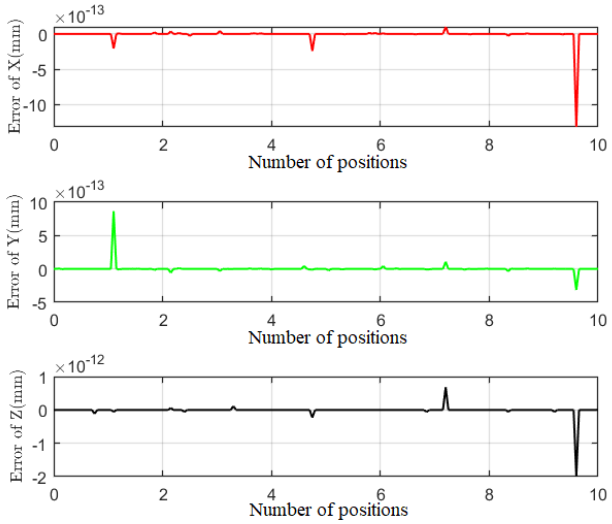

Figure. 3.9: Euclidean errors between the desired and the generated spiral trajectory for the two-section continuum robot.

3.3.4.4 Free-collision during the follow up of a circular trajectory

In this example, a VL two-sections continuum robot is considered to follow the circular trajectory (Figure 3.10), defined by equation (3.17), in the presence of a static obstacle. The robot has to follow the prescribed circular trajectory in the condition that it does not collide into the obstacle.

$$X = 30cos(\frac{\pi}{5}t); \quad Y = 30sin(\frac{\pi}{5}t); \quad z = 440 + 30sin(\frac{\pi t}{5}) \tag{3.17}$$

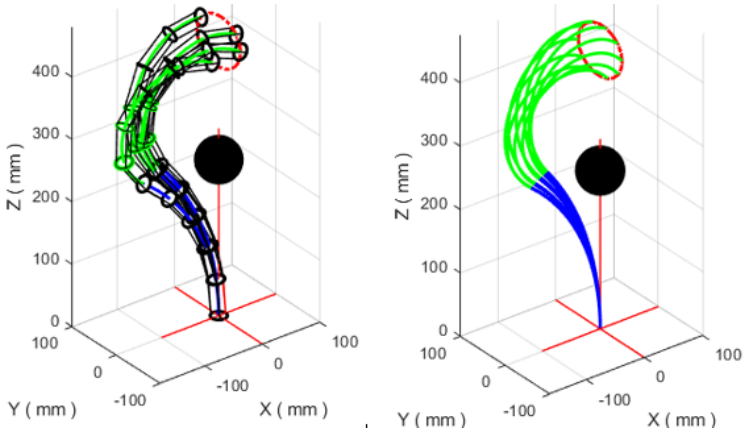

Figure. 3.10: (Left) VL continuum robot following a circular trajectory in the presence of a static obstacle; (Right) Different configuration of the central axis of the robot.

As it can be seen from Figure 3.10, the variable length continuum robot follows the circular trajectory with a free collision. The whole operation is performed based on TLBO algorithm which generates the required angles allowing the robot to properly follow the circular trajectory with respect to the length variation.

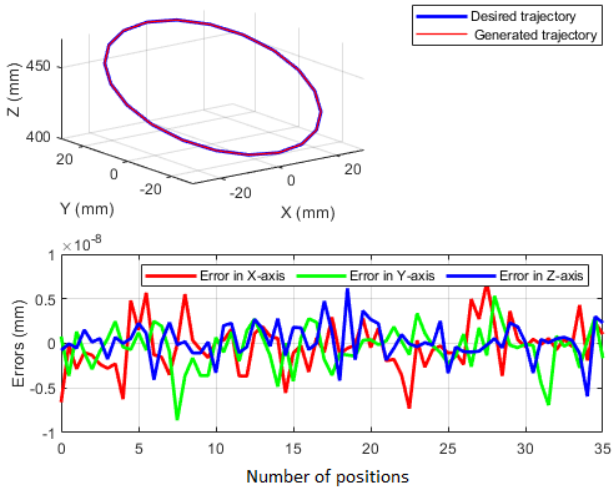

Figure. 3.11: Error between the desired circular trajectory and the generated one by TLBO

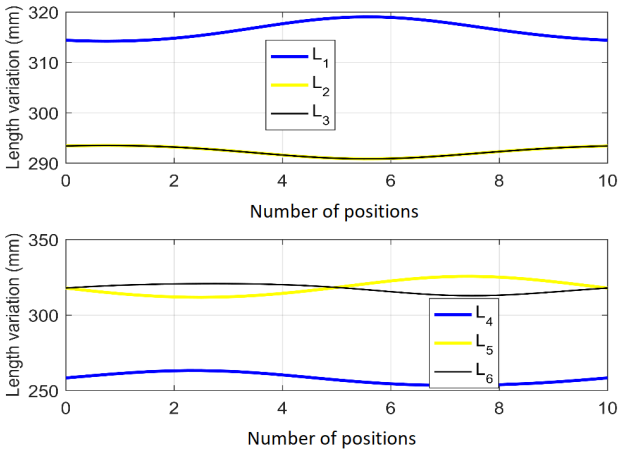

Figure. 3.12: The cables length generated by TLBO ensuring the free-collision during circular trajectory

Remarkably, based on the Euclidean error between the generated trajectory by TLBO and the desired trajectory (Figure 3.11), TLBO can be considered as a powerful optimization algorithm for solving the inverse kinematic model of continuum robots.

Figure 3.12 represents the cables length allowing the robot to follow the circular trajectory with free collision.

It is noteworthy to say that the calculation of the cables length is mainly based on angles which are calculated from the proposed algorithm and on the strategy of calculating the parallel robots' IKMs, in other words, the three cables for each unit are considered as the three segments connecting the parallel robot's platforms, namely two platforms are linked through three segments with prismatic articulation .

3.3.4.5 Three sections continuum robot following a linear trajectory

In this simulation example, a variable length three-section continuum robot is considered to follow the linear trajectory, defined by equation (3.18). The characteristics of the three-section continuum robot are described in Table 3.3.

$$X = 12t; \quad Y = 0; \quad Z = 295 - 10t \tag{3.18}$$

Table 3.3: Parameters of the three-section continuum robot.

Robot's parameters	Description
$m_k = 8(k:1,2,3)$	Number of disks per section
$l_{k_{min}} = 100mm$	Minimum contraction length in each section
$l_{k_{max}} = 200mm$	Maximum extension length in each section
$r = 12mm$	The radius of disks

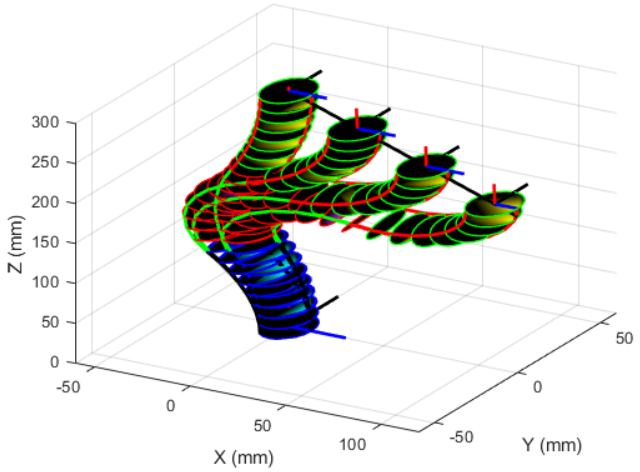

Figure. 3.13: Three-section continuum robot following a linear trajectory.

As it is shown in Figure 3.13, since the robot is following the prescribed linear trajectory, the TLBO algorithm is capable of solving the IKM even for a three section continuum robot which is similar to a real robot called bionic handling assisting [31]. Each section can range between 100 mm (contraction) and 200 mm (extension).

The purpose of using a three section continuum robot resides in showing that the proposed algorithm does not depend by no means on the complexity of the tackled models. In other words, by adding more sections, the mathematical equations become more complicated but since the TLBO algorithm does not rely on this complexity, its IKM model can be easily figured out. Furthermore, besides the used TLBO algorithm, increasing the number of sections can help in manipulating the robot inside a much more twisted path as well as avoiding a potential obstacle during the desired operation.

3.4 ANN for solving the IKM of constant length continuum robot with variable curvature

Conical-shaped robots or the so-called variable curvature continuum robots such as BHA and CBHA robots are usually adopted in direct and open applications that require accuracy, stability, and response time especially when dealing with real-time applications.Moreover, they do not require dealing with clustered paths and avoiding obstacles.

In this section, to develop the inverse kinematic model of the continuum robot with VC through neural networks, the forward kinematic model that was calculated in previous chapter is mainly adopted to train the neural networks.

3.4.1 Problem formulation

Neural Networks have achieved a great success in many areas due to their learning and generalization capabilities as well as their parallelism. They have been successfully used in many applications, such as classification, noise filtering, system modeling and control...etc. One of the fields where NN has received an increasing interest is that of solving the robots' IKMs.

Due to the complexity of variable curvature continuum robots models, very few works which aim at solving their IKMs have been carried out. To this end, the Multi-Layer Perceptron (MLP) neural networks are used and developed to find the IKMs of a single as well as a two-section continuum robot with variable curvature. The hidden layers contains neurons with sigmoid activation function and a linear activation function

in output layers. For the sake of avoiding the complexity of the neural networks a minimum number of neurons and hidden layers that gives the good learning are chosen.

The forward kinematic model is calculated for the sake of obtaining the P_{x_i},P_{y_i}, and P_{z_i} coordinates of the robot's end tip which themselves are used to train the proposed MLP. the used objective function for training neural networks is given by the following equation: (3.19):

$$F = \frac{1}{N}\sum_{i=1}^{N}\left((P_{x_i} - X_{c_i})^2 + (P_{y_i} - Y_{c_i})^2 + (P_{z_i} - Z_{c_i})^2\right) \tag{3.19}$$

Where N represent the number of data. X_{c_i},Y_{c_i}, and Z_{c_i} represent the spatial coordinates of a located position on the prescribed trajectory. P_{x_i},P_{y_i}, and P_{z_i} represent the position of the robot's end tip for each specific position of the prescribed trajectory, which are obtained from the FKM. Explicitly, they represent the three first components of the forth column of equation (2.25) which describe the FKM of the considered robot (Table 2.1).

3.4.2 Outline and simulation

Two simulations examples are considered, for the first simulation; a single spatial section continuum robot with variable curvature must follow up arc-shaped trajectory and circular trajectories.

For the second simulation, a planar two-section continuum robot with variable curvature must follow up linear and an arc-shaped trajectories. The characteristics of the considered robot are given in Table 2.1.

3.4.2.1 IKM of spacial single section continuum robot

The FKM of a spatial single section is first calculated using equation (2.25), and the orientation angle is then calculated analytically using FKM by dividing the position P_y by the position P_x. Finally, the static MLP (Figure 3.14) with the following configuration is used to calculate the bending angles:

- The input layer contains four inputs (x, y, z, ϕ)
- One hidden layer with 20 neurons.
- One linear output neuron that gives the approximated θ.
- Learning rate: $\alpha = 0.01$.

- Type of optimizer: Levenberg-Marquardt backpropagation.

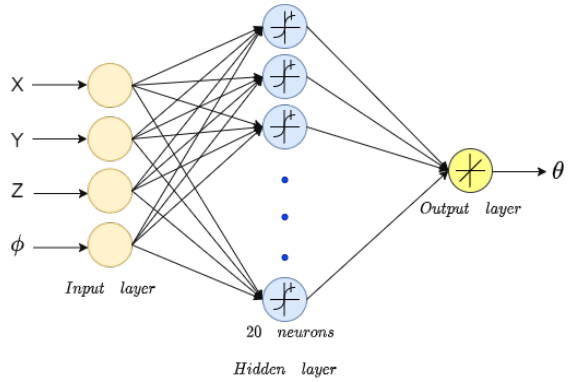

Figure. 3.14: Neural network structure for spacial single section continuum robot

A random dataset that covers all-inclusive possible positions which can be attained by the robot's first section, namely its workspace, are generated using the FKM to train the developed model.

The training result error value to the bending angle is given by Figure 3.15.

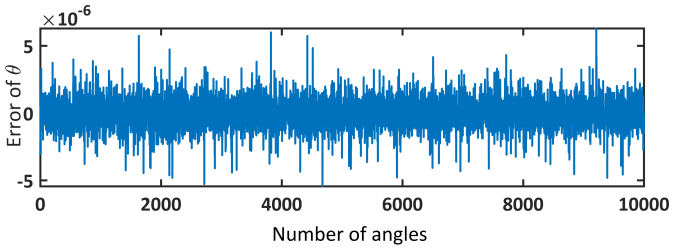

Figure. 3.15: Training error results of the neural model for the bending angle θ.

To evaluate the effectiveness of the obtained IKM. A second randomly dataset that cover all-inclusive possible positions in the robot's workspace is generated using the FKM. Figure 3.16 gives the error test results of the developed neural model for the bending angle θ .

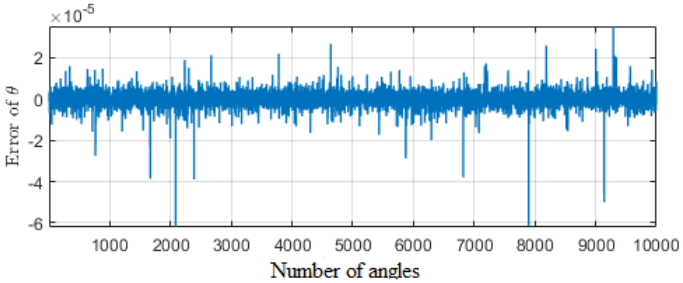

Figure. 3.16: Error test results of the neural model for the bending angle θ.

Figures 3.15 and 3.16 show the accuracy and the effectiveness of the obtained IKM. The values of the mean square error (MSE) of the achieved model are given in Figure 3.17.

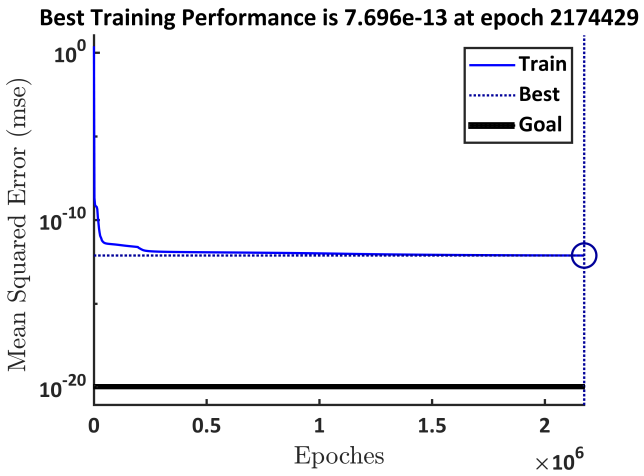

Figure. 3.17: Training performance of the model

After tested the effectiveness of the obtained model (IKM), the considered robot is tested on practically realistic-like trajectories (circular and arc-shaped trajectories) in order to assess the robot's behavior via 3D simulations.

As it is shown in Figure 3.18, the considered single section continuum robot with VC can accurately follow the arc-shaped trajectory within its 3D workspace (yellow curved arcs).

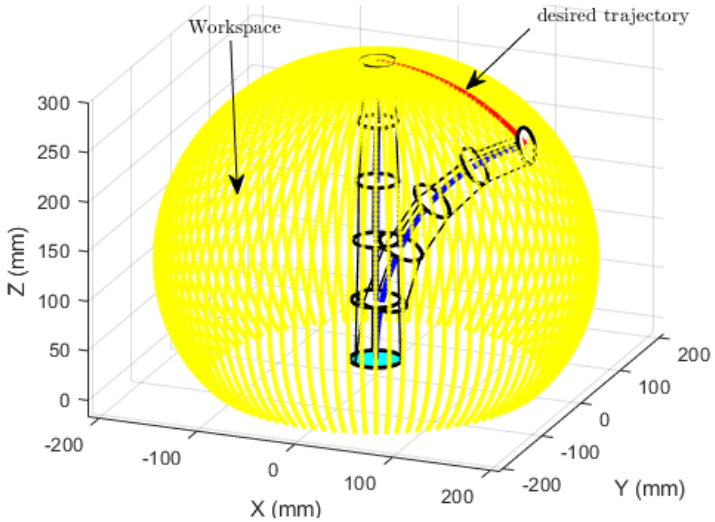

Figure. 3.18: Two configurations of a single section continuum robot following an arc shaped trajectory within its 3D workspace

To show the accuracy of the generated trajectory, euclidean errors are calculated. As it is shown in Figure 3.19, the maximum error between the generated and the desired trajectory is of the order of 0.002 mm.

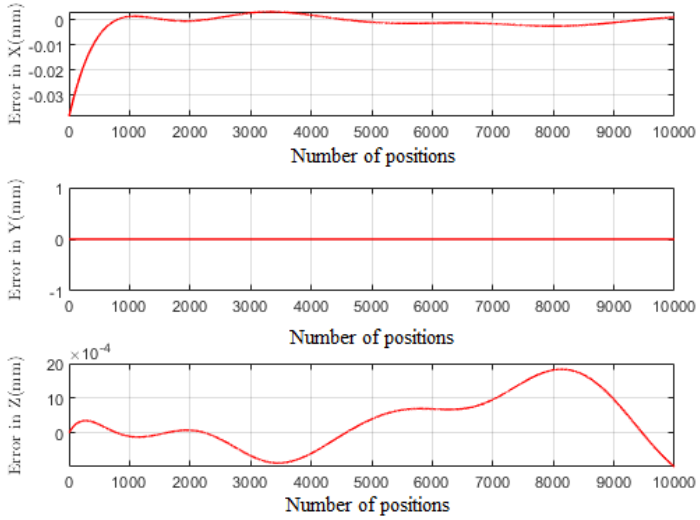

Figure. 3.19: Error between the reference trajectory (arc-shaped) and the trajectory (arc-shaped) given by the NN

Similarly to the first simulation example, the continuum robot track a circular trajectory within its workspace. Figure 3.21, shows the euclidean error of the trained NN.

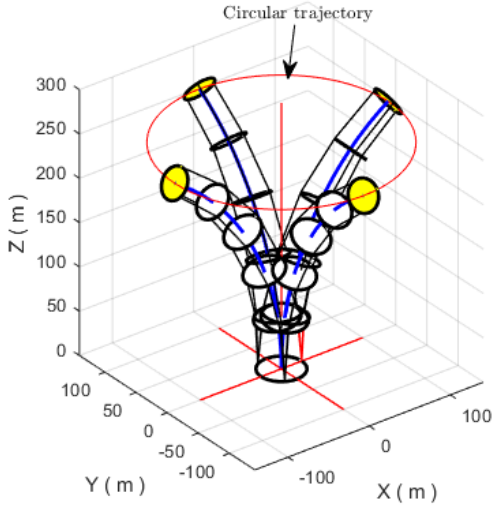

Figure. 3.20: Representation of the continuum robot's first section tracking the desired circular trajectory

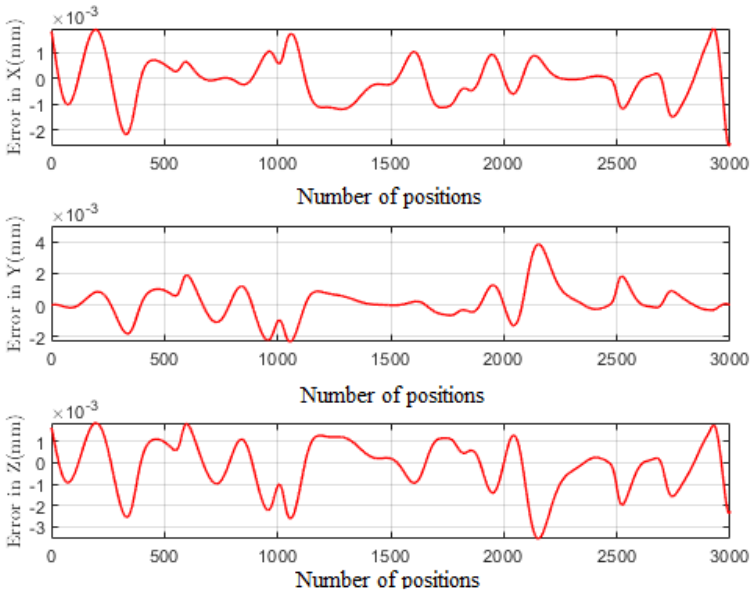

Figure. 3.21: Error between the reference circular trajectory and the circular trajectory given by the NN

3.4.2.2 IKM of planar two-section continuum robot

In the second simulation, two database have been created from the FKM of a two-section VC continuum robot with fixed orientation angles ($\phi_i = 0$) using random values of the bending angles within the robot's workspace. After that, to calculate the IKM of the considered robot, an artificial neural network with two hidden layers is built up (Figure 3.22). Using the generated data the error between the generated random bending angles and angles obtained from the trained NN is shown in Figure 3.23.

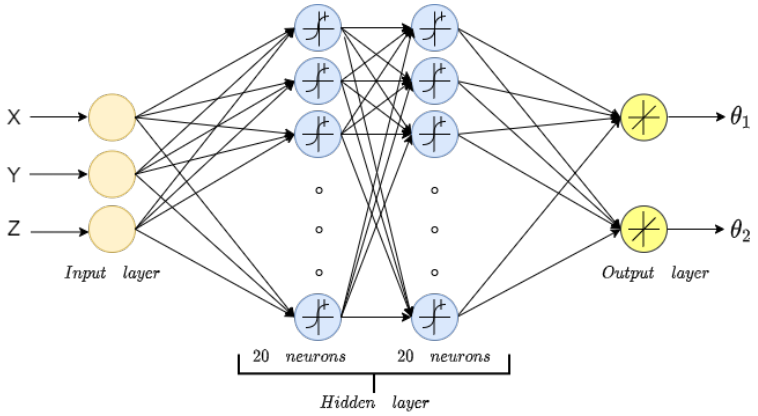

Figure. 3.22: The architecture of the neural model for a planer two-section continuum robot

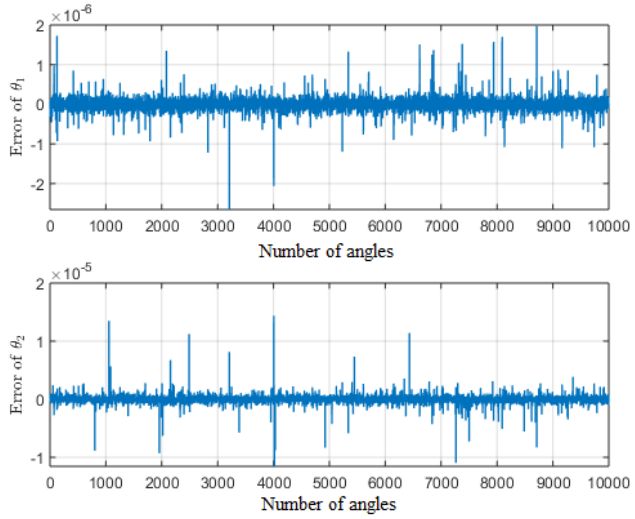

Figure. 3.23: Training results of the neural model for the two-section continuum robot

Finally, the IKM accuracy is evaluated by applying the second created database and the error in its bending angles is shown in Figure 3.24.

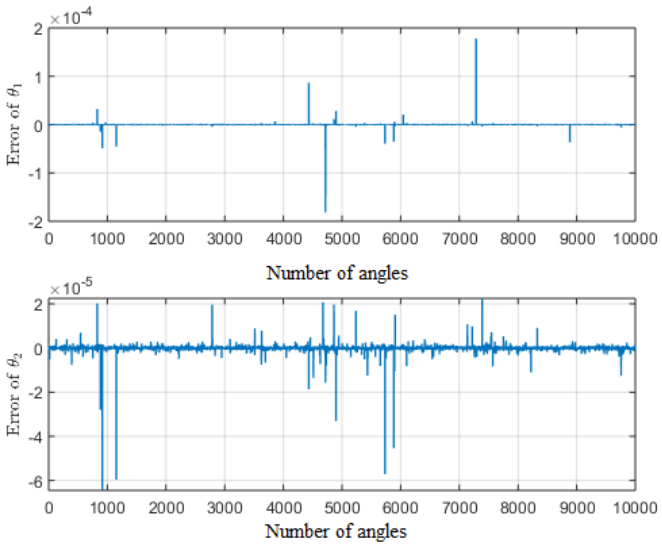

Figure. 3.24: Test results of the obtained model for the two-section continuum robot

Figure 3.26 shows that the considered two-section continuum robot with variable curvature can accurately follow the linear trajectory expressed by equation (3.20). It is noteworthy to say that each position on the linear trajectory can be reached by the robot's end-effector through at least three configurations (redundancy), as it is shown in Figure 3.25. Therefore, only one existing configuration (solution) is taken

which allows the robot to track the linear trajectory and that can be achieved by adding constraints to the objective function during the learning phase according to many norms such as velocity sensitivity and minimum curvature, etc. In this work, the minimum curvature norm is chosen with the aim of keeping the robot from more undesirable curvatures. To emphasize, through the added constraints only one solution can be considered which allows the robot to reach the specific position through one configuration as shown in Figure 3.26.

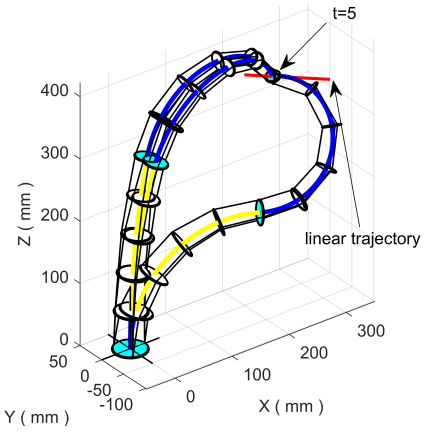

Figure. 3.25: Possible solutions for each desired point on the linear trajectory (redundancy)

$$X = 10t + 200; \quad Y = 0; \quad Z = 370 - 4t \tag{3.20}$$

with $t = 0 : 0.1 : 15$

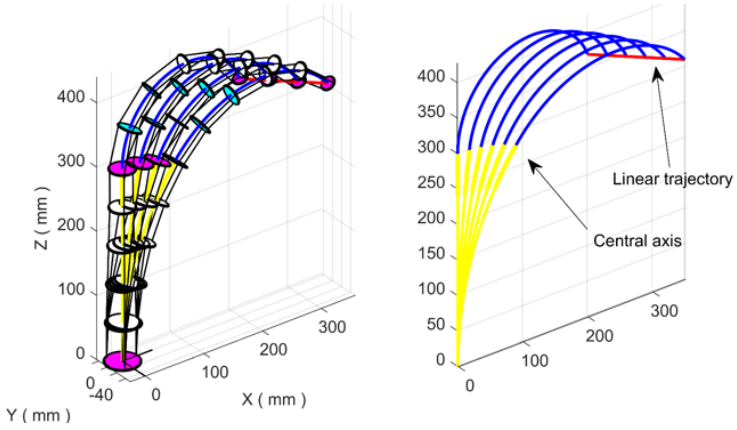

Figure. 3.26: (Right) Different configurations for the robot following the linear trajectory; (Left) Central axis of the robot following the linear trajectory

The euclidean error between the generated and the desired linear trajectory is shown in Figure 3.27.

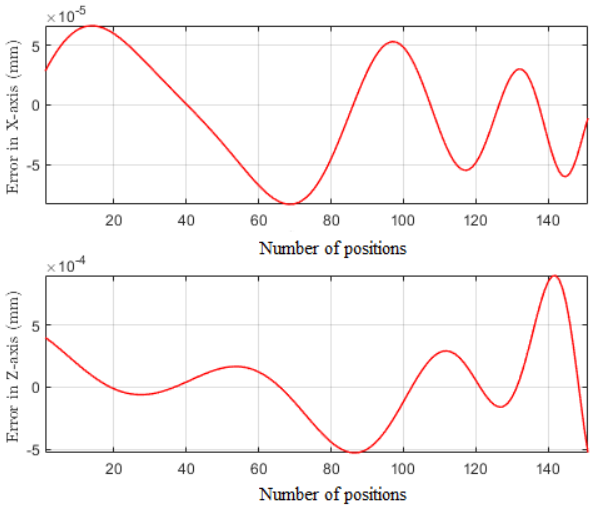

Figure. 3.27: Euclidean errors between the desired and the obtained trajectory (linear trajectory)

In the last simulation, an arc-shaped trajectory is followed up by a two-section continuum robot as shown in Figure 3.28. This kind of trajectory is deliberately used since it allows the robot to considerably bend and in order to assess the NN when dealing with large bending angles. Furthermore, the cables length are calculated based on the bending angles (Figure 3.30) which are provided by the obtained NN as it is shown in Figure 3.31.

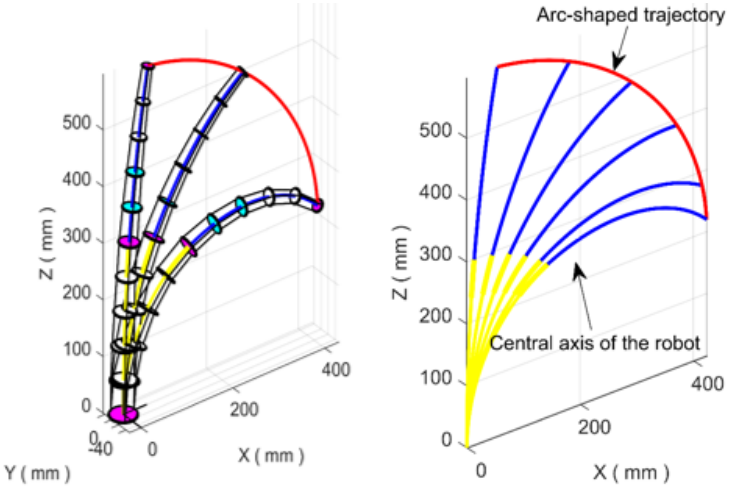

Figure. 3.28: (Right) Different configuration for the robot following the arc-shaped trajectory; (Left) Central axis of the robot following the arc-shaped trajectory

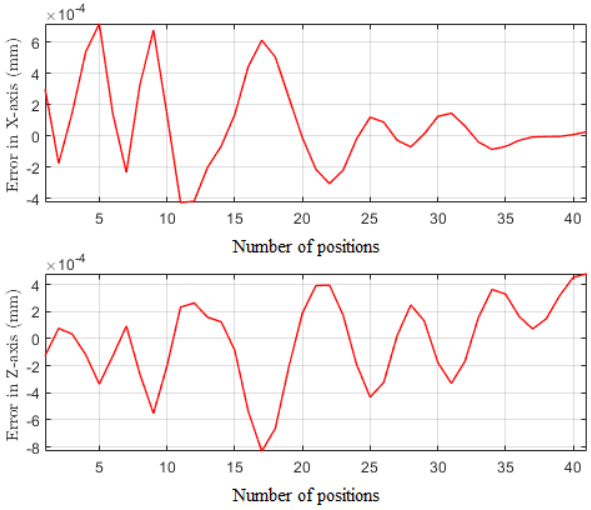

Figure. 3.29: Euclidean errors between the desired and the obtained trajectory (arc-shaped) for the two-section continuum robot

Although the tackled trajectory which is shown in Figure 3.28 is relatively difficult compared to the previously proposed trajectories, the NN IKM gives satisfactory tracking accuracy (Figure 3.29).

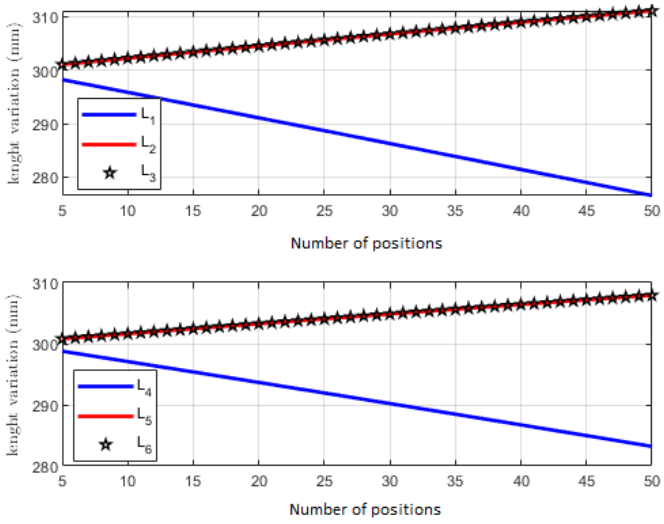

Figure. 3.30: Lengths Variation of the two-section continuum robot while tracking the arc-shaped trajectory

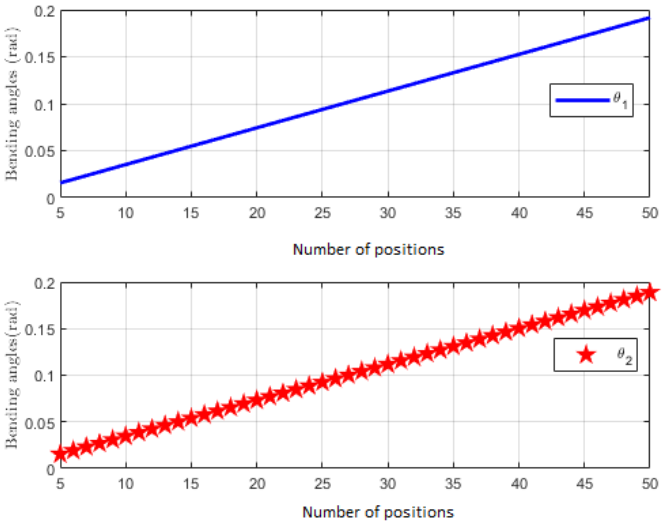

Figure. 3.31: Needed bending angles for the two-section continuum robot following the arc-shaped trajectory

3.5 Conclusion

In this chapter, the teaching learning based optimization algorithm was adopted to build the inverse kinematic model of a two-section continuum robot as well as the IKM of three-section continuum robot with variable length. The accuracy and the efficiency of the proposed algorithm were evaluated by considering several trajectories with and without the presence of static obstacles. The obtained results have showed the effectiveness of the proposed algorithm in solving the inverse kinematic model of the variable length continuum robot. Additionally, the used algorithm is not fussy and does not require any specific parameters to be tuned up.

in the second section, an artificial neural network was used to obtain the inverse kinematic model of a spatial single section continuum robot as well as a planar two-section continuum robot with variable curvature. To evaluate the efficiency of the obtained neural model, various types of trajectories were considered. It is found that the developed neural model is a powerful tool to deal with the high complexity of continuum robots' inverse kinematic models, in particular when it comes to solving the inverse kinematic model of variable curvature continuum robots. Moreover, it is a needed tool for real time application since it does not depend on the complexity inverse kinematic models.

CHAPTER 4

DYNAMIC MODELING AND CONTROL

4.1 Introduction

the dynamic modeling and control of continuum robots, are quite complicated due to their infinite degrees of freedom, particularly variable curvature continuum robots. In this chapter a simplified dynamic model for a variable curvature continuum robot is thoroughly developed based on Euler-Lagrange method. for the sake of narrowing down the number of the generated coordinates in the equation of motion an approximate formula relating each unit of the robot is integrated in the dynamic model. Then, an Optimized Proportional Integral Derivative (OPID) controller is designed to control the developed dynamic model. After that, to achieve satisfactory performance an optimized nonlinear sliding mode control algorithm (ONSMC) is developed for the sake of controlling a continuum robot with constant curvature. Furthermore, the performance of the proposed controller is compared with an optimized proportional integral derivative controller and an optimized sliding mode control scheme.

4.2 Dynamic modeling of a single section continuum robot with variable curvature

In this section, we present the forward dynamic model of a VC continuum robot with a single section ($k = 1$) composed of 5 units using the Lagrange-Euler method. The bending and orientation angles represent the generalized coordinates. The equation of

motion of a VC continuum robot can be expressed as follows:

$$\begin{cases} \frac{d}{dt}\left(\frac{dT}{\partial\dot{\theta}_{j,k}}\right) - \frac{dT}{\partial\theta_{j,k}} + \frac{\partial U}{\partial\theta_{j,k}} = Q_1 \\ \frac{d}{dt}\left(\frac{dT}{\partial\dot{\varphi}_k}\right) - \frac{dT}{\partial\varphi_k} + \frac{\partial U}{\partial\varphi_k} = Q_2 \end{cases} \tag{4.1}$$

where Q_1 and Q_2 are the generalized forces, T is the total kinetic energy of the robot, U is the total potential energy of the robot, $\theta_{j,k}$ is the bending angle for each unit, ϕ_k is the orientation angle for the whole section

For a VC continuum robot, each unit has its own bending angle, thus different generalized coordinates are considered. On the other hand, if we use the previously developed equation as in [77], in which the bending angles of the robot's units are expressed in function of the robot's first bending angle (first unit), the generalized coordinates will be reduced to a single generalized coordinate $\theta_{1,k}$, which can be mathematically expressed as follows [77]:

$$\theta_{j,k} = \frac{r_{1,k}}{r_{j,k}}\theta_{1,k} \tag{4.2}$$

4.2.1 Kinetic and potential energy

The kinetic energy of the robot under consideration resides in the flexible backbone as well as the disks. As mentioned before, the flexible backbone is composed of a concatenation of units, each unit has its own bending angle. Thus, the kinetic energy of the backbone is the sum of the kinetic energy of each unit.

Each point on the central axis of the flexible unit (j,k) is specified by the curvilinear abscissa ' h' which represents the length from the origin of the reference frame $o_{j,k-1}$ to the specified point (Figure 4.1).

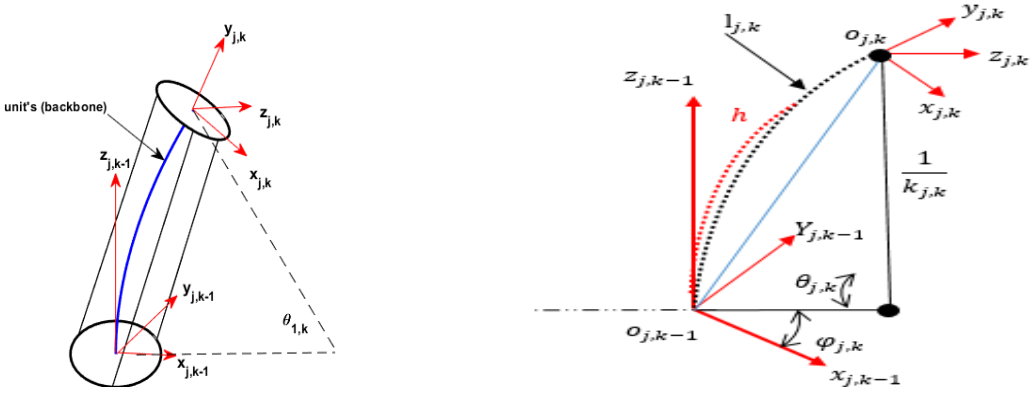

Figure. 4.1: (Left) Unit representation; (Right) Unit central axe description

where k is the curvature, $ł_{i,k}$ refers to the length of the unit's arc, h is the position for each point located on the central axis at each unit. The position vector $U_{j,k}$ of any point distant from the origin of the reference frame can be expressed as follows:

$$U_{j,k} = \begin{cases} x_{U_{j,k}}(h) = \frac{h_{U_{j,k}}}{\theta\left(h_{U_{j,k}}\right)}\left(1-\cos\left(\theta\left(h_{U_{j,k}}\right)\right)\right)\cos(\varphi_k) \\ y_{U_{j,k}}(h) = \frac{h_{U_{j,k}}}{\theta\left(h_{U_{j,k}}\right)}\left(1-\cos\left(\theta\left(h_{U_{j,k}}\right)\right)\right)\sin(\varphi_k) \\ z_{U_{j,k}}(h) = \frac{h_{U_{j,k}}}{\theta\left(h_{U_{j,k}}\right)}\sin\left(\theta\left(h_{U_{j,k}}\right)\right) \end{cases} \tag{4.3}$$

With $\theta\left(h_{U_{j,k}}\right) = \frac{h_{U_{j,k}}\theta_{j,k}}{l_{j,k}}$ and $h_{U_{j,k}}$ refers to the arc length at h point. The linear velocity of any point h away from the origin can be calculated by differentiation with respect to time:

$$v_{h,j} = \begin{cases} \dot{x}_{U_{j,k}}(h) = \dot{\theta}_{j,k}\left[\frac{h_{U_{j,k}}}{\theta_{j,k}}\sin\left(\frac{h_{U_{j,k}}}{l_{j,k}}\theta_{j,k}\right) - \frac{l_{j,k}}{\theta_{j,k}^2}H\right]\cos(\varphi_k) - \frac{l_{j,k}}{\theta_{j,k}}H\dot{\varphi}_k \\ \dot{y}_{U_{j,k}}(h) = \dot{\theta}_{j,k}\left[\frac{h_{U_{j,k}}}{\theta_{j,k}}\sin\left(\frac{h_{U_{j,k}}}{l_{j,k}}\theta_{j,k}H\right) - \frac{l_{j,k}}{\theta_{j,k}^2}\right]\sin(\varphi_k) - \frac{l_{j,k}}{\theta_{j,k}}H\dot{\varphi}_k \\ \dot{z}_{U_{j,k}}(h) = \dot{\theta}_{j,k}\left[\frac{h_{U_{j,k}}}{\theta_{j,k}}\cos\left(\frac{h_{U_{j,k}}}{l_{j,k}}\theta_{j,k}\right) - \frac{l_{j,k}}{\theta_{j,k}^2}\sin\left(\frac{h_{U_{j,k}}}{l_{j,k}}\theta_{j,k}\right)\right] \end{cases} \tag{4.4}$$

with $H = 1-\cos\left(\frac{h_{U_{j,k}}}{l_{j,k}}\theta_{j,k}\right)$.

The kinetic energy of the flexible backbone is given by :

$$T_b = \sum_{j=1}^{n=5}\frac{1}{2}m_b\int_0^{l_{j,k}}\left(\left(\dot{x}_{U_{j,k}}(h)\right)^2 + \left(\dot{y}_{U_{j,k}}(h)\right)^2 + \left(\dot{z}_{U_{j,k}}(h)\right)^2\right)dh \tag{4.5}$$

where n is the unit's number and m_b is the mass of the flexible backbone.

For the kinetic energy of the disks, it can be obtained using equation (4.6). Since each unit has its own bending angle, the kinetic energy for each unit is considered. Thus, the total kinetic energy of the disks can be expressed as follows:

$$T_d = \frac{1}{2}\sum_{j=1}^{5} v_{h,j}^T m_j v_{h,j} \tag{4.6}$$

where m_j is the mass of each disk.

The total kinetic energy of a single section is given by:

$$T = T_b + T_d \tag{4.7}$$

For potential energy, the flexible backbone can be virtually divided into a series of a flexible backbones (arcs) where each flexible arc has its own bending angle $\theta_{j,k}$. As long as the disks have a low weight, we can only consider the potential energy of the backbone, which can be considered as follows:

$$E_p = \frac{EI_b}{2L} \sum_{i=1}^{5} \theta_{j,k}^2 \quad , \qquad (k = 1) \tag{4.8}$$

The parameters of the considered continuum robot which are used to calculate its kinetic and potential energy are defined in Table 4.1.

Table 4.1: The parameters of the considered section

Robot parameters	Description	values
L	The length of the robot's backbone	0.800 m
g	Gravity	9.81 m/s^2
E	Young modulus	210 GPa
I_b	Backbone's moment of inetia	1.257 10^{-11} m^4
m_b	Mass of the backbone	32,6 10^{-3} kg
r	Radial distance of the applied force	19 mm
m_1	Mass of disk 1 (base)	50 10^{-4} kg
m_2	Mass of disk 2	40 10^{-4} kg
m_3	Mass of disk 3	30 10^{-4} kg
m_4	Mass of disk 4	20 10^{-4} kg
m_5	Mass of disk 5	10 10^{-4} kg
d_b	Diameter of the backbone	4 10^{-3} m
r_1	radius of disk 1 (base)	25 mm
r_2	radius of disk 2	23.5 mm
r_3	radius of disk 3	22 mm
r_4	radius of disk 4	20.5 mm
r_5	radius of disk 5	19 mm

4.2.2 Generalized forces

The generalized forces are given by [67] :

$$\begin{cases} Q_1 = F_1 r\cos(\gamma_1-\varphi) + F_2 r\cos(\gamma_2-\varphi) \\ Q_2 = F_1 r\sin(\gamma_1-\varphi) + F_2 r\sin(\gamma_2-\varphi) \end{cases} \tag{4.9}$$

where F_1 and F_2 are the applied forces, φ the orientation angle, $\gamma_1 = 0$ and $\gamma_2 = \frac{2\pi}{3}$.

4.2.3 Dynamic model

The equation of motion is given as follows:

$$M_t \begin{bmatrix} \ddot{\theta} \\ \ddot{\varphi} \end{bmatrix} + C_t \begin{bmatrix} \dot{\theta}^2 \\ \dot{\theta}\dot{\varphi} \\ \dot{\varphi}^2 \end{bmatrix} + K_t \begin{bmatrix} \theta \\ \varphi \end{bmatrix} = D_t \begin{bmatrix} F_1 \\ F_2 \end{bmatrix} \tag{4.10}$$

where:

$$M_t = \begin{bmatrix} M_{11} & M_{12} \\ M_{21} & M_{22} \end{bmatrix},\ C_t = \begin{bmatrix} C_{11} & C_{12} & C_{13} \\ C_{21} & C_{22} & C_{23} \end{bmatrix},\ K_t = \begin{bmatrix} K_{11} & K_{12} \\ K_{21} & K_{22} \end{bmatrix}$$
$$D_t = \begin{bmatrix} D_{11} & D_{12} \\ D_{21} & D_{22} \end{bmatrix}$$

Applying the Euler-Lagrange formalism (4.1), Taylor expansions, and using the obtained equations of the kinetic energy (4.5),(4.6),(4.7) and the potential energy (4.8) and the generalized forces (4.9), the elements of the motion equation are given as follows:

$$\begin{aligned} M_{11} =& \frac{9739\,L^2\,\mathrm{m_1}}{16918} + \frac{L^3\,\mathrm{m_b}}{154} - \frac{163\,L^2\,\theta^2\,\mathrm{m_2}}{10000} + \frac{4\,L^2\,\theta^2\,\mathrm{m_3}}{29} + \frac{2000\,L^2\,\theta^4\,\mathrm{m_4}}{34657} \\ &+ \frac{21897\,L^4\,\theta^3\,\mathrm{m_5}}{472109} - \frac{L^3\,\theta^2\,\mathrm{m_b}}{396} + \frac{L^3\,\theta^4\,\mathrm{m_b}}{21911} \end{aligned}$$

$$\begin{aligned} M_{22} =& \frac{\mathrm{m_5}\,L^4\,\theta^3}{19991} - \frac{\mathrm{m_b}\,L^3\,\theta^4}{122} + \frac{\mathrm{m_b}\,L^3\,\theta^2}{100} - \frac{330513\,\mathrm{m_1}\,L^2\,\theta^4}{6505015} + \frac{61938\,\mathrm{m_3}\,L^2\,\theta^3}{2299369} \\ &+ \frac{467\,\mathrm{m_2}\,L^2\,\theta^2}{1058} + \frac{\mathrm{m_4}\,L^2\,\theta}{145678} \end{aligned}$$

$$M_{12} = M_{21} = 0$$

$$C_{11} = -\frac{\mathrm{m_b}\, L^3 \theta^5}{839204} + \frac{\mathrm{m_b}\, L^3 \theta^3}{18769} - \frac{126\,\mathrm{m_3}\, L^3 \theta^2}{10000} - \frac{\mathrm{m_b}\, L^3 \theta}{381} + \frac{2.1010\,\mathrm{m_5}\, L^2 \theta^5}{100000} + \frac{1.1364\,\mathrm{m_4}\, L^2 \theta^4}{14286000} + \frac{6.5829\,\mathrm{m_2}\, L^2 \theta^3}{10000} - \frac{200000\,\mathrm{m_1}\, L^2 \theta}{12300403}$$

$$C_{13} = -\frac{17862\,\mathrm{m_4}\, L^4 \theta^3}{282109} - \frac{\mathrm{m_b}\, L^3 \theta^5}{364} + \frac{\mathrm{m_b}\, L^3 \theta^3}{119} + \frac{15983\,\mathrm{m_5}\, L^3 \theta^2}{28982109} - \frac{\mathrm{m_b}\, L^3 \theta}{115} - \frac{138\,\mathrm{m_3}\, L^2 \theta^5}{10000} + \frac{591879\,\mathrm{m_2}\, L^2 \theta^3}{5030069} - \frac{2807\,\mathrm{m_1}\, L^2 \theta}{4700}$$

$$C_{22} = \frac{\mathrm{m_b}\, L^3 \theta^5}{383} - \frac{\mathrm{m_b}\, L^3 \theta^3}{30} + \frac{281\,\mathrm{m_5}\, L^3 \theta^2}{203196} + \frac{\mathrm{m_b}\, L^3 \theta}{69} + \frac{214\,\mathrm{m_2}\, L^2 \theta^5}{10000} - \frac{670011\,\mathrm{m_1}\, L^2 \theta^3}{2210041} - \frac{19337\,\mathrm{m_4}\, L^2 \theta^2}{10000} + \frac{1978\,\mathrm{m_3}\, L^2 \theta}{21129}$$

$$C_{12} = C_{21} = C_{23} = 0$$

$$K_{11} = \frac{32573\, E\, \mathrm{I_b}}{10000\, L}$$

$$K_{12} = K_{21} = K_{22} = 0$$

$$D_{11} = r\cos(\gamma_1 - \varphi)$$

$$D_{12} = r\cos(\gamma_2 - \varphi)$$

$$D_{21} = r\sin(\gamma_1 - \varphi)$$

$$D_{22} = r\sin(\gamma_1 - \varphi)$$

A state variable representation of the dynamic robot can be obtained by adoption the following state variable:

$$\begin{cases} x_1(t) = \theta \\ x_2(t) = \dot{\theta} \\ x_3(t) = \varphi \\ x_4(t) = \dot{\varphi} \end{cases} \tag{4.11}$$

Using equation (4.10), we can write:

$$\begin{cases} M_{11}\ddot{\theta} + C_{11}\dot{\theta}^2 + C_{13}\dot{\varphi}^2 + K_{11}\theta = D_{11}F_1 + D_{12}F_2 \\ M_{22}\ddot{\varphi} + C_{22}\dot{\theta}\dot{\varphi} = D_{21}F_1 + D_{22}F_2 \end{cases} \tag{4.12}$$

By substituting equation (4.11) in (4.12) we will have:

$$\begin{aligned}\ddot{\theta} =& \frac{D_{11}F_1 + D_{12}F_2 - C_{11}\dot{\theta}^2 - C_{13}\dot{\varphi}^2 - K_{11}\theta}{M_{11}} \\ =& \frac{D_{11}F_1 + D_{12}F_2 - C_{11}x_2^2 - C_{13}x_4^2 - K_{11}x_1}{M_{11}}\end{aligned} \tag{4.13}$$

and :

$$\begin{aligned}\ddot{\varphi} =& \frac{D_{21}F_1 + D_{22}F_2 - C_{22}\dot{\theta}\dot{\varphi}}{M_{22}} \\ =& \frac{D_{21}F_1 + D_{22}F_2 - C_{22}x_2x_4}{M_{22}}\end{aligned} \tag{4.14}$$

If we derive $x_2(t)$ and $x_4(t)$, the acceleration can be written as follows :

$$\begin{cases} \dot{x}_2(t) = \ddot{\theta} \\ \dot{x}_4(t) = \ddot{\varphi} \end{cases} \tag{4.15}$$

Finally, equation (4.11) can be written as follows:

$$\begin{cases} \dot{x}_1 = x_2 \\ \dot{x}_2 = \frac{1}{M_{11}}\left(D_{11}F_1 + D_{12}F_2 - C_{11}x_2^2 - C_{13}x_4^2 - K_{11}x_1\right) \\ \dot{x}_3 = x_4 \\ \dot{x}_4 = \frac{1}{M_{22}}\left(D_{21}F_1 + D_{22}F_2 - C_{22}x_2x_4\right) \end{cases} \tag{4.16}$$

For the sake of validating the developed dynamic model of a variable curvature continuum robot, simulation examples through matlab are carried out and presented in the following sections.

4.2.4 Simulation examples

The Runge Kutta method is used to solve the state model given by equation (4.16) In the first example, the continuum robot is initially inclined by a bending angle of $\theta = \frac{\pi}{8}$ without any tension on its cables.

After the robot reaches the given bending angle ($\pi/8$), it is released. Basically, the flexibility of the robot's backbone helps it to bend according to the needed position.

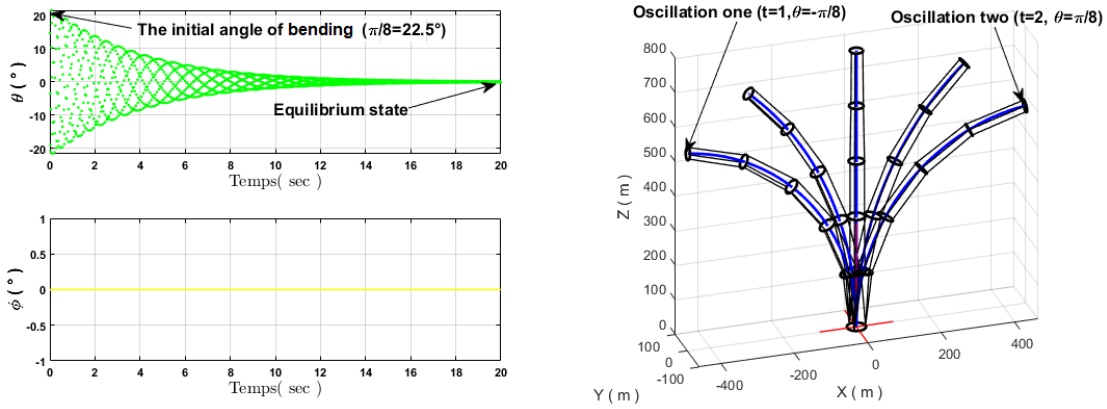

Figure. 4.2: (Left) Oscillation of the bending angle for $\theta = \frac{\pi}{8}$ and $\varphi = 0$; (Right) Visualization of the robot's oscillations

After releasing the robot, it clearly oscillates from 22.5 to -22.5 degree (see Figure 4.2). Just right after this maximum level of θ that the robot can reach, it is observed that the robot's oscillation starts to decrease until it stabilizes at roughly 18 seconds as shown in Figure 4.2.

For the second simulation example, a force equal to 3N is applied on the robot's first cable, after releasing it we can observe that the robot takes the equilibrium position given by $\theta = 32.6$ degrees, as shown in Figure 4.3.

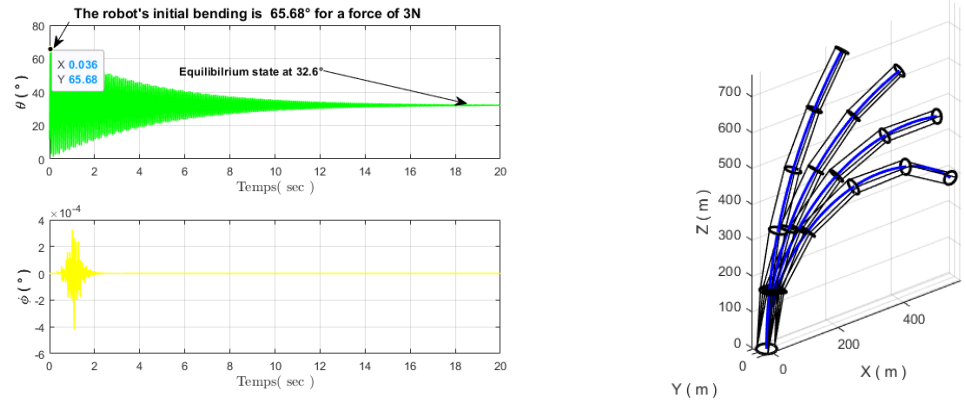

Figure. 4.3: (Left) Oscillations at the bending angle when subjected to a force of 3N on one of its cables ; (Right) Visualization of the robot's oscillations

It should be noted that when implementing the Runge-Kutta method for solving the matrix system defined by equation (4.16), we deliberately assumed that the robot

initially bends by an angle of pi/5000 which is approximately equal to zero for the sake of avoiding the non-convergence of the used method. This can be noticed in Figure 4.3, namely the robot is initially tilted by an angle of pi/5000 (0.036 degree) before applying the force.

4.3 Continuum robot control

4.3.1 Optimized PID controller for a VL continuum robot

The PID controller does not require a perfect knowledge of the robot's parameters to properly operate. Thanks to its intuitiveness and relative simplicity, it has become the standard controller in industrial environments. It has a good response to unmeasured and unexpected disturbances. In order to control the continuum robot's end effector, a discrete PID controller is implemented using the transformations as follows:

$$\begin{aligned} F_1(k+1) &= F_1(k) + \left(K_{p1} + k_{i1}\tfrac{T_s}{2} + \tfrac{k_{d1}}{T_s}\right) e_1(k) \\ &+ \left(-k_{p1} + k_{i1}\tfrac{T_s}{2} - \tfrac{2k_{d1}}{T_s}\right) e_1(k-1) + \tfrac{k_{d1}}{T_s} e_1(k-2) \end{aligned} \tag{4.17}$$

$$\begin{aligned} F_2(k+1) &= F_2(k) + \left(K_{p2} + k_{i2}\tfrac{T_s}{2} + \tfrac{k_{d2}}{T_s}\right) e_2(k) \\ &+ \left(-k_{p2} + k_{i2}\tfrac{T_s}{2} - \tfrac{2k_{d2}}{T_s}\right) e_2(k-1) + \tfrac{k_{d2}}{T_s} e_2(k-2) \end{aligned} \tag{4.18}$$

where : F_1 and F_2 are the applied forces on the robot's cables and e_1, e_2 are the error signal between the reference trajectory $R_{\theta_i}(k)$ and the output signal $\theta_i(k)$. T_s is the sampling time. To find the best values of K_{p1}, K_{i1}, K_{d1}, K_{p2}, K_{i2}, K_{d2}, adaptive particle swarm optimization is used with following minimized cost function:

$$F = \sum_{k=1}^{samples} (R_{\theta_i}(k) - \theta_i(k))^2, \qquad i = 1,2 \tag{4.19}$$

In this part, a spatial single section with variable curvature is considered to follow a sinusoidal trajectory. Basically, the PID controller developed for this section is based on the dynamic model obtained previously and defined by equation (4.10).

Table 4.2: Obtained values of the PID controllers for the VC single section using the PSO algorithm

The obtained paramters by PSO	Values
K_{p1}	17.4
K_{i1}	39
K_{d1}	2.1
K_{p2}	20
K_{i2}	28
K_{d2}	0.36

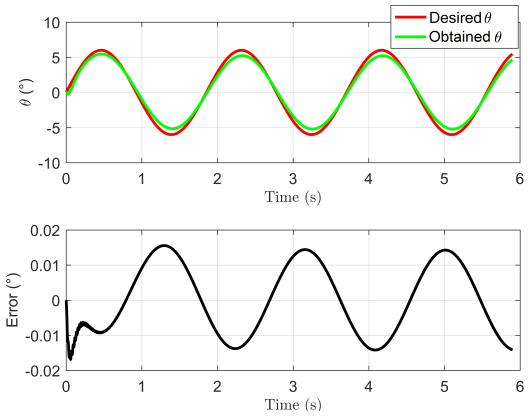

Figure. 4.4: Obtained and desired bending angles for the VC single section continuum robot using the optimized PID

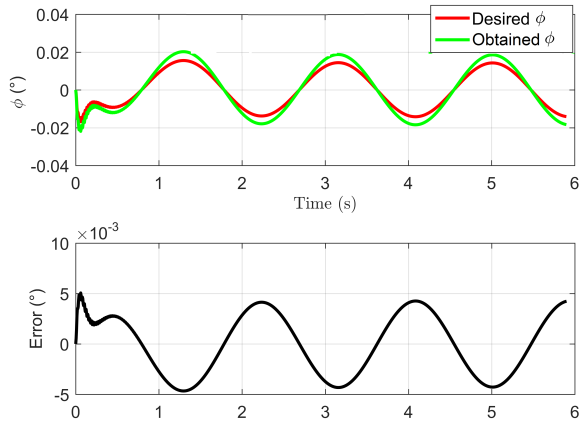

Figure. 4.5: Obtained and desired orientation angles for the VC single section continuum robot using the optimized PID

As shown in Figures 4.4 and 4.5, the obtained and desired angles for the considered single section continuum robot are approximately the same.

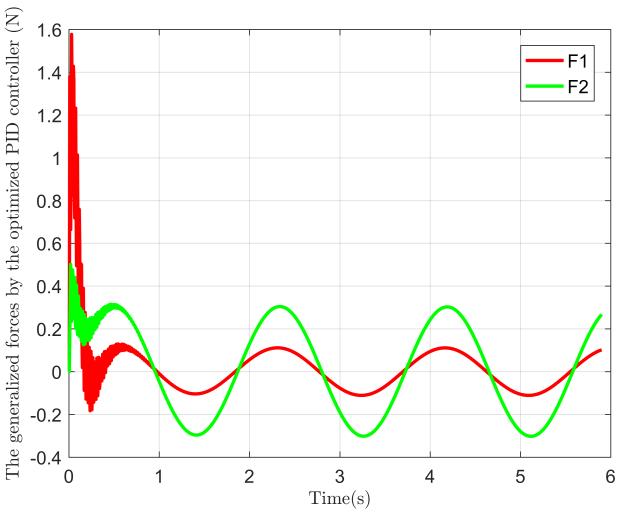

Figure. 4.6: Obtained control using the optimized PID controllers for the VC single section continuum robot

4.3.2 Optimized nonlinear sliding mode controller of multi-section continuum robot with constant curvature

In this section, we consider the control of the two-section continuum robot described in [125].

The dynamic model of this robot is given by [125]:

$$\begin{bmatrix} M_{11} & M_{12} \\ M_{21} & M_{22} \end{bmatrix} \begin{bmatrix} \ddot{\theta}_1 \\ \ddot{\theta}_2 \end{bmatrix} + \begin{bmatrix} C_{11} & C_{12} & C_{13} \\ C_{21} & C_{22} & C_{23} \end{bmatrix} \begin{bmatrix} \dot{\theta}_1^2 \\ \dot{\theta}_1\dot{\theta}_2 \\ \dot{\theta}_2^2 \end{bmatrix} + \begin{bmatrix} K_1 \\ K_2 \end{bmatrix} = \begin{bmatrix} Q_1 \\ Q_2 \end{bmatrix} \quad (4.20)$$

and its parameters value are defined in Table 4.3.

Table 4.3: The continuum robot's parameters [125]

Robot parameters	Description	values
L	The length of the robot's backbone	0.3 m
m	The mass of the disks	0.01 Kg
g	Gravity	9.81 m/s^2
E	Young modulus	2.1 10^{11} Pa
I_b	Inertia moment of the backbone	3.97 10^{-12} m^4
I_{xx}	Inertia moment of the disks	3.06 10^{-7} m^4

4.4 Controller design

In this subsection, an optimized nonlinear sliding mode control for the two-section continuum robot described by the dynamic model given by equation (4.20). The control bloc diagram of the considered continuum robot is given by Figure 4.7, where two controllers are used to control the robot's position so that the angles θ_1 and θ_2 track their desired reference trajectories R_{θ_1} and R_{θ_2}. The control laws U_1 and U_2 (control forces) are obtained as follows:

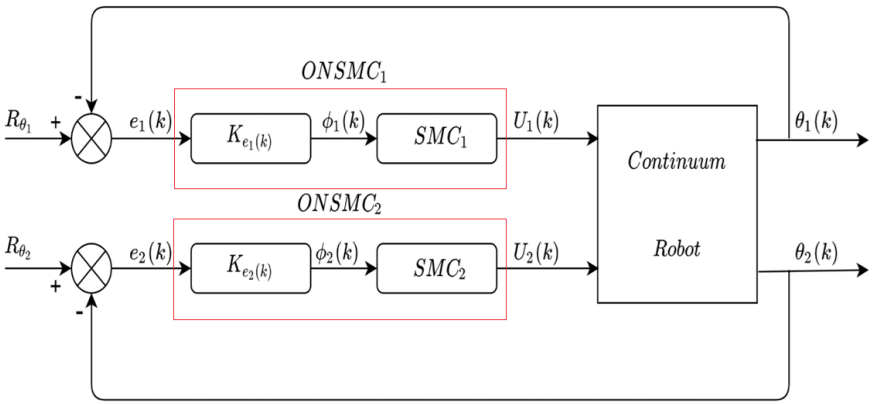

Figure. 4.7: Continuum robot control block diagram

The conventional Sliding Mode Control (SMC) law is given by:

$$S(t) = \lambda e(t) + \dot{e}(t) \tag{4.21}$$

$$U(t) = S(t)sign(\phi)K \tag{4.22}$$

where:
$S(t)$ is the sliding mode surface, $e(t)$ is the tracking error, λ, ϕ and K are constant gains. The discrete version of the SMC is given as follows:

$$S(k) = \lambda e(k) + \frac{e(k) - e(k-1)}{T_s} \tag{4.23}$$

$$U(k) = S(k)sign(\phi)K \tag{4.24}$$

where: T_s is the sampling time.

To enhance the robustness and the accuracy of the controller against external disturbances, the feedback error is reformulated, using a proposed nonlinear function,

as follows:

$$S(k) = \lambda\varphi(k) + \frac{\varphi(k) - \varphi(k-1)}{T_s} \tag{4.25}$$

Such that:

$$\varphi(k) = K_e(k)e(k) \tag{4.26}$$

$$K_e(k) = \beta\frac{exp(\alpha e(k)) + exp(-\alpha e(k))}{2} \tag{4.27}$$

where: $\alpha \in [0 \quad 1]$ and β are constants.
Finally, to control the position of each section of the considered robot, the ONSMC is implemented as follows:

$$\begin{cases} U_1(k) = S_1(k)sign(\phi_1)K_1 \\ U_2(k) = S_2(k)sign(\phi_2)K_2 \end{cases} \tag{4.28}$$

where:

$$\begin{cases} S_1(k) = \lambda_1\varphi_1(k) + \dfrac{\varphi_1(k) - \varphi_1(k-1)}{T_s} \\ \varphi_1(k) = K_{e_1}(k)e_1(k) \\ K_{e_1}(k) = \beta_1\dfrac{exp(\alpha_1 e_1(k)) + exp(-\alpha_1 e_1(k))}{2} \end{cases} \tag{4.29}$$

$$\begin{cases} S_2(k) = \lambda_2\varphi_2(k) + \dfrac{\varphi_2(k) - \varphi_2(k-1)}{T_s} \\ \varphi_2(k) = K_{e_2}(k)e_2(k) \\ K_{e_2}(k) = \beta_2\dfrac{exp(\alpha_2 e_2(k)) + exp(-\alpha_2 e_2(k))}{2} \end{cases} \tag{4.30}$$

The main objective from developing the proposed control ONSMC by reformulating the feedback error as a non-linear function, is to give the system faster response, accuracy, and better robustness, especially when the system is subjected to unwanted external disturbances. To implement the control scheme illustrated in Figure 4.7 and given by equations (4.29) and (4.30), the control parameters ($X_i = [\beta_i, \alpha_i, \lambda_i, \phi_i, K_i]^T, \quad i = 1, 2$) must be computed. To this end, the efficient adaptive particle swarm optimization [126] is adopted to obtain the value of the needed parameters. The minimized cost function is given by:

$$min_{X_i} J_i(X_i) = \sum_{k=1}^{samples} (R_{\theta_i}(k) - \theta_i(k))^2, \qquad i = 1, 2 \tag{4.31}$$

4.4.1 Control algorithm

For each controller $ONSMC_i$ (i=1,2) do the following steps:

1. Step 0: initialization

   - The reference trajectory R_{θ_i} is randomly chosen.
   - Choose the value of ϵ and k_{max} (the precision and the maximal iterations number).
   - $m = size(X_i), i = 1, 2$; the number of parameters of each controller.
   - Choose the number of particles n_p (population size).
   - Randomly generate the initial population (X_{ij}) of the adaptive PSO algorithm using the following equation:

     $$x_{ij}^{l} = rand, \quad i = 1, 2, \quad j = 1, ..., m, \quad l = 1, ..., n_p$$

     where $X_{ij} = [x_{ij}^{1}, x_{ij}^{2}, ..., x_{ij}^{n_p}]$, are n_p solutions of the j^{th} parameters of the controller i.
   - Set the initial velocity $(v_{ij}^{l} = 0; j = 1, 2, ..., m; l = 1, 2, ..., n_p)$, and choose the values of C_1, C_2.

2. Step 1: evaluation of the fitness of the entire population

   - Evaluate the fitness J_i for each solution $X_{ij}, j = 1, ..., m$, as follows
     - For $l = 1 : n_p$
       - $J_i^l = 0$ (the cost function of the solution l)
       - Use x_{ij}^{l} $(j = 1, ..., m)$ as the $ONSMC$ gains
       - For $k = 1 : samples$
         - Calculate the control effort using equation (4.28)
         - Apply the control effort to the system input
         - Evaluate the cost function as follows: $J_i^l = J_i^l + \left(R_{\theta_i}(k) - \theta_i^l(k)\right)^2$ θ_i^l is the angle that corresponds to the solution l
       - End
     - End

3. Step 2: personal best and global best updating

- Update the values of the personal best position $P_{ij}^{l}(j=1,\ldots,m)$ of each particle and the global best (G) of the entire population, as follows:
  - For $l=1:n_p$
    - If $J_i^l(x_{ij}^l) < J_i^l(P_{ij}^l), j=1,\ldots,m$
      - $P_{ij}^l = x_{ij}^l$
      - If $J_i^l(P_{ij}^l) < J_i^l(G_i)$
        $G_i = P_{ij}^l, j=1,\ldots,m$
      - End if
    - End if
  - End

4. Step 3: position updating

- Update the position $x_{ij}^{l}(j=1,\ldots,m)$ and the velocity $v_{ij}^{l}(j=1,\ldots,m)$ of each particle, as follows:
  - For $l=1:n_p$
    - Calculate the new position using the following equation: $x_{ij}^l = x_{ij}^l + v_{ij}^l, \quad j=1,\ldots,m$
    - Calculate the new velocity using the following equation: $v_{ij}^l = w\cdot v_{ij}^l + C_1\cdot r_1\cdot(P_{ij}^l - x_{ij}^l) + C_2\cdot r_2\cdot(G_i - x_{ij}^l), \quad j=1,\ldots,m$
  - End

5. Step 4: termination criteria

- If $J_i(G_i) < \epsilon$ or k_{max} is reached
  - Report the global best solution (G_i)
  - Exit
- Else
  - Go to step 1 to perform the next iteration

4.5 Results and Discussion

In this section, the control performance of the considered continuum robot using the proposed control algorithm is investigated. The optimized parameters of the ONSMC using the adaptive PSO algorithm are given in Table 4.4.

Table 4.4: Optimized parameters values of the ONSMC

Parameter	Value	Parameter	Value
β_1	-2.16	β_2	9.16
α_1	-0.76	α_2	0.95
λ_1	12.09	λ_2	85.27
Φ_1	0.41	Φ_2	0.23
K_1	11.57	K_2	0.72

To highlight the control performance of the proposed ONSMC controller, a comparative study of the proposed controller, the OSMC algorithm and the OPID controller is carried out. Considering different operating conditions, several simulations are conducted with the sampling time $T_s = 0.5\ ms$. In the first simulation, a multistep reference trajectory is chosen for both sections of the continuum robot. The obtained control results are shown in Figures 4.8, 4.9 and 4.10. Using the same initial conditions, the values of the Mean Squared Error (MSE) and the Mean Absolute Error (MAE) are computed for all considered controllers and given in Table 4.5. According to the obtained results, it is clear that the proposed controller gives better control performance than the OSMC and the OPID controller.

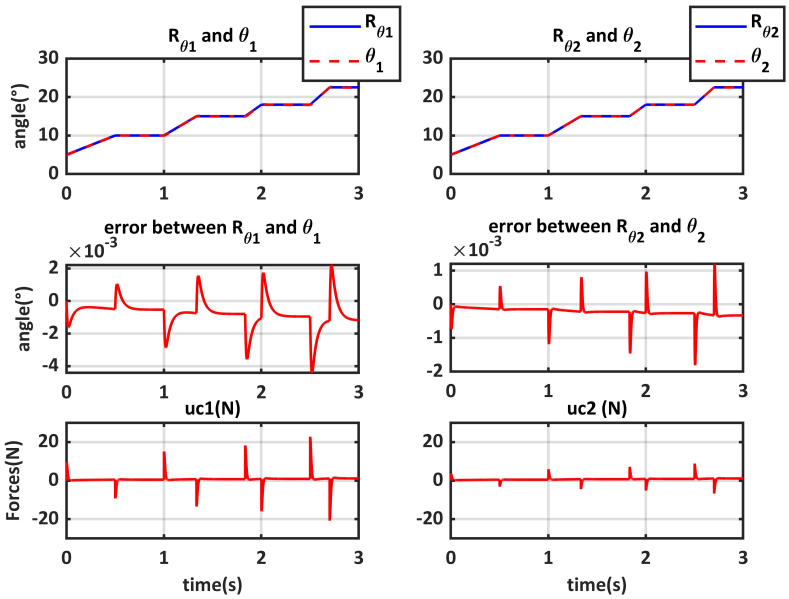

Figure. 4.8: ONSMC results of the continuum robot in case of multistep reference trajectory

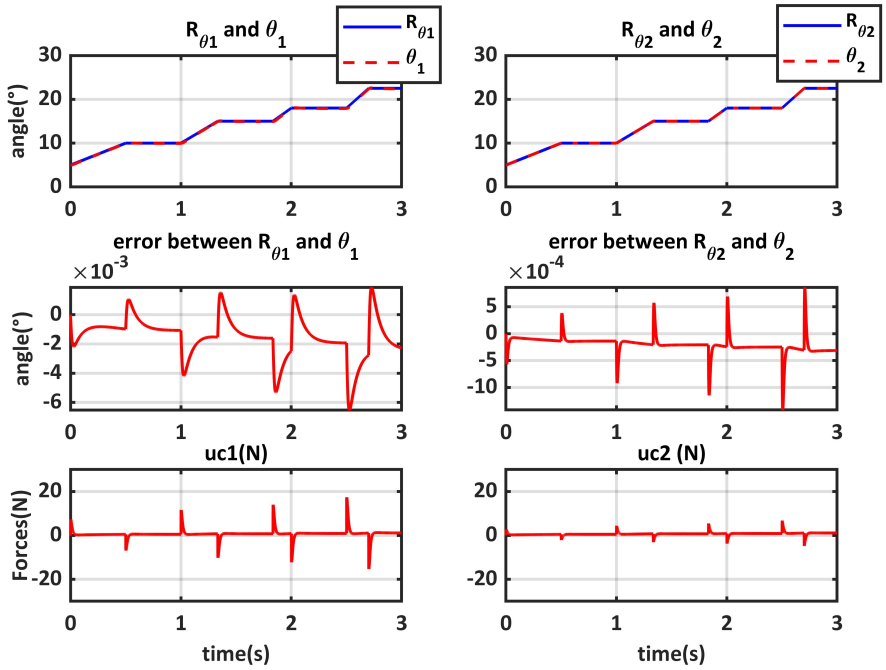

Figure. 4.9: OSMC results of the continuum robot in case of multistep reference trajectory

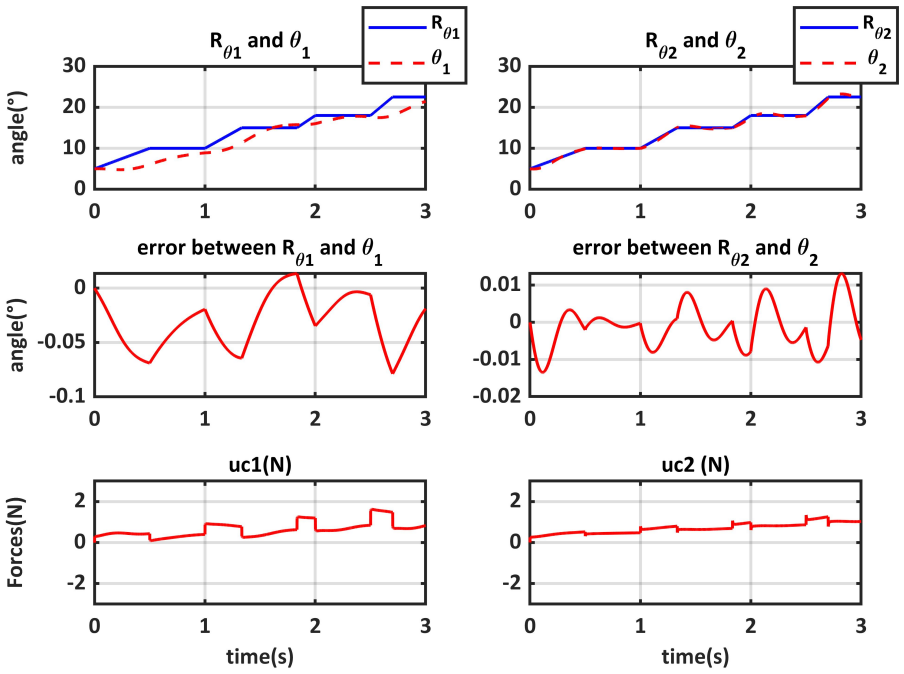

Figure. 4.10: OPID control results of the continuum robot in case of multistep reference trajectory

Table 4.5: MAE and MSE values in case of multistep reference trajectory

	MAE	MSE
ONSMC	7.4719	1.3616e-06
OSMC	12.2935	4.2126e-06
OPID	232.2291	0.0015

In the second case, a sinusoidal trajectory is chosen for both sections of the continuum robot. Starting from the same initial conditions, the control performance of the three considered controllers is shown in figures 4.11, 4.12 and 4.13. The MSE and the MAE values are given by Table 4.6. It is clear that the proposed ONSMC algorithm gives better control performance than the other ones.

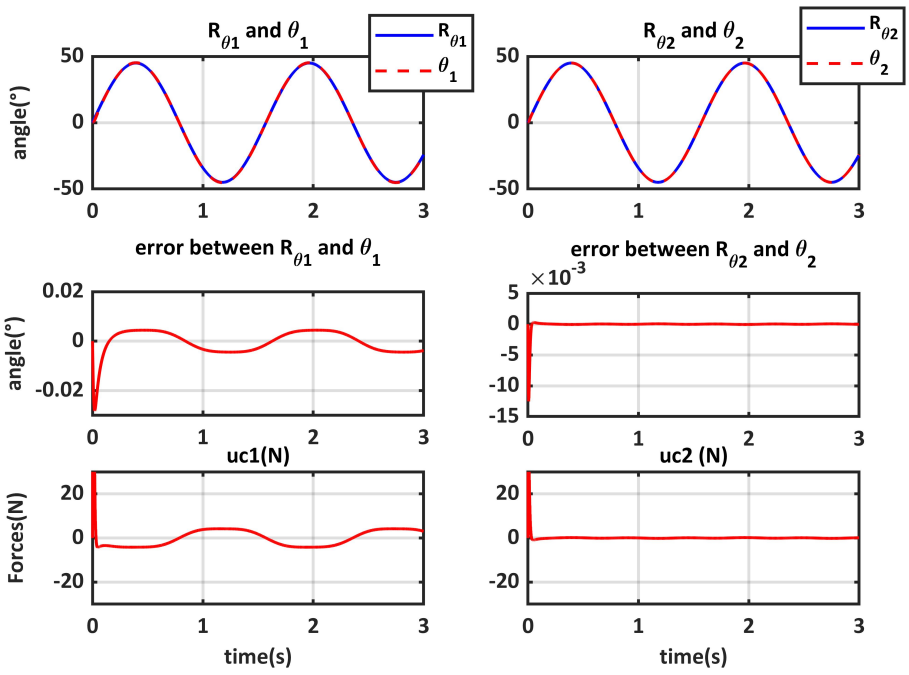

Figure. 4.11: ONSMC control results of the continuum robot in case of sinusoidal reference trajectory

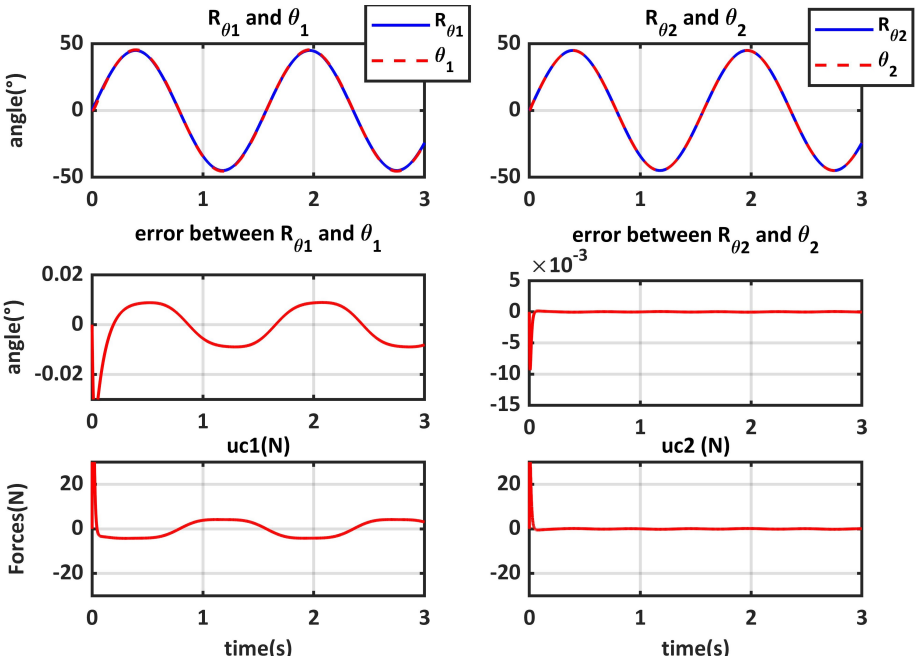

Figure. 4.12: OSMC control results of the continuum robot in case of sinusoidal reference trajectory

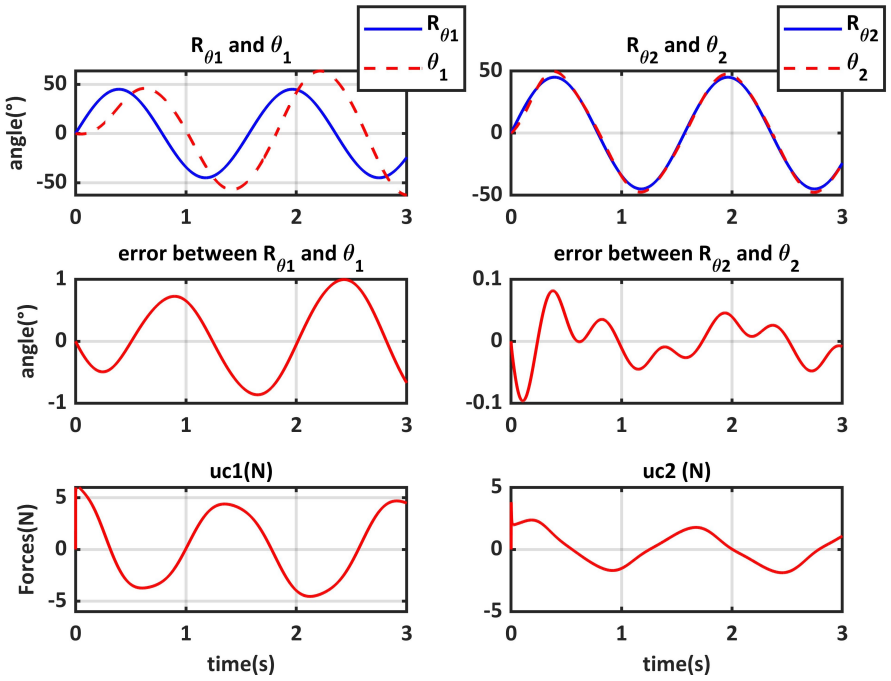

Figure. 4.13: OPID control results of the continuum robot in case of sinusoidal reference trajectory

Table 4.6: MSE and MAE values in case of sinusoidal reference trajectory

	MAE	MSE
ONSMC	22.8141	2.3069e-05
OSMC	43.2870	7.3141e-05
OPID	3.1898+03	0.0383

In the last simulation, the robustness of the ONSMC algorithm is investigated. A disturbance of 40% is added to the outputs of the continuum robot during the time interval $[1\ 2]s$ and a single step reference trajectory is chosen. The obtained results are given by figures 4.14,4.15 and 4.16 and the values of the MSE and the MAE are given in Table 4.7. It can be seen that the proposed controller compensates the imposed disturbance more rapidly than the other considered controllers.

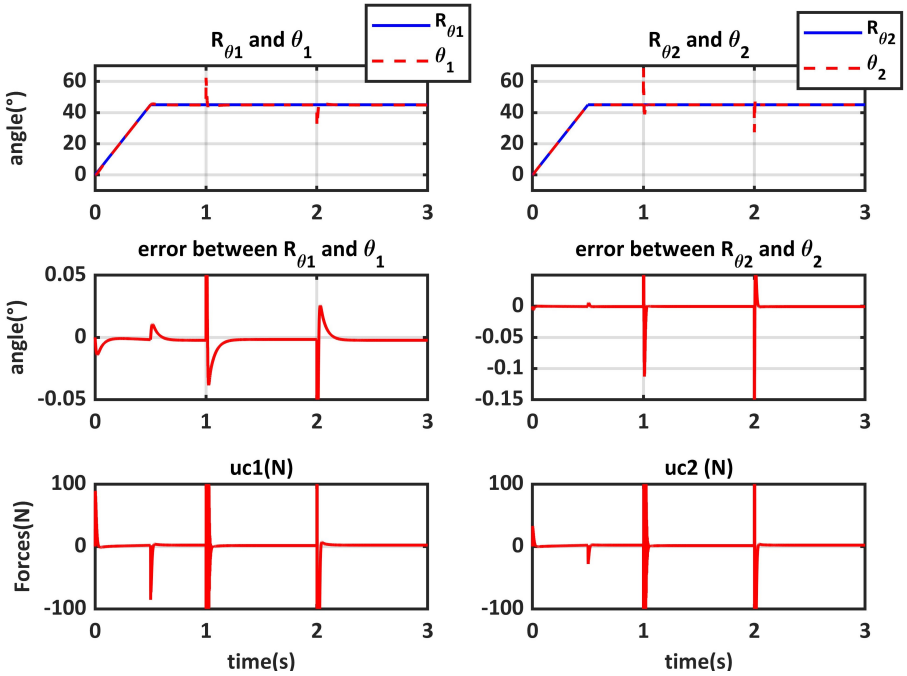

Figure. 4.14: ONSMC control results of the continuum robot in case of an added disturbance

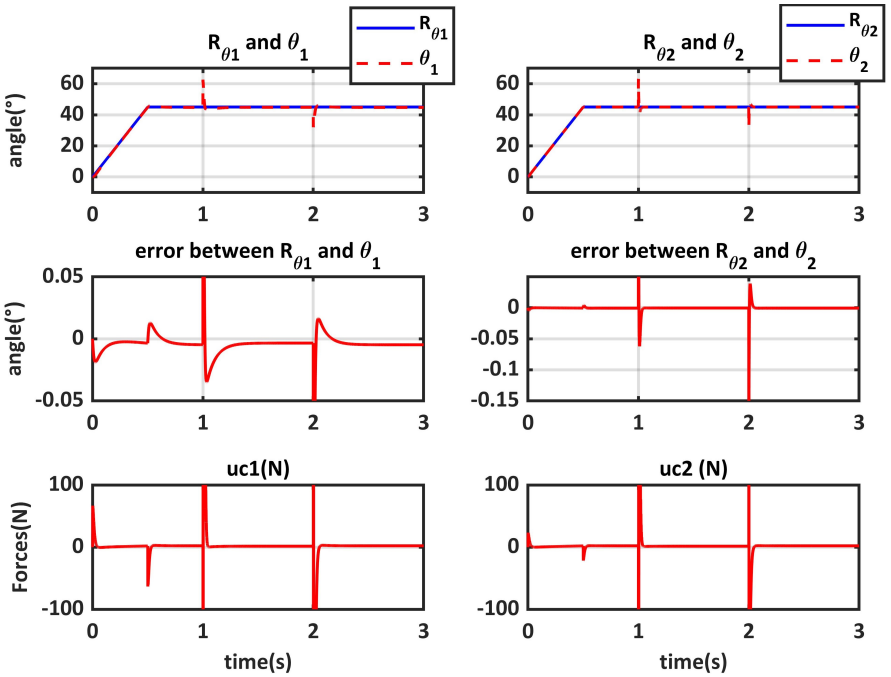

Figure. 4.15: OSMC control results of the continuum robot in case of an added disturbance

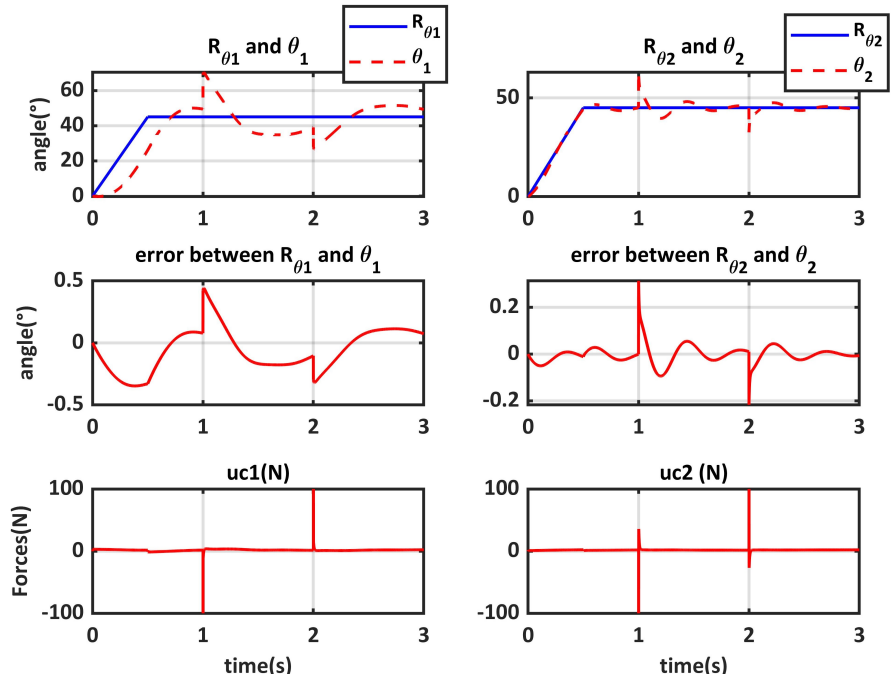

Figure. 4.16: OPID control results of the continuum robot in case of an added disturbance

Table 4.7: MSE and MAE values in case of an added disturbance

	MAE	MSE
ONSMC	37.4462	4.3745e-04
OSMC	51.4019	4.6902e-04
OPID	1.0779+03	0.0348

It should be highlighted that the introduced modifications are not of big deal in terms of complexity; and that the resulting control scheme, has almost similar computational burden as its competitors, however with better performance.

A poor selection of any parameter's value of the optimization algorithm leads to a slow convergence rate and a high possibility to be trapped in local minima. Therefore, several simulations have been conducted in order to determine the best values of the optimization algorithm's parameters. After that, the optimization algorithm (PSO) was used to optimize the controller parameters.

4.6 Conclusion

In This chapter, a simplified dynamic model for a single section variable curvature continuum robot was introduced by exploiting the equation that express the bending angle of each unit in function of the angle of first unit. This equation significantly narrows down the number of variables to be considered in the dynamic model. Then, an optimized proportional integral derivative controller was designed to control the developed dynamic model. As well as, an efficient robust control algorithm based on the nonlinear sliding mode control and the PSO algorithm has been designed and successfully used to control a two-section continuum robot. To assess the efficiency of the proposed controller two different reference trajectories were used and a comparative study between the OPID controller, the OSMC and the proposed ONSMC has been carried out. The simulation results have shown that the proposed controller gives satisfactory control performance in term of the tracking accuracy and the robustness against external disturbances.

CONCLUSION AND FUTURE WORK

The aim of this thesis was to develop methods for modeling and control of continuum robots, which can provide satisfactory and effective performance. In fact, neural networks and optimization methods have been widely used for modeling and controlling nonlinear systems. The secret of neural networks' success lies in the fact that any non-linear system can be modeled with a certain precision using a simple neural network having learning and generalization capabilities. On the other hand, the emergence of many optimization methods has made it possible to consider more complex optimization problems for which numerical methods cannot give acceptable solutions.

In this thesis, the different types of continuum robots and their modeling were properly studied. This study allowed us to examine the limitations and advantages of the adopted approaches and maked it easier for us to suggest several ways to improve the modeling and control methods based on artificial intelligence tools. The accomplished work can be summarized as follows:

- ✓ A recently developed meta-heuristic approach so-called teaching learning based optimization was adopted to solve the inverse kinematic model of a continuum robot with variable length as well as the resolution of the inverse kinematic model of a three-section continuum robot. The TLBO algorithm is not fussy and does not require any specific parameters to be tuned up. In other words, unlike the other developed meta-heuristic algorithms which need specific parameters to perform correctly, TLBO can be considered as the best optimization method to tackle the complexity of continuum robots. To emphasize, based on the available state of art about optimization methods, it is concluded that the TLBO algorithm is way better accurate than the other optimization algorithms for solving the IKM. Furthermore, the TLBO algorithm has managed to properly solve the IKM of three sections continuum robot with and without the presence of a static obstacle. From a practical point of view, the variable length continuum robot

is of a great interest since it can extend its backbone and broad the workspace of the robot yet its realization require a specific type of material. The chosen material of this bind of robots must satisfy certain extensibility without badly deforming the robot's backbone.

- ✓ An artificial neural network is developed to solve the inverse kinematic model of multi-section continuum robot with variable curvature. The development of the used artificial neural network is done through the forward kinematic model which is mainly used to train the ANN. At the training of the neural network is performed based on a random generated database from the fKM. The obtained neural network is tested on solving the IKM of continuum robots through various examples. The bending angles which allow the robot to the trained properly follow a desired trajectory can be easily and accurately generated by ANN. Furthermore, it is crucially important to say that the ANN is an appropriate tool to deal with real time application unlike other meta-heuristic approaches that cannot respond to the needs of the industry and that can be found in the real time application. While ANN proves its dexterity towards real time application with further accuracy.

- ✓ A simplified dynamic model for a class of variable curvature continuum robots was developed based on Euler-Lagrange method and by adopting the equation which links each of the continuum robot's bending angles to each other. It significantly narrows down the number of variables to be dealt with in the dynamic model. To verify the effectiveness of the developed dynamic model, simulation examples through Matlab were carried out. The first simulation was dedicated to a single section variable curvature continuum robot, in which the robot was given a bending angle as initial point and its behavior is theoretically assessed using Runge-Kutta method. The second simulation example has addressed the behavior of a variable curvature continuum robot subjected to a force.

- ✓ An proportional integral derivative controller and optimized using the reliable particle swarm optimization was developed to control a continuum robot. It is proved that the OPID controller can be used with various type of trajectories. Its robustness in tracking trajectories has also been confirmed against some external disturbances. As well as an efficient robust control algorithm based on the nonlinear sliding mode control and the adaptive PSO algorithm was designed and successfully used to control a continuum robot. To assess the efficiency of the proposed controller two different reference trajectories were used and a

comparative study between the OPID controller, the OSMC and the proposed ONSMC is carried out. The simulation results have shown that the proposed controller gives satisfactory control performance in term of the tracking accuracy and the robustness against the output disturbances.

The possible extensions of this current work are numerous, among the perspectives that can be supported we cite:

- ✓ Coupling the TLBO algorithm with artificial neural networks for the sake of achieving accuracy and real-time response in solving the continuum robots inverse kinematic models.
- ✓ Addition of frictional forces, torsional effect and gravitational terms in the robot equations of motion to get closer to its real dynamic behavior.
- ✓ Developing robust adaptive controllers to deal with different disturbances that face continuum robots.
- ✓ Making a prototype for a continuum robot in order to experimentally evaluate the different techniques.

REFERENCES

[1] P. Wilkening, F. Alambeigi, R. J. Murphy, R. H. Taylor, and M. Armand, "Development and experimental evaluation of concurrent control of a robotic arm and continuum manipulator for osteolytic lesion treatment," *IEEE robotics and automation letters*, vol. 2, no. 3, pp. 1625–1631, 2017.

[2] A. W. Mahoney, P. L. Anderson, P. J. Swaney, F. Maldonado, and R. J. Webster, "Reconfigurable parallel continuum robots for incisionless surgery," in *2016 IEEE/RSJ International Conference on Intelligent Robots and Systems (IROS)*, pp. 4330–4336, IEEE, 2016.

[3] M. M. Tonapi, I. S. Godage, and I. D. Walker, "Next generation rope-like robot for in-space inspection," in *2014 IEEE Aerospace Conference*, pp. 1–13, IEEE, 2014.

[4] A. Bajo and N. Simaan, "Finding lost wrenches: Using continuum robots for contact detection and estimation of contact location," in *2010 IEEE international conference on robotics and automation*, pp. 3666–3673, IEEE, 2010.

[5] A. L. Orekhov, C. B. Black, J. Till, S. Chung, and D. C. Rucker, "Analysis and validation of a teleoperated surgical parallel continuum manipulator," *IEEE Robotics and Automation Letters*, vol. 1, no. 2, pp. 828–835, 2016.

[6] F. Alambeigi, Y. Wang, S. Sefati, C. Gao, R. J. Murphy, I. Iordachita, R. H. Taylor, H. Khanuja, and M. Armand, "A curved-drilling approach in core decompression of the femoral head osteonecrosis using a continuum manipulator," *IEEE Robotics and Automation Letters*, vol. 2, no. 3, pp. 1480–1487, 2017.

[7] T. Qu, J. Chen, S. Shen, Z. Xiao, Z. Yue, and H. Y. K. Lau, "Motion control of a bio-inspired wire-driven multi-backbone continuum minimally invasive surgical manipulator," in *2016 IEEE International Conference on Robotics and Biomimetics (ROBIO)*, pp. 1989–1995, IEEE, 2016.

[8] J. Fraś, J. Czarnowski, M. Maciaś, J. Główka, M. Cianchetti, and A. Menciassi, "New STIFF-FLOP module construction idea for improved actuation and sensing," in *2015 IEEE international conference on robotics and automation (ICRA)*, pp. 2901–2906, IEEE, 2015.

[9] M. Cianchetti, T. Ranzani, G. Gerboni, I. De Falco, C. Laschi, and A. Menciassi, "STIFF-FLOP surgical manipulator: Mechanical design and experimental characterization of the single module," in *2013 IEEE/RSJ international conference on intelligent robots and systems*, pp. 3576–3581, IEEE, 2013.

[10] J. Burgner-Kahrs, D. C. Rucker, and H. Choset, "Continuum robots for medical applications: A survey," *IEEE Transactions on Robotics*, vol. 31, no. 6, pp. 1261–1280, 2015.

[11] B. L. Conrad, J. Jung, R. S. Penning, and M. R. Zinn, "Interleaved continuum-rigid manipulation: An augmented approach for robotic minimally-invasive flexible catheter-based procedures," in *2013 IEEE International Conference on Robotics and Automation*, pp. 718–724, IEEE, 2013.

[12] J. Li, Z. Teng, and J. Xiao, "Can a continuum manipulator fetch an object in an unknown cluttered space?," *IEEE Robotics and Automation Letters*, vol. 2, no. 1, pp. 2–9, 2016.

[13] D. Trivedi, C. D. Rahn, W. M. Kier, and I. D. Walker, "Soft robotics: Biological inspiration, state of the art, and future research," *Applied bionics and biomechanics*, vol. 5, no. 3, pp. 99–117, 2008.

[14] G. Robinson and J. B. C. Davies, "Continuum robots-a state of the art," in *Proceedings 1999 IEEE international conference on robotics and automation (Cat. No. 99CH36288C)*, vol. 4, pp. 2849–2854, IEEE, 1999.

[15] I. D. Walker, "Continuous backbone "continuum" robot manipulators," *International Scholarly Research Notices*, vol. 2013, 2013.

[16] H.-S. Yoon and B.-J. Yi, "Development of a 4-DOF Continuum Robot Using a Spring Backbone," *The Journal of Korea Robotics Society*, vol. 3, no. 4, pp. 323–330, 2008.

[17] M. Li, R. Kang, S. Geng, and E. Guglielmino, "Design and control of a tendon-driven continuum robot," *Transactions of the Institute of Measurement and Control*, vol. 40, no. 11, pp. 3263–3272, 2018.

[18] G. Gao, H. Wang, J. Fan, Q. Xia, L. Li, and H. Ren, "Study on stretch-retractable single-section continuum manipulator," *Advanced Robotics*, vol. 33, no. 1, pp. 1–12, 2019.

[19] C. Laschi, B. Mazzolai, M. Cianchetti, V. Mattoli, L. Bassi-Luciani, and P. Dario, "Design of a biomimetic robotic octopus arm, Bioinspiration and Biomimetics," 2009.

[20] F. Renda, M. Cianchetti, M. Giorelli, A. Arienti, and C. Laschi, "A 3D steady-state model of a tendon-driven continuum soft manipulator inspired by the octopus arm," *Bioinspiration & biomimetics*, vol. 7, no. 2, p. 25006, 2012.

[21] F. Renda, M. Giorelli, M. Calisti, M. Cianchetti, and C. Laschi, "Dynamic model of a multibending soft robot arm driven by cables," *IEEE Transactions on Robotics*, vol. 30, no. 5, pp. 1109–1122, 2014.

[22] Y. Peng, Y. Liu, Y. Yang, N. Liu, Y. Sun, Y. Liu, H. Pu, S. Xie, and J. Luo, "Development of continuum manipulator actuated by thin McKibben pneumatic artificial muscle," *Mechatronics*, vol. 60, pp. 56–65, 2019.

[23] V. C. Anderson, "Tensor arm manipulator design," *Trans. ASME*, vol. 67, pp. 1–12, 1967.

[24] V. C. Anderson and R. C. Horn, "Tensor arm manipulator," *United State Patent*, no. 3,497,083, 1970.

[25] G. S. Chirikjian and J. W. Burdick, "A modal approach to hyper-redundant manipulator kinematics," *IEEE Transactions on Robotics and Automation*, vol. 10, no. 3, pp. 343–354, 1994.

[26] G. Robinson, J. B. C. Davies, and J. P. P. Jones, "Development of the Amadeus dextrous robot end-effectors," in *IEEE Oceanic Engineering Society. OCEANS'98. Conference Proceedings (Cat. No. 98CH36259)*, vol. 2, pp. 703–707, IEEE, 1998.

[27] J. B. C. Davies, D. M. Lane, G. C. Robinson, D. J. O'Brien, M. Pickett, M. Sfakiotakis, and B. Deacon, "Subsea applications of continuum robots," in *Proceedings of 1998 International Symposium on Underwater Technology*, pp. 363–369, IEEE, 1998.

[28] I. D. Walker and M. W. Hannan, "A novel'elephant's trunk'robot," in *1999 IEEE/ASME International Conference on Advanced Intelligent Mechatronics (Cat. No. 99TH8399)*, pp. 410–415, IEEE, 1999.

[29] K. C. Walker and D. W. L. Wang, "Analytical modelling of deformable objects for haptics virtual environments," *International Journal of Robotics and Automation*, vol. 27, no. 1, p. 92, 2012.

[30] T. Mahl, A. Hildebrandt, and O. Sawodny, "Forward kinematics of a compliant pneumatically actuated redundant manipulator," in *2012 7th IEEE Conference on Industrial Electronics and Applications (ICIEA)*, pp. 1267–1273, IEEE, 2012.

[31] T. Mahl, A. Hildebrandt, and O. Sawodny, "A variable curvature continuum kinematics for kinematic control of the bionic handling assistant," *IEEE transactions on robotics*, vol. 30, no. 4, pp. 935–949, 2014.

[32] C. Escande, P. M. Pathak, R. Merzouki, and V. Coelen, "Modelling of multisection bionic manipulator: Application to robotinoxt," in *2011 IEEE International Conference on Robotics and Biomimetics*, pp. 92–97, IEEE, 2011.

[33] W. McMahan, V. Chitrakaran, M. Csencsits, D. Dawson, I. D. Walker, B. A. Jones, M. Pritts, D. Dienno, M. Grissom, and C. D. Rahn, "Field trials and testing of the OctArm continuum manipulator," in *Proceedings 2006 IEEE International Conference on Robotics and Automation, 2006. ICRA 2006.*, pp. 2336–2341, IEEE, 2006.

[34] M. D. Grissom, V. Chitrakaran, D. Dienno, M. Csencits, M. Pritts, B. Jones, W. McMahan, D. Dawson, C. Rahn, and I. Walker, "Design and experimental testing of the octarm soft robot manipulator," in *Unmanned Systems Technology VIII*, vol. 6230, p. 62301F, International Society for Optics and Photonics, 2006.

[35] W. McMahan, B. A. Jones, and I. D. Walker, "Design and implementation of a multi-section continuum robot: Air-octor," in *2005 IEEE/RSJ International Conference on Intelligent Robots and Systems*, pp. 2578–2585, IEEE, 2005.

[36] O. Salomon and A. Wolf, "Inclined links hyper-redundant elephant trunk-like robot," *Journal of Mechanisms and robotics*, vol. 4, no. 4, 2012.

[37] C. Laschi, B. Mazzolai, V. Mattoli, M. Cianchetti, and P. Dario, "Design of a biomimetic robotic octopus arm," *Bioinspiration & biomimetics*, vol. 4, no. 1, p. 15006, 2009.

[38] E. Guglielmino, N. Tsagarakis, and D. G. Caldwell, "An octopus anatomy-inspired robotic arm," in *2010 IEEE/RSJ International Conference on Intelligent Robots and Systems*, pp. 3091–3096, IEEE, 2010.

[39] E. Guglielmino, L. Zullo, M. Cianchetti, M. Follador, D. Branson, and D. G. Caldwell, "The application of embodiment theory to the design and control of an octopus-like robotic arm," in *2012 IEEE International Conference on Robotics and Automation*, pp. 5277–5282, IEEE, 2012.

[40] M. Sfakiotakis, A. Kazakidi, N. Pateromichelakis, and D. P. Tsakiris, "Octopus-inspired eight-arm robotic swimming by sculling movements," in *2013 IEEE International Conference on Robotics and Automation*, pp. 5155–5161, IEEE, 2013.

[41] M. Cianchetti, M. Calisti, L. Margheri, M. Kuba, and C. Laschi, "Bioinspired locomotion and grasping in water: the soft eight-arm OCTOPUS robot," *Bioinspiration & biomimetics*, vol. 10, no. 3, p. 35003, 2015.

[42] M. Jha and N. R. Chauhan, "A review on Snake-like Continuum Robots for Medical Surgeries," in *IOP Conference Series: Materials Science and Engineering*, vol. 691, p. 12093, IOP Publishing, 2019.

[43] B. Rosa, V. Bordoux, and F. Nageotte, "Combining differential kinematics and optical flow for automatic labeling of continuum robots in minimally invasive surgery," *Frontiers in Robotics and AI*, vol. 6, p. 86, 2019.

[44] H. Hu, P. Wang, B. Zhao, M. Li, and L. Sun, "Design of a novel snake-like robotic colonoscope," in *2009 IEEE International Conference on Robotics and Biomimetics (ROBIO)*, pp. 1957–1961, IEEE, 2009.

[45] B. Ouyang, Y. Liu, and D. Sun, "Design of a three-segment continuum robot for minimally invasive surgery," *Robotics and biomimetics*, vol. 3, no. 1, pp. 1–4, 2016.

[46] T. Wang, Z. Wang, G. Wu, L. Lei, B. Zhao, P. Zhang, and P. Shang, "Design and analysis of a snake-like surgical robot with continuum joints," in *2020 5th International Conference on Advanced Robotics and Mechatronics (ICARM)*, pp. 178–183, IEEE, 2020.

[47] N. Simaan, K. Xu, W. Wei, A. Kapoor, P. Kazanzides, R. Taylor, and P. Flint, "Design and integration of a telerobotic system for minimally invasive surgery of the throat," *The International journal of robotics research*, vol. 28, no. 9, pp. 1134–1153, 2009.

[48] R. E. Goldman, A. Bajo, L. S. MacLachlan, R. Pickens, S. D. Herrell, and N. Simaan, "Design and performance evaluation of a minimally invasive telerobotic platform for transurethral surveillance and intervention," *IEEE transactions on biomedical engineering*, vol. 60, no. 4, pp. 918–925, 2012.

[49] J. Ding, K. Xu, R. Goldman, P. Allen, D. Fowler, and N. Simaan, "Design, simulation and evaluation of kinematic alternatives for insertable robotic effectors platforms in single port access surgery," in *2010 IEEE International Conference on Robotics and Automation*, pp. 1053–1058, IEEE, 2010.

[50] A. Bajo and N. Simaan, "Hybrid motion/force control of multi-backbone continuum robots," *The International journal of robotics research*, vol. 35, no. 4, pp. 422–434, 2016.

[51] N. Simaan, "Snake-like units using flexible backbones and actuation redundancy for enhanced miniaturization," in *Proceedings of the 2005 IEEE international conference on robotics and automation*, pp. 3012–3017, IEEE, 2005.

[52] R. J. Webster, A. M. Okamura, and N. J. Cowan, "Toward active cannulas: Miniature snake-like surgical robots," in *2006 IEEE/RSJ international conference on intelligent robots and systems*, pp. 2857–2863, IEEE, 2006.

[53] Y. Kim, G. A. Parada, S. Liu, and X. Zhao, "Ferromagnetic soft continuum robots," *Science Robotics*, vol. 4, no. 33, 2019.

[54] G. S. Chirikjian, "Conformational modeling of continuum structures in robotics and structural biology: A review," *Advanced Robotics*, vol. 29, no. 13, pp. 817–829, 2015.

[55] J. D. Greer, T. K. Morimoto, A. M. Okamura, and E. W. Hawkes, "Series pneumatic artificial muscles (sPAMs) and application to a soft continuum robot," in *2017 IEEE International Conference on Robotics and Automation (ICRA)*, pp. 5503–5510, IEEE, 2017.

[56] I. Singh, *Curve Based Approach for Shape Reconstruction of Continuum Manipulators*. PhD thesis, Universite de Lille, 2018.

[57] R. J. Webster III and B. A. Jones, "Design and kinematic modeling of constant curvature continuum robots: A review," *The International Journal of Robotics Research*, vol. 29, no. 13, pp. 1661–1683, 2010.

[58] D. C. Rucker and R. J. Webster III, "Statics and dynamics of continuum robots with general tendon routing and external loading," *IEEE Transactions on Robotics*, vol. 27, no. 6, pp. 1033–1044, 2011.

[59] M. T. Chikhaoui and J. Burgner-Kahrs, "Control of continuum robots for medical applications: State of the art," in *ACTUATOR 2018; 16th International Conference on New Actuators*, pp. 1–11, VDE, 2018.

[60] J. Till, V. Aloi, and C. Rucker, "Real-time dynamics of soft and continuum robots based on Cosserat rod models," *The International Journal of Robotics Research*, vol. 38, no. 6, pp. 723–746, 2019.

[61] V. K. Venkiteswaran, J. Sikorski, and S. Misra, "Shape and contact force estimation of continuum manipulators using pseudo rigid body models," *Mechanism and machine theory*, vol. 139, pp. 34–45, 2019.

[62] R. J. Roesthuis and S. Misra, "Steering of multisegment continuum manipulators using rigid-link modeling and FBG-based shape sensing," *IEEE transactions on robotics*, vol. 32, no. 2, pp. 372–382, 2016.

[63] S. Bruno, S. Lorenzo, V. Luigi, and O. Giuseppe, "Robotics: modelling, planning and control," 2010.

[64] S. Grazioso, G. Di Gironimo, and B. Siciliano, "A geometrically exact model for soft continuum robots: The finite element deformation space formulation," *Soft robotics*, vol. 6, no. 6, pp. 790–811, 2019.

[65] D. C. Rucker, B. A. Jones, and R. J. Webster III, "A geometrically exact model for externally loaded concentric-tube continuum robots," *IEEE transactions on robotics*, vol. 26, no. 5, pp. 769–780, 2010.

[66] Y. Bailly and Y. Amirat, "Modeling and control of a hybrid continuum active catheter for aortic aneurysm treatment," in *Proceedings of the 2005 IEEE International Conference on Robotics and Automation*, pp. 924–929, IEEE, 2005.

[67] B. He, Z. Wang, Q. Li, H. Xie, and R. Shen, "An analytic method for the kinematics and dynamics of a multiple-backbone continuum robot," *International Journal of Advanced Robotic Systems*, vol. 10, no. 1, p. 84, 2013.

[68] B. A. Jones and I. D. Walker, "Kinematics for multisection continuum robots," *IEEE Transactions on Robotics*, vol. 22, no. 1, pp. 43–55, 2006.

[69] V. Falkenhahn, T. Mahl, A. Hildebrandt, R. Neumann, and O. Sawodny, "Dynamic modeling of bellows-actuated continuum robots using the Euler–Lagrange formalism," *IEEE Transactions on Robotics*, vol. 31, no. 6, pp. 1483–1496, 2015.

[70] G. Runge, M. Wiese, L. Günther, and A. Raatz, "A framework for the kinematic modeling of soft material robots combining finite element analysis and piecewise constant curvature kinematics," in *2017 3rd International Conference on Control, Automation and Robotics (ICCAR)*, pp. 7–14, IEEE, 2017.

[71] C. Della Santina, A. Bicchi, and D. Rus, "On an improved state parametrization for soft robots with piecewise constant curvature and its use in model based control," *IEEE Robotics and Automation Letters*, vol. 5, no. 2, pp. 1001–1008, 2020.

[72] L. Fryziel, "Modélisation et calibrage pour la commande d'un micro-robot continuum dédié à la chirurgie mini-invasive," 2010.

[73] C. Escande, "Towards modeling of a class of bionic manipulator robots," 2013.

[74] M. W. Hannan and I. D. Walker, "Kinematics and the implementation of an elephant's trunk manipulator and other continuum style robots," *Journal of robotic systems*, vol. 20, no. 2, pp. 45–63, 2003.

[75] Z. Li and R. Du, "Design and analysis of a bio-inspired wire-driven multi-section flexible robot," *International Journal of Advanced Robotic Systems*, vol. 10, no. 4, p. 209, 2013.

[76] S. Neppalli and B. A. Jones, "Design, construction, and analysis of a continuum robot," in *2007 IEEE/RSJ International Conference on Intelligent Robots and Systems*, pp. 1503–1507, IEEE, 2007.

[77] S. Djeffal, C. Mahfoudi, and A. Amouri, "Comparison of Three Meta-heuristic Algorithms for Solving Inverse Kinematics Problems of Variable Curvature Continuum Robots," in *2021 European Conference on Mobile Robots (ECMR)*, pp. 1–6, IEEE.

[78] J. Lu, F. Du, T. Zhang, D. Wang, and Y. Lei, "An efficient inverse kinematics algorithm for continuum robot with a translational base," in *2020 IEEE/ASME International Conference on Advanced Intelligent Mechatronics (AIM)*, pp. 1754–1759, IEEE, 2020.

[79] S. Iqbal, S. Mohammed, and Y. Amirat, "A guaranteed approach for kinematic analysis of continuum robot based catheter," in *2009 IEEE International Conference on Robotics and Biomimetics (ROBIO)*, pp. 1573–1578, IEEE, 2009.

[80] A. M. Chu, X. B. Duong, and C. H. Le, "Forward and inverse kinematics analysis of a spatial three-segment continuum robot," 2021.

[81] I. Singh, O. Lakhal, Y. Amara, V. Coelen, P. M. Pathak, and R. Merzouki, "Performances evaluation of inverse kinematic models of a compact bionic handling assistant," in *2017 IEEE International Conference on Robotics and Biomimetics (ROBIO)*, pp. 264–269, IEEE, 2017.

[82] A. Ammar, M. Chawki, Z. Abdelouahab, and M. Halim, "A New Approach to Solve Inverse Kinematics of a Planar Flexible Continuum Robot," in *International Conference of Computational Methods in Science and Engineering, ICCMSE*, 2014.

[83] J. Santoso and C. D. Onal, "An origami continuum robot capable of precise motion through torsionally stiff body and smooth inverse kinematics," *Soft Robotics*, 2020.

[84] A. Amouri, C. Mahfoudi, and A. Zaatri, "Contribution to inverse kinematic modeling of a planar continuum robot using a particle swarm optimization," in *Conference on Multiphysics Modelling and Simulation for Systems Design*, pp. 141–150, Springer, 2014.

[85] A. Amouri, C. Mahfoudi, A. Zaatri, O. Lakhal, and R. Merzouki, "A metaheuristic approach to solve inverse kinematics of continuum manipulators," *Proceedings of the Institution of Mechanical Engineers, Part I: Journal of Systems and Control Engineering*, vol. 231, no. 5, pp. 380–394, 2017.

[86] O. Lakhal, A. Melingui, A. Chibani, C. Escande, and R. Merzouki, "Inverse kinematic modeling of a class of continuum bionic handling arm," in *2014 IEEE/ASME International Conference on Advanced Intelligent Mechatronics*, pp. 1337–1342, IEEE, 2014.

[87] A. Melingui, R. Merzouki, J. B. Mbede, C. Escande, and N. Benoudjit, "Neural networks based approach for inverse kinematic modeling of a compact bionic handling assistant trunk," in *2014 IEEE 23rd International Symposium on Industrial Electronics (ISIE)*, pp. 1239–1244, IEEE, 2014.

[88] T. G. Thuruthel, E. Falotico, M. Cianchetti, and C. Laschi, "Learning global inverse kinematics solutions for a continuum robot," in *Symposium on robot design, dynamics and control*, pp. 47–54, Springer, 2016.

[89] A. Melingui, R. Merzouki, J. B. Mbede, C. Escande, B. Daachi, and N. Benoudjit, "Qualitative approach for inverse kinematic modeling of a compact bionic handling assistant trunk," in *2014 International Joint Conference on Neural Networks (IJCNN)*, pp. 754–761, IEEE, 2014.

[90] O. Lakhal, A. Melingui, and R. Merzouki, "Hybrid approach for modeling and solving of kinematics of a compact bionic handling assistant manipulator," *IEEE/ASME Transactions on Mechatronics*, vol. 21, no. 3, pp. 1326–1335, 2015.

[91] D. Y. Kolpashchikov, N. V. Laptev, V. V. Danilov, I. P. Skirnevskiy, R. A. Manakov, and O. M. Gerget, "FABRIK-based inverse kinematics for multi-section continuum robots," in *2018 18th International Conference on Mechatronics-Mechatronika (ME)*, pp. 1–8, IEEE, 2018.

[92] L. Jiajia, D. Fuxin, L. Yibin, L. Yanqiang, Z. Tao, and Z. Gang, "A novel inverse kinematics algorithm using the Kepler oval for continuum robots," *Applied Mathematical Modelling*, vol. 93, pp. 206–225, 2021.

[93] E. Shahabi and C.-H. Kuo, "Solving inverse kinematics of a planar dual-backbone continuum robot using neural network," in *European Conference on Mechanism Science*, pp. 355–361, Springer, 2018.

[94] W. S. Rone and P. Ben-Tzvi, "Continuum robot dynamics utilizing the principle of virtual power," *IEEE Transactions on Robotics*, vol. 30, no. 1, pp. 275–287, 2013.

[95] F. Xu, H. Wang, K. W. S. Au, W. Chen, and Y. Miao, "Underwater dynamic modeling for a cable-driven soft robot arm," *IEEE/ASME transactions on Mechatronics*, vol. 23, no. 6, pp. 2726–2738, 2018.

[96] W. S. Rone and P. Ben-Tzvi, "Mechanics modeling of multisegment rod-driven continuum robots," *Journal of Mechanisms and Robotics*, vol. 6, no. 4, 2014.

[97] H. El-Hussieny, S.-G. Jeong, and J.-H. Ryu, "Dynamic modeling of a class of soft growing robots using euler-lagrange formalism," *Society of Instrument and Control Engineers*, 2019.

[98] J. Yang, H. Peng, W. Zhou, J. Zhang, and Z. Wu, "A modular approach for dynamic modeling of multisegment continuum robots," *Mechanism and Machine Theory*, vol. 165, p. 104429, 2021.

[99] I. A. Seleem, S. F. M. Assal, H. Ishii, and H. El-Hussieny, "Guided pose planning and tracking for multi-section continuum robots considering robot dynamics," *IEEE Access*, vol. 7, pp. 166690–166703, 2019.

[100] M. M. Dalvand, S. Nahavandi, and R. D. Howe, "An analytical loading model for n-tendon continuum robots," *IEEE Transactions on Robotics*, vol. 34, no. 5, pp. 1215–1225, 2018.

[101] H. Mochiyama and T. Suzuki, "Kinematics and dynamics of a cable-like hyper-flexible manipulator," in *2003 IEEE International Conference on Robotics and Automation (Cat. No. 03CH37422)*, vol. 3, pp. 3672–3677, IEEE, 2003.

[102] G. S. Chirikjian, "A continuum approach to hyper-redundant manipulator dynamics," in *Proceedings of 1993 IEEE/RSJ International Conference on Intelligent Robots and Systems (IROS'93)*, vol. 2, pp. 1059–1066, IEEE, 1993.

[103] V. Falkenhahn, T. Mahl, A. Hildebrandt, R. Neumann, and O. Sawodny, "Dynamic modeling of constant curvature continuum robots using the Euler-Lagrange formalism," in *2014 IEEE/RSJ International Conference on Intelligent Robots and Systems*, pp. 2428–2433, IEEE, 2014.

[104] A. Ehsani-Seresht and S. Hashemi-Pour Moosavi, "Dynamic modeling of the cable-driven continuum robots in hybrid position-force actuation mode," *Journal of Mechanisms and Robotics*, vol. 12, no. 5, p. 51002, 2020.

[105] S. M. Mustaza, Y. Elsayed, C. Lekakou, C. Saaj, and J. Fras, "Dynamic modeling of fiber-reinforced soft manipulator: A visco-hyperelastic material-based continuum mechanics approach," *Soft robotics*, vol. 6, no. 3, pp. 305–317, 2019.

[106] S. Norouzi-Ghazbi and F. Janabi-Sharifi, "Dynamic modeling and system identification of internally actuated, small-sized continuum robots," *Mechanism and Machine Theory*, vol. 154, p. 104043, 2020.

[107] I. A. Gravagne, C. D. Rahn, and I. D. Walker, "Large deflection dynamics and control for planar continuum robots," *IEEE/ASME transactions on mechatronics*, vol. 8, no. 2, pp. 299–307, 2003.

[108] D. Trivedi, A. Lotfi, and C. D. Rahn, "Geometrically exact dynamic models for soft robotic manipulators," in *2007 IEEE/RSJ International Conference on Intelligent Robots and Systems*, pp. 1497–1502, IEEE, 2007.

[109] E. Tatlicioglu, I. D. Walker, and D. M. Dawson, "New dynamic models for planar extensible continuum robot manipulators," in *2007 IEEE/RSJ International Conference on Intelligent Robots and Systems*, pp. 1485–1490, IEEE, 2007.

[110] A. A. Alqumsan, S. Khoo, and M. Norton, "Robust control of continuum robots using Cosserat rod theory," *Mechanism and Machine Theory*, vol. 131, pp. 48–61, 2019.

[111] "scholar."

[112] S. Heidari, F. Piltan, M. Shamsodini, K. Heidari, and S. Zahmatkesh, "Design new nonlinear controller with parallel fuzzy inference system compensator to control of continuum robot manipulator," *International Journal of Control and Automation*, vol. 6, no. 4, pp. 115–134, 2013.

[113] A. Mousa, S. Khoo, and M. Norton, "Robust control of tendon driven continuum robots," in *2018 15th International Workshop on Variable Structure Systems (VSS)*, pp. 49–54, IEEE, 2018.

[114] F. Piltan and S. T. Haghighi, "Design gradient descent optimal sliding mode control of continuum robots," *IAES International Journal of Robotics and Automation*, vol. 1, no. 4, p. 175, 2012.

[115] M. Li, R. Kang, D. T. Branson, and J. S. Dai, "Model-free control for continuum robots based on an adaptive Kalman filter," *IEEE/ASME Transactions on Mechatronics*, vol. 23, no. 1, pp. 286–297, 2017.

[116] A. Melingui, R. Merzouki, and J. B. Mbede, "Compact bionic handling arm control using neural networks," *Electronics letters*, vol. 50, no. 14, pp. 979–981, 2014.

[117] W. Xu, J. Chen, H. Y. K. Lau, and H. Ren, "Data-driven methods towards learning the highly nonlinear inverse kinematics of tendon-driven surgical manipulators," *The International Journal of Medical Robotics and Computer Assisted Surgery*, vol. 13, no. 3, p. e1774, 2017.

[118] P. Lloyd, A. K. Hoshiar, T. da Veiga, A. Attanasio, N. Marahrens, J. H. Chandler, and P. Valdastri, "A learnt approach for the design of magnetically actuated shape forming soft tentacle robots," *IEEE Robotics and Automation Letters*, vol. 5, no. 3, pp. 3937–3944, 2020.

[119] T. George Thuruthel, E. Falotico, M. Manti, A. Pratesi, M. Cianchetti, and C. Laschi, "Learning closed loop kinematic controllers for continuum manipulators in unstructured environments," *Soft robotics*, vol. 4, no. 3, pp. 285–296, 2017.

[120] H. Jiang, Z. Wang, X. Liu, X. Chen, Y. Jin, X. You, and X. Chen, "A two-level approach for solving the inverse kinematics of an extensible soft arm considering viscoelastic behavior," in *2017 IEEE International Conference on Robotics and Automation (ICRA)*, pp. 6127–6133, IEEE, 2017.

[121] I. A. Gravagne and I. D. Walker, "Kinematic transformations for remotely-actuated planar continuum robots," in *Proceedings 2000 ICRA. Millennium Conference. IEEE International Conference on Robotics and Automation. Symposia Proceedings (Cat. No. 00CH37065)*, vol. 1, pp. 19–26, IEEE, 2000.

[122] S. Neppalli, M. A. Csencsits, B. A. Jones, and I. Walker, "A geometrical approach to inverse kinematics for continuum manipulators," in *2008 IEEE/RSJ International Conference on Intelligent Robots and Systems*, pp. 3565–3570, IEEE, 2008.

[123] R. V. Rao, V. J. Savsani, and D. P. Vakharia, "Teaching–learning-based optimization: a novel method for constrained mechanical design optimization problems," *Computer-Aided Design*, vol. 43, no. 3, pp. 303–315, 2011.

[124] R. V. Rao, V. J. Savsani, and D. P. Vakharia, "Teaching–learning-based optimization: an optimization method for continuous non-linear large scale problems," *Information sciences*, vol. 183, no. 1, pp. 1–15, 2012.

[125] A. Amouri, A. Zaatri, and C. Mahfoudi, "Dynamic modeling of a class of continuum manipulators in fixed orientation," *Journal of Intelligent & Robotic Systems*, vol. 91, no. 3, pp. 413–424, 2018.

[126] Y. Shi and R. Eberhart, "A modified particle swarm optimizer," in *1998 IEEE international conference on evolutionary computation proceedings. IEEE world congress on computational intelligence (Cat. No. 98TH8360)*, pp. 69–73, IEEE, 1998.